AN AB INITIO ANALYSIS OF BIMETALLIC OLIGOANILINE MOLECULAR JUNCTIONS

A Thesis

by

MICHAEL WEI-LUENG WANG

Submitted to the Office of Graduate Studies of
Texas A&M University
in partial fulfillment of the requirements for the degree of

MASTER OF SCIENCE

May 2006

Major Subject: Chemical Engineering

AN AB INITIO ANALYSIS OF BIMETALLIC OLIGOANILINE MOLECULAR JUNCTIONS

A Thesis

by

MICHAEL WEI-LUENG WANG

Submitted to the Office of Graduate Studies of
Texas A&M University
in partial fulfillment of the requirements for the degree of

MASTER OF SCIENCE

Approved by:

Chair of Committee,	Jorge Seminario
Committee Members,	David Ford
	Jun Zou
Head of Department,	Kenneth Hall

May 2006

Major Subject: Chemical Engineering

ABSTRACT

An Ab Initio Analysis of Bimetallic Oligoaniline Molecular Junctions. (May 2006)
Michael Wei-Leung Wang, B.S., University of Washington
Chair of Advisory Committee: Dr. Jorge Seminario

The electron transport characteristics of Oligoaniline molecular junctions terminated with thiol-ends are analyzed with the density functional theory and the Green's function approach. The molecular junction consists of an Oligoaniline molecule attached to metal electrodes at each end. By applying an electric field, the molecule conducts a current that depends on either the molecular conformation or the ionization state. Ab initio optimization methods are performed on various Oligoaniline systems to analyze how different conformational changes are associated with different conductivities. The density functional theory and Green's function are used to calculate the density of states, transmission probability functions, and current-voltage calculations for each Oligoaniline system to complement the results from the molecular analysis. An inelastic tunneling spectrum analysis is also performed through frequency calculations to examine the different characteristics of each conducting state. Molecular orbits of each conformation was used to investigate further the relation between structure and electrical properties of the molecular junction. The combined results from the different calculations provided insight into the possible mechanisms for electron transfer throughout the junction.

DEDICATION

To my grandparents, parents

and

my lifelong friend, Jeff Su

ACKNOWLEDGEMENTS

I would like to express gratitude to my committee chair and advisor, Prof. Jorge Seminario for his support and guidance throughout this research assignment. Selecting him as my advisor has served as an eye-opening experience towards the research aspect of the nanotechnology world. I would also like to thank Dr. Juan Sotelo for his valuable insights and comments that have helped this research take form. I would like to express my special thanks to Dr. Liuming Yan whose guidance, support and assistance have proven invaluable in this research. I also want to extend my gratitude to various members of the Seminario research group, A. Zacarias, P. Derosa, and L. Agapito, who all expended great effort in providing key developments towards the software used. In addition, I would like to give special mention to the DURIP and ARO institutes for providing the super computer system and the necessary funds, and also DARPA who provided funds towards developing the software used in this research.

I would also like to give special mention to my friends and colleagues in the Chemical Engineering Department for giving me encouragement and daily discussion about engineering problems or just life in general. I am also thankful towards the departmental staff and faculty for providing me with an education and a mindset that will more than prepare me to succeed in my future endeavors.

Finally, I would like to express gratitude towards my parents, my father for his support and my mother for her patience and encouragement.

TABLE OF CONTENTS

Page

CHAPTER Page

LIST OF FIGURES

FIGURE Page

FIGURE Page

LIST OF TABLES

CHAPTER I

INTRODUCTION

1.1 Background

Downscaling dimensions of IC devices has always served as the impetus for the microelectronics industry. Reducing the size of IC components, namely transistors allow for higher density packing on a chip, which translates to higher circuit speed and power dissipation (per transistor). Gordon Moore, one of the founders of Intel, made a prediction, later termed "Moore's Law" that the number of transistors on one chip will double in approximately 18-24 months. Currently, the thickness of the gate oxide is 1.2 nanometers, along with the gate length being 35 nanometers. These dimensions are approaching the order of magnitude of individual molecules. At this scale, the problem of current leakage becomes more prominent due to the thermal diffusion of electrons and gate-oxide tunneling, a quantum-mechanical effect[1]. Research has yielded temporary solutions such as high-k dielectrics to address the leakage problems, but material limitations and the incessant need to downscale dimensions will soon mark the end of the CMOS era. It is evident then, that new technologies must be founded to address the data storage and information-processing needs of today.

One of the viable alternatives to conventional CMOS technology includes using specialized molecular structures such as carbon nanotubes or even individual molecules to serve as the gate structure. Although carbon nanotube gate designs are similar to current CMOS devices, schemes that involve individual molecules and nanowires utilize an entirely different set of mechanics. Termed "moletronics", the concept of using only a few molecules as a switching device was first realized by Arieh Aviram and Mark Ratner in 1974, who demonstrated rectifier properties in a single organic molecule[2].

This thesis follows the style of the *Journal of the Electrochemical Society*

In order to exhibit rectifier properties, the candidate molecule must have electrical characteristics similar to a *p-n* junction; *p* refers to *hole* reach regions while *n* refers *electron* rich regions, and can be altered on the molecule by implementing various side groups. In addition, the molecule must contain conducting properties, which is represented by the overlap of atomic orbitals throughout its length to form delocalized electron clouds. The delocalization of the molecular orbitals is necessary in that it provides inhabitable energy states for the electrons to traverse across the molecule.

The delocalization of electron clouds occurs mainly through resonant chemical structures consisting of alternating single and double or triple bonds. Electrons that take part in this resonant behavior are referred to as π electrons, electrons inhabiting the parallel p orbitals of the two bonding atoms. However, if the chemical structure contains a lot of aliphatic molecules, or singled-bonded molecules, delocalization is almost nonexistent due to the absence of pi electrons. Many of the molecules that exhibit a strong degree of resonance contain the benzene(C_6H_6) molecule, which contains six π electrons delocalized throughout the ring. Moletronics takes advantage of the delocalized molecular orbitals of the benzene molecule and the fact that the delocalization can be extended by inserting alternating single and double-triple bonds between the benzene groups. In addition, by outfitting different side groups on the benzene molecules, additional holes and electrons can be created, a concept to silicon doping in CMOS technology. A typical molecule used in moletronics is shown below in Figure 1, illustrating the conjugated bonds and the various side groups that can be attached to the Benzene molecule to alter electron densities.

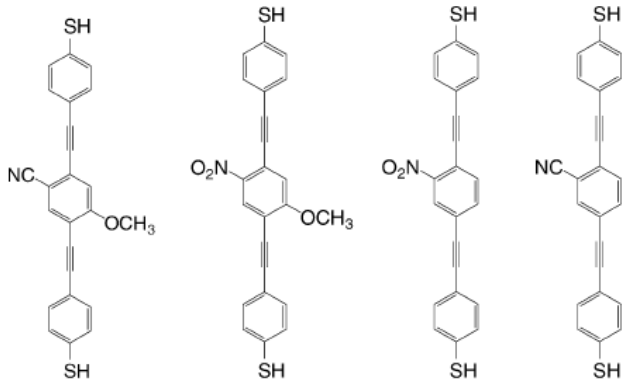

Figure 1. Typical molecules used in moletronics

1.2 Moletronics

Moletronics technology can be grouped into two main areas: Molecular junctions and molecular optoelectronics[3]. As its name suggests, molecular optoelectronics is associated with the absorbing and emission of photons, light energy. Molecular junctions encompasses the utilization of molecules into interconnects, interconnects, diodes, gates, transistors and more. The scope of this thesis only covers molecular junctions in the form of interconnects and gate switches.

A typical molecular junction system includes attaching a molecule via self assembly methods between two metal electrodes (usually gold) and then applying an electric field along the length of the molecule to generate current. The overall current flow occurs through two regimes, the metal electrode-molecule interface, and the molecule itself. When the electrode is first attached to the molecule, a mixing of allowable energy states will occur since the metal contains essentially a continuous spectrum of allowable energies while the molecule contains only discrete energy states. After coming to equilibrium, a single Fermi level will form, representative of the electrode-molecule interface as a single system.[3] In addition, the discontinuity of energy states at the interface leads to a deviation from ohmic behavior, where the current is proportional to the applied voltage. This discontinuity can also lead to the formation of a Schottky barrier, where the magnitude of its potential depends on the electronegativity

differences between the bonding atoms at the interface. In spite of all these complications, the conductance at the interface can be characterized theoretically through the Landauer theory.[4] This theoretical approach utilizes the product of Green's Function and the mixing matrix, which combines the Hamiltonian matrices of the molecule and electrode. All of the terminology will be explained more in detail in the ab initio section.

Due to the lack of a discontinuous interface, charge transport through the molecule itself is relatively more straightforward. Depending on the length and the complexity of the molecule, conduction can occur through five possible mechanisms: resonant and nonresonant coherent electron tunneling, incoherent tunneling (ohmic behavior), quasiparticle diffusion, and gated electron transfer.[5] Incoherent tunneling is mostly observed in metal interconnects, which follow ohmic behavior. Nonresonant coherent electron tunneling involves elastic transfer of electrons throughout the molecule, which means that a lot of the kinetic energy of the electron is transferred to the molecule. This transport mechanism leads to an exponential decay in conductivity as the length increases. This mode of transportation is usually observed in linear aliphatic molecules such as thiol-terminated alkanes attached between two metal electrodes.[6] Resonant coherent electron tunneling also involves elastic transfer of electrons, except that the conductance is affected by the electrons scattering from the collisions with the molecule. In this case the conductivity is independent of molecule length but depends on the degree of delocalization. Chemical compounds such as carbon nanotubes are a perfect example of this type of charge transfer, as the branched assortment of benzene rings provides for a high degree of delocalization. Quasiparticle diffusion involves extra charges resulting from degenerate electronic ground states. This type of charge transfer usually occurs only in nonrigid polymers. Gated electron transfer involves different electron transfer rates depending on the conformation of the molecule. By applying an electric field to the system, isomers exhibiting notably different conductivities may form, depending on the strength of the field. However, electron transport in the molecule is not necessarily limited to just one transfer mechanism. Depending on the molecule's

structure, many possibilities for charge transfer can occur. One example is a donor-bridge-acceptor (DBA) molecule, where the electron donor and acceptor sites are on the molecule itself, compared to the electrodes for a linear aliphatic thiolalkane. In this case two possibilities for electron transport can occur: the electrons may transfer from the acceptor state to the donor state before the electrode through coherent means, or an electron can jump from the donor to the acceptor incoherently, which is ohmic behavior.[4] The fact that the electric characteristics of the molecule can be altered through simple chemical modification illustrate the diversity and degree of control associated with moletronics systems.

1.3 Ab Initio Methods

Computational chemistry has always been a significant factor in advancing the field of moletronics. It consists of three areas: ab initio methods, semi-empirical methods, and molecular mechanics. Molecular mechanics utilizes classical physics to solve large systems of molecules and is considered the least accurate due to the fact that no electron behavior is factored in. Semi-empirical methods are more accurate because utilization of quantum physics to account for some of the electron behavior, but its scope is still limited since it relies on extensive approximations and empirical parameters. Ab initio methods are based purely on quantum physics and use no approximations from classical physics to describe the electronic structure of the molecule very accurately. The drawback of using ab initio methods is that the computations are extremely taxing and so is limited to much smaller systems such as individual molecules. However, ab initio methods complements moletronics perfectly since it gives a lot of information on the electronic structure without having to actually synthesize the molecule experimentally. This can either help guide researchers in synthesizing or modifying molecules to exhibit certain electric characteristics or even help to explain experimental results.

The fundamental idea behind ab initio calculations is to solve Schrodinger's equation with a set of mathematical functions called a "basis set". Schrodinger's

equation is used to apply the Hamiltonian operator to the wavefunction of the molecule to predict its behavior in a given space and time. Additionally, the quantized state energies are calculated. The time independent Schrodinger equation for three dimensions is defined mathematically as:[7]

$$\hat{\mathrm{H}}_{mol}\Psi_{mol}(x,y,z) = E\Psi_{mol}(x,y,z) \tag{1}$$

The $\hat{\mathrm{H}}_{mol}$ represents the Hamiltonian of the molecule while Ψ_{mol} represents the wavefunction of the molecule. The Hamiltonian of the molecule is defined as the sum of all the molecule's particles kinetic and potential energies added together. It is represented by a differential equation:[8]

$$\hat{\mathrm{H}}_{mol} = \hat{\mathrm{T}}_{mol} + \hat{V}_{mol} \tag{2}$$

where $\hat{\mathrm{T}}_{mol}$ is the kinetic energy summed over all the particles in the molecule:[8]

$$\hat{\mathrm{T}}_{mol} = \frac{-\hbar^2}{2m}\sum\frac{1}{m_i}\left(\frac{\partial^2}{\partial x_i^2}+\frac{\partial^2}{\partial y_i^2}+\frac{\partial^2}{\partial z_i^2}\right) \tag{3}$$

and $\hat{V}_{mol}$ is the potential energy resulting from the Coulomb interaction between electron-nucleus attraction, nucleus-nucleus repulsion and electron-electron repulsion:[8]

$$\hat{V}_{mol} = \frac{1}{4\pi\varepsilon_0}\sum_j\sum_{k<j}\frac{q_j q_k}{\left|r_k - r_j\right|} \tag{4}$$

'm' is the mass of the particle, $\hbar$ is Planck's constant, ε_0 is the permittivity of free space, $\left|r_k - r_j\right|$ is the distance between charges q_j and q_k. The time-dependent Schrodinger equation is seldom used because ab initio calculations typically involve only the spatial behavior of the wavefunction.

As mentioned previously, the Hamiltonian operator $\hat{\mathrm{H}}_{mol}$ in (1) acts on the molecular wavefunction $\Psi_{mol}(t)$ to yield the molecular wavefunction, which is calculated by solving the Schrodinger equation. However, for systems containing more than one electron the molecular wavefunction cannot be solved explicitly and must be determined through numerical methods. It is these types of computer intensive calculations that

characterize the ab initio method; software such as Gaussian utilize different basis sets to solve for the wavefunction through self-consistent calculations until convergence is reached. Due to the complex nature of the calculations for systems with more than one electron, some mathematical approximations must be made, such as the single-particle approximation, linear combinations of atomic orbitals (LCAO), and the Born Oppenheimer approximation.[8] The single-particle approximation uses the product of single-electron wavefunctions to emulate the total wavefunction of a molecule. The Born-Oppenheimer approximation states that since electrons have a much higher velocity than the heavier nuclei, the nuclei can be thought of as being stationary relative to the electrons. Neglecting the nuclei velocity translates to a zero for the nuclear kinetic energy. The LCAO theory states that the molecular orbitals can be represented as the sum of basis functions that are based on hydrogenic wavefunctions. Its general form is:[8]

$$\phi_i(r) = \sum_{\mu=i}^{N} c_{\mu i}\chi_\mu(r) \tag{5}$$

where $\phi_i(r)$ are the individual molecular orbitals, $\chi_\mu(r)$ are the basis functions based on hydrogenic wavefunctions and $c_{\mu i}$ are the expansion coefficients. A consequence of using this approximation is that the hydrogenic wavefunctions are derived from Slater-type orbitals, which is an exponential function. For example, for s-states is of the form:[8]

$$\chi_{STO}(r) \approx Ce^{-\alpha r} \tag{6}$$

Mathematically, exponential functions yield complicate calculations thus they are preferably approximated by linear combinations of Gaussian functions:[8]

$$\chi_{STO}(r) \approx \sum_{\nu} d_{\mu\nu} e^{-\alpha_\nu r^2} \tag{7}$$

where $d_{\mu\nu}$ and α_ν are fitted parameters.

Although the single-particle approximation simplifies calculations notably, it does not account for electron-electron interaction leading to systematic errors for systems calculated with the Hartree-Fock method. Additional modifications have been implemented alongside with the previous approximations to account for electron correlation. There are three methods, among several, that account for electron

correlation: Configuration-Interaction, Moller-Plesset perturbation, and Density Functional Theory. The only method of concern in this work is the Density Functional Theory (DFT) and will be the only one discussed. The DFT method expands the energy as a functional of the electron density. The energy is now represented as

$$E = E^T + E^V + E^J + E^{XC} \quad (8)$$

where 'E^T' stands for Kinetic energy, 'E^V' is the Potential energy resulting from interactions between nuclei-nuclei and nuclei-electrons, E^J is the energy from electron-electron interactions and E^{XC} is the electron correlation term that accounts for electron spin and the energy from the motion of individual electrons. Now, every term except for nuclei-nuclei interaction portion depends on the electron density and must be modified from equations (3) and (4) to account for this new dependence. The modified forms of these equations are referred to as the Kohn-Sham equations. The new set of equations must be solved self-consistently, where an initial "guess" density is used to calculate a new potential, which is then used in the Kohn-Sham set of equations to generate a new electronic density.[9] This cycle is repeated until the differences in the electronic densities are minimized. Different sets of DFT methods involve pairing different exchange functional with different correlation functionals to give the best results for a particular system. A renowned DFT method that can be used for almost any system is the B3PW91, which combines Becke's three-parameter hybrid functional with the gradient – corrected correlation functionals of Perdew and Wang.[10-13]

1.4 Motivation

The purpose of this study is to investigate the electron transport behavior of thiol-terminated Oligoanilines with ab initio methods. The molecule demonstrated NDR properties through a two-state switching mechanism that makes it a potential candidate as a molecular transistor. The bistable switching behavior was observed and recorded experimentally, but the reasons and understanding for it were still unclear. Ab initio methods utilizing the density functional theorem in conjunction with Green's function help to explain some of the observed phenomena of the molecule through

conformational analyses and current-voltage plots. By understanding the traits that lead to this behavior, current Oligoaniline systems can be further modified to enhance the observed properties, or new systems containing the desirable can be created with relative simplicity and ease.

1.5 Outline

Chapter II includes a short compilation of the literature that inspired this study. It covers the first moletronics system that exhibited NDR behavior to the most recent experimental study of thiol-substituted Oligoaniline molecular junctions. The switching characteristics are illustrated in an I-V curve and an inelastic tunneling spectroscopy plot, demonstrating the two distinct conducting states. An Arrhenius plot shows that conductance is independent of temperature and leads to the reasoning that the electron transport mechanism for the Oligoaniline is most likely coherent tunneling.

Chapter III outlines the methodology behind the conformational optimization and I-V calculations. All of the conformation analyses were done with Gaussian 03 in conjunction with GaussView while the I-V calculations were computed with a UNIX program called MoCAF.

Chapter IV focuses on the geometrical analysis of each different conformation and provides a comparison on the relevant attributes of each molecule. The bond lengths, angles and dihedral angles of each conformation are presented in tables along with the molecular orbital diagrams.

Chapter V focuses on the electrical characterization for the different conformations. This includes a comparison of the I-V plots for each different conformation, and also for the charged states of each conformation.

Finally, Chapter VI summarizes all of the results and provides the appropriate conclusions.

CHAPTER II

BACKGROUND INFORMATION*

With the use of self-assembly techniques and innovative fabrication techniques, the synthesis of various moletronics systems with metal electrode attachments have been made possible. Despite the fact that certain molecules exhibit a good level of conductivity, the overall goal of moletronics is to take this concept farther and construct electronic devices from the molecules. In order to do so, the molecule must exhibit properties that emulate the functions of common electronic components such as transistors, diodes and rectifiers. These characteristics include negative differential resistance (NDR), switching, and rectification. Rectification is the process of converting an input of AC current into an output of DC current and was demonstrated in an organic molecule by Aviram and Ratner[2]. NDR is the phenomena where the current actually decreases when the voltage is increased. A well known molecule that demonstrated this property was the nitro benzenethiolate molecule synthesized by M. Reed, J. Tour, J. Chen, and A. Rawlett.[14]

---

*Parts of the figures reported in this chapter are reprinted with permission from

"Reversible Bistable Switching in Nanoscale Thiol-Substituted Oligoaniline Molecular Junctions" by L. Cai, M.A. Cabassi, H. Yoon, O.M. Cabarcos, C.L. McGuiness, A.K. Flatt, D.L. Allara, J.M. Tour, T.S. Mayer, 2005. *Nano Letters*, 5, 2365-2372. Copyright 2005 by American Chemical Society.

"Room Temperature Negative Differential Resistance in Nanoscale Molecular Junctions" by J. Chen, W. Wang, M.A. Reed, 2000. *Applied Physics Letters*, 77, 1224-1226. Copyright 2000 by American Institute of Physics.

"Large On-Off Ratios and Negative Differential Resistance in a Molecular Electronic Device" by J. Chen, M.A. Reed, A.M. Rawlett, J.M. Tour, 1999. *Science*, 286, 1550-1552. Copyright 1999 by AAAS.

Switching is the process of having two states, usually an “ON” state and “OFF” state depending on the voltage applied. For an electronic component such as a transistor, these two states refer to whether current is flowing through the device or not.

Recently, the need to find a replacement for standard CMOS technology has lead to increased effort in researching molecules with potential as gate devices. The ultimate goal is to incorporate the molecular device into a 3-terminal system, which includes the source, drain and the gate, which is the molecule. When a gate voltage is supplied, an electric field surrounds the molecule.Depending on the strength of the electric field, the molecule should exhibit two states where the current flow is increased (high conductivity) or the current flow is impeded (low conductivity). However, due to the Angstrom-scale dimensions of the molecule, a method of fabricating a suitable gate terminal that acts only on the molecule is extremely difficult. Therefore, in order for a molecule to be used as a gate device with only two terminals, NDR and switching characteristics are essential. Figure 2 shows a general schematic of a three terminal device.[15]

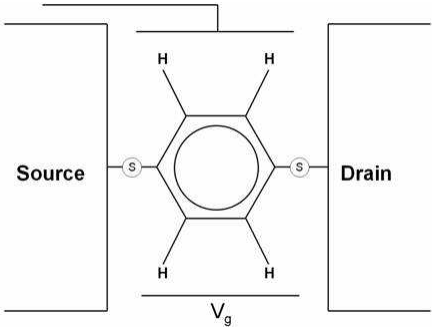

Figure 2. Three terminal molecular transistor

While desired, NDR was a trait observed in very few moletronics systems. Of the few, one of the more eminent molecules that exhibited NDR behavior is the 2’-amino-nitro-1-benzenethiolate molecule with gold electrode attachments synthesized by J. Chen, M.A. Reed, A.M. Rawlett and J.M. Tour[14], shown below in Figure 3.

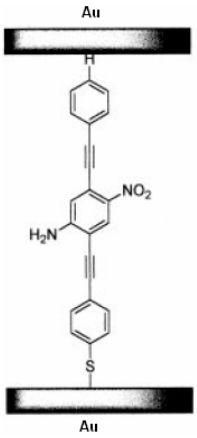

Figure 3. Nitro-benzenethiolate molecule exhibiting NDR[14]

The proposed explanation for the NDR effect was a two-step reduction process, which was later supported by ab initio calculations.[16] In the first step, as the voltage reaches a certain amount, the molecule acquires one electron which transforms it into a charged radical anion. In this state, the molecule essentially becomes a charge carrier and contributes to current flow. As the voltage is increased even further, the molecule undergoes the second reduction step process as it acquires another electron which pairs up with the first one to form an insulating dianion state and effectively blocks the current flow. The factor responsible for the NDR effects is the presence of the nitrate functional group NO_2, an electron withdrawing group, on the center benzene ring. It was found that the molecule shown in Fig. 3 lacking the nitrate group did not exhibit any NDR behavior, but the phenomenon was still present if only the amine group was missing. Temperature was also found to be a major factor in determining the behavior of the NDR curve, as temperature decreases the NDR curve turns much steeper and a proposed explanation for this result is that the decrease in temperature leads to decreased inelastic scattering of the electrons.[17] Figure 4 below presents I-V curves of the nitrate-only benzenethiolate molecules at different temperatures.

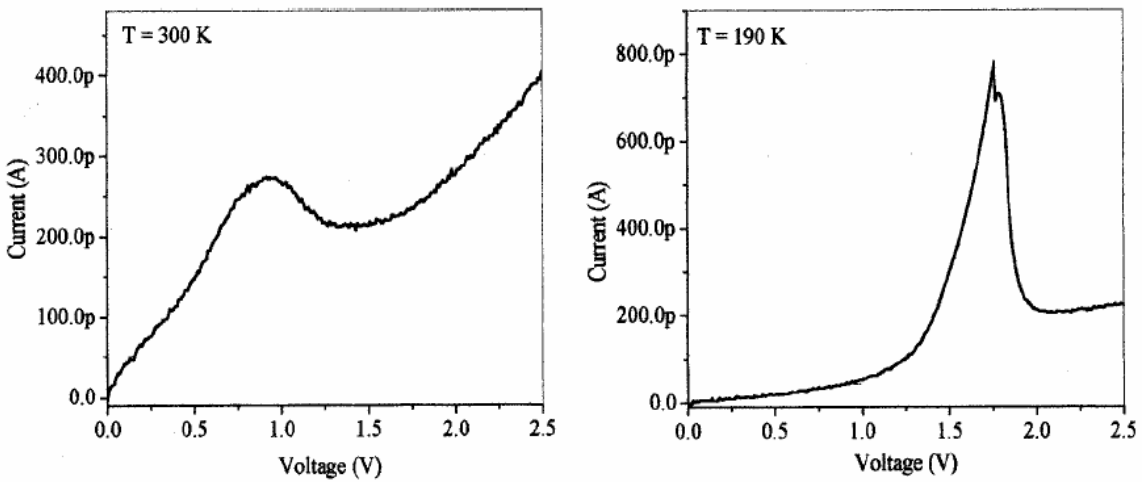

Figure 4. IV curves for nitrate-only benzenethiolates exhibiting NDR behavior at different temperatures[17]

Recently, another molecule demonstrating NDR behavior was synthesized by a collaborative group consisting of members from the department of EE, Chemistry and Materials Research from Penn State university, and Rice University.[18] This molecule, a thiol-substituted Oligoaniline shown below in Figure 5, was much different in the sense in that the bridging molecules did not include any conjugated bonds as the ones present in the molecule shown in Fig. 3.

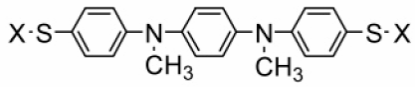

(**1a**, X = Ac or $COCH_3$; **1b**, X = H)

Figure 5. Thiol-terminated oligoaniline[18]

This molecule also demonstrates NDR behavior, similar to the molecule discussed previously, but in a more advantageous fashion as it leads directly to a switching phenomenon, demonstrated by the IV curve in Figure 6.

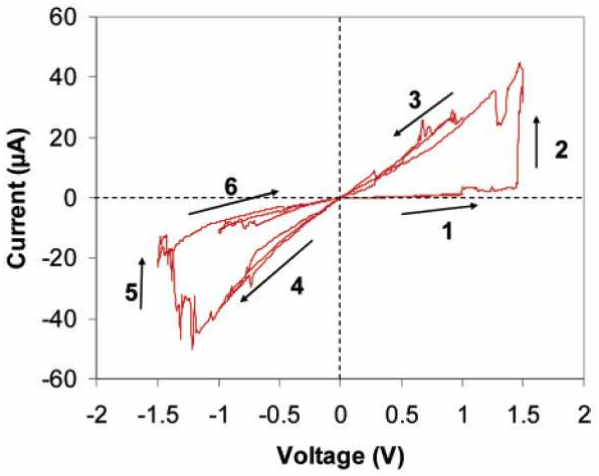

Figure 6. IV curve for an Pd-oligoaniline-Pd junction[18]

The NDR and switching behavior is can be illustrated in a cycle-like process shown in Figure 6, where a voltage increase from 0 to 2 Volts causes the current to jump at the threshold voltage at about 1.5 Volts. The jump represents the switching behavior, as the molecule remains at this relatively high current state until the bias voltage is reversed to a threshold voltage around -1.5 Volts, where it resumes its low current state. This is similar to a standard CMOS transistor, in that a threshold voltage must be reached before current can flow through the channel (ON state). Note that the molecular junction is still a two-terminal device, but has the characteristics of a three-terminal device. An inelastic electron tunneling spectroscopy analysis, shown below in Figure 7, revealed that there was a broadening in the C-N stretching peak at the high current state, which suggests a higher charge delocalization. The peak seen at 184 mV for the low conducting state is replaced by two peaks 178 and 190 mV, which further supports the reasoning that electron delocalization around the nitrogen atom and benzene carbons is increased upon the switching.

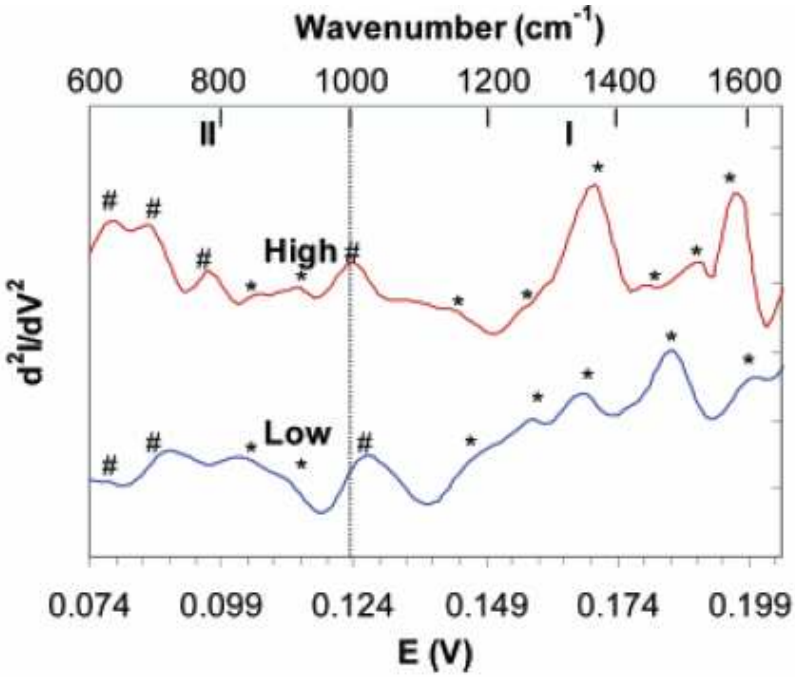

Figure 7. IETS for the high conducting state and low conducting state[18]

Unlike the previous benzenethiolate molecules, the Oligoaniline junctions did not exhibit a dependence on temperature. Arrhenius relationships involving the natural log of the current was plotted against the inverse temperature at different biases from 0.1 to 1.0 volts. The linear plots under different temperatures shown in Figure 8 signify that the I-V behavior at the junction is not a function of temperature and that coherent tunneling is most likely the dominant electron transport mechanism.

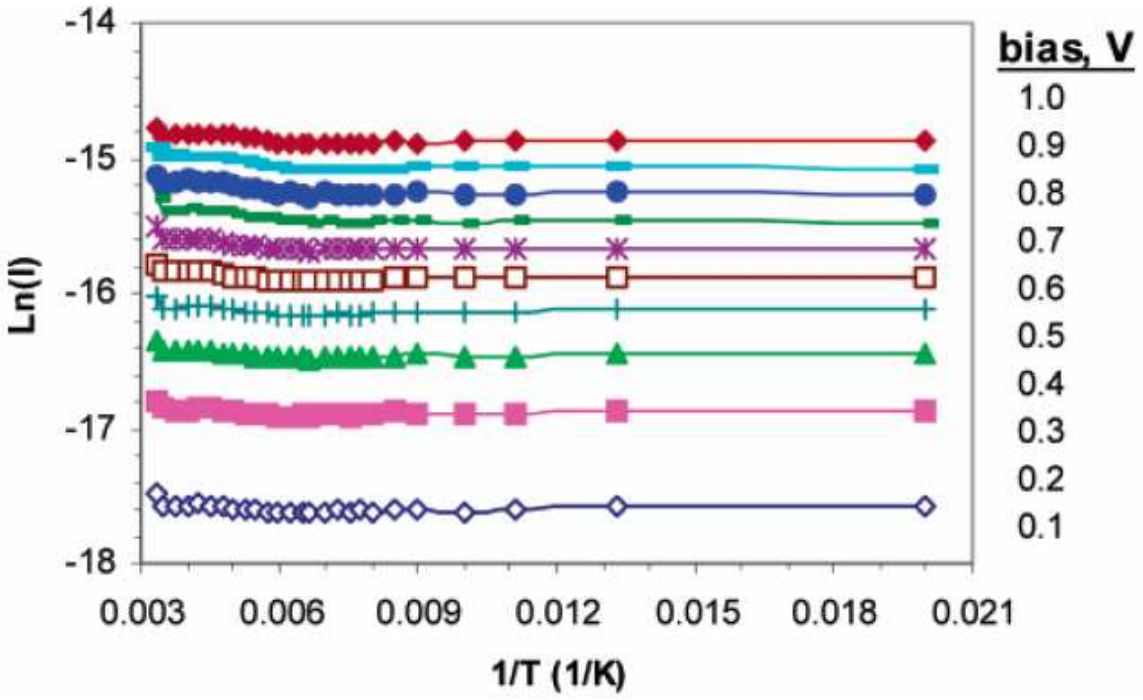

Figure 8. Arrhenius plot of the Pd-oligoaniline-Pd junction[18]

CHAPTER III

METHODOLOGY

3.1 Geometry Optimization

The ab initio calculations of the Oligoaniline molecule itself are performed at varying levels of theory as implemented in the GAUSSIAN 2003 program.[19] 5 different Oligoaniline systems were analyzed, as illustrated in the Figure 9.

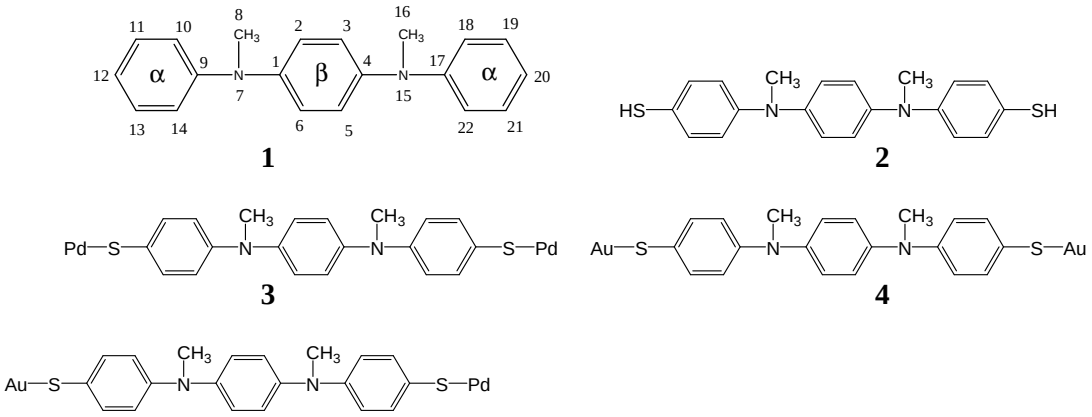

Figure 9. Oligoaniline systems analyzed

In order to find all the conformational isomers, the geometrical optimizations are run from several initial geometries for each system. All the conformational isomers are verified to be situated at the local minimum through the Hessian matrix (or frequency calculations). The frequency calculations represent the second derivative of the current with respect to voltage; a positive value denotes a region of the total energy plot where the concavity is faced upwards while a negative value represents a concavity region faced downwards. The results of the frequency calculation are also used to predict inelastic electron transport or the energy transfer from electron to the vibrational mode of the molecule. Their relative stabilities of the conformational isomers are compared on

the basis of their corresponding total energies. In order to save time and to maximize the possibilities for convergence, an optimization hierarchy was utilized as follows:

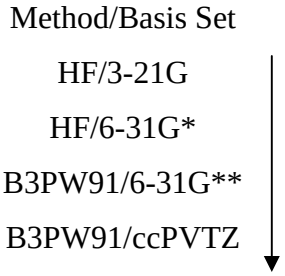

Each pair of method and basis set corresponds to a full geometrical optimization. The initial geometries were constructed with Gaussview and then were each slightly modified to ensure a fully varied assortment of starting conformations. If the initial geometry did not yield convergence or if any part of the molecule was broken up at the HF/3-21G level, the log file of the failed run was modified with respect to the error and resubmitted until convergence was reached. After the molecule has undergone the final optimization step, Gaussview is used to plot the molecular orbital diagrams using the wavefunction orbital data.

HF stands for the Hartree-Fock method used to solve for the molecular Hamiltonian. It was mentioned in the introduction, where it was described as a method to solve for the Schrodinger equation as given in equations (1) and (2). Unfortunately, it does not account for electron correlation which leads to systematic errors such as underestimated bond lengths.

The 3-21G Basis Set is a split-valence basis set first proposed by Binkley, Pople, and Hehre.[20] The split-valence method stresses importance on the valence electrons by performing a double-zeta calculation, which utilizes two Slater type orbitals. Since inner shell electrons aren't considered as important in split-valence calculations, they are represented by only a single Slater type orbital. The general format for split-valence basis sets is x-yzG, where each letter stands for the number of Gaussian type functions used to approximate a Slater type orbital. The '3' corresponds to 3 Gaussian functions being used to approximate the Slater type orbital electrons in the inner shell. The '2'

stands for the 2 Gaussian functions approximating the first Slater type orbital for the valence electrons. The '1' represents the 1 Gaussian function approximating the second Slater type orbital. The 'G' tells that the Slater type orbitals are being approximated with Gaussian type functions.

The 6-31G* is also a split-valence basis set,[21] following the same nomenclature as the 3-21 basis set. 6 Gaussian functions are used for the one Slater type orbital electrons in the inner shell, 3 Gaussian functions are used for the first Slater type orbital representing the valence shell, and 1 Gaussian function is used for the second Slater type orbital in the valence shell. The '*' states that polarization effects are now being taken into account. The polarization results from the charge distribution between atoms, which shouldn't be uniform as assumed previously, and leads to the mixing of the 's', 'p' and 'd' orbitals. One star accounts for polarization effects in the 'd' orbitals, and two stars account for polarization effects in the 'p' orbitals. Therefore, the 6-31G** basis set utilizes the same number of Gaussian functions, but accounts for additional polarization effects in the 'p' and 'd' orbitals.[22] As expected, the 6-31G** basis set requires more computing time as it needs to account for additional atomic interactions now.

B3PW91 is the modified density functional theorem method utilizing Becke's three-parameter hybrid functional with the gradient –corrected correlation functionals of Perdew,. Typical DFT calculations are based on Kohn-Sham equations utilizing the local spin-density approximation for the electron exchange-correlation energy:[10-11]

$$E_{XC}^{LDA} = -C_X \sum_{\sigma} \int \rho_{\sigma}^{4/3} d^3 r \qquad (9)$$

σ represents the different spin states "up" or "down", and the integrand is the volume exchange-correlation energy density as a function of the uniform electron gas with different spin densities ρ_α and ρ_β. As expected, the assumption that the electron gas density is uniform falls short for certain systems, namely individual molecules. Axel Becke addresses nonuniformity through a 3 parameter gradient corrected exchange-energy functional in the form of [12-13]

$$E_X^{SE} = E_{XC}^{LDA} - \beta \sum_{\sigma} \int \rho_{\sigma}^{4/3} \frac{x_{\sigma}^2}{(1+\gamma x_{\sigma}^2)} d^3 r \qquad (10)$$

β and γ are semiempirical parameters and x_σ is a dimensionless ratio of the gradient of the spin density and the spin density to the 4/3 power. The main factor that distinguishes the Becke's methods from standard DFT methods is the correct asymptotic form for points infinitely far from the system:[10-11]

$$E_{XC} = -\frac{1}{2} \int \frac{\rho}{r} d^3 r \qquad (11)$$

Perdew and Wang incorporate an additional correlation correction to Becke's 3 parameter electron exchange correction to form the modified hybrid DFT method. The PW91 electron correlation correction utilizes a new parameterization system that consists of two parts. Depending on whether the correlation energy lies within the random- phase approximation, different parameters are utilized for the same analytical correction equation[12-13].

The ccPVTZ is a computation intensive basis set that involves the use of triply split (Triple Zeta, TZ), for the valence orbitals.[23] The 'cc-PV' is the abbreviation for 'correlation consistent polarized valence', which denotes that additional polarization functions has been added and may include d and even f functions for first row atoms. Although Gaussian functions are still used to approximate the Slater type orbitals, this basis set is much more accurate due to the fact that correlation and polarization effects from multiple shells are taken into effect along with the triple zeta calculations.

3.2 Metal Contacts

Metal contacts are implemented as a single Au or Pd atom or as a set of trimer metal atoms at the sulfur terminated ends of the molecule. For the case of one single metal contact at each end, the geometry of the entire organometallic system was optimized with the method and basis pair B3PW91/LANL2DZ. For the case of the trimer metal atoms, only the geometry of timer metal contacts and a benzene ring with a

sulfur attachment was optimized due to the difficulty of convergence issues for transition metals. The details of this optimization can be found in Chapter IV.

The LANL2DZ basis set is practically required for any molecular system containing elements beyond Xe in the period table. Therefore, for systems involving gold atoms, the LANL2DZ basis set is used in place of the cc-pVTZ. The accuracy tradeoff is not too significant, as the LANL2DZ utilizes a double zeta calculation (DZ). Although palladium is included in the previous basis sets, the lanl2dz basis set is still used in order to compare the different Oligoaniline systems on equal grounds. What sets the LANL2DZ basis set apart from the previous basis sets is that it uses ab initio effective core potentials (ECP) to perform valence-electron calculations. By using ECP, relativistic effects in the inner atomic core for heavy atoms (Atomic # >54) can be accounted for. Transition metals have an unusual characteristic where sometimes the outermost core orbitals have the same size as the valence orbitals, leading to the ambiguity of which electrons should be considered towards the electron core potential. The Gaussian functions used for the LANL2DZ basis set is:[24]

$$\sum d_k r^{n_k} \exp\left[-\xi_k r^2\right] \qquad (12)$$

where n_k is a parameter that can be 0,1 or 2. ξ_k is the electron core potential, where specific values for various transitions metals are provided in the paper[24].

3.3 Geometry Optimization under a Bias

In order to find out whether the Oligoaniline molecule exhibits switching behavior, each of the fully optimized conformation with single metal contacts were subjected to an electric field along the Z-axis. The fields employed were (–30, -25, -20, -15, 15, 20, 25, 30) x 10^{-4} atomic units. The range was chosen in order to match the voltage range applied in the experiment as mentioned in Chapter II. Switching was demonstrated experimentally at approximately under 1.5 and -1.5 Volts; -30 and 30 a.u. corresponds to approximately $\pm$ 2.4 Volts. Each conformation then underwent another geometry optimization under the B3PW91/LANL2DZ method and basis set.

3.4 Charged States

As mentioned previously in the introduction, electron transport in the molecule is not necessarily limited to just one transfer mechanism. Section 3.1 deals with the possibility that gated electron transfer will be the dominant electron transport mechanism, which involves different electron transfer rates depending on the conformation of the molecule. However, by providing a -1 or +1 charge to the molecule, the possibility that the transfer scheme may also consist of a hopping or tunneling mechanism will be tested. The prospect that a charged state may contribute to electron transport was inspired by the nitro benzenethioloate molecule[14] where the NDR behavior was attributed to a -1 and -2 state of the molecule. The charged state analysis will only be performed on the optimized geometries of the organometallic systems with 1 metal contact atom at each end due to convergence issues. The jobs will be run with a single point calculation (no geometry optimization) to account for only electron hopping and/or tunneling effects.

3.5 DOS of Metal Electrodes

The Density of States (DOS) of the Pd and Au contact metals are required in order to compute the Green's Functional, theorem, as outlined in section 3.6. Crystal '03 was selected to generate the DOS of the metal contacts used in Green's function as it provides a highly detailed DFT analysis with periodic boundary conditions on the electronic structure of bulk crystal materials at the atomistic level. Similar to Gaussian '03, Crystal utilizes Gaussian Type functions to approximate the Slater orbitals describing the crystal wavefunction. The electron density of an arbitrary electron system for a crystal is given by:[25]

$$\rho(r) = \int dk \sum_{i}^{OccupiedBands} \left|\varphi_{ki}(r)\right|^2 \theta(\varepsilon_F - \varepsilon_i(k)) \qquad (13)$$

where θ is the Heaviside step function, ε_i(k) is the eigenvalue of the ith crystal orbital, and ε_F is the Fermi energy of the metal. Besides the different expression for the

electron density term, the wavefunctions for the metal are still calculated in the same manner as the molecule's.

3.6 The DFT-GF Approach

The Green's function (GF) and density functional theory (DFT) are used to study the electrical characteristics of the bimetallic Oligoaniline junction, $[X_{bulk}\ X_n]$-[S-1-S]-$[Y_n Y_{bulk}]$, n=1,3; X=Y=Au, Pd. This notation [26] indicates that the standalone molecule, [S-1-S], is extended to, say, Au_3-[S-1-S]-Pd_3 and, through the extending atoms, interfaced to a semi-infinite bulk of gold at the left-end and of palladium at the right-end.

The procedure in calculating the I-V plots are as follows[26], and references therein. First, the geometry of the extended molecule is optimized using the Gaussian03 program[19] until a local energy minimum is obtained. As varying the initial geometry usually leads to several local minima, several optimized geometries may result at this stage. However, following the optimization hierarchy proposed previously, the number of valid conformations is significantly reduced to yield the most likely geometries. Second, a frequency calculation is performed on each optimized geometry to guarantee the stability of the extended molecule, that the total energy is at the minimum. Third, the Hamiltonian and overlap matrices of the extended molecule in an electric field are computed for each applied bias electric field at which the current is going to be calculated. Thus, every point of the *I-V* curve corresponds to a full ab initio calculation. Fourth, the DOS for the bulk materials is obtained using the Crystal03 program.[27] Fifth, through a Green's function transport scheme explained below, the Hamiltonian and overlap matrices obtained in step three are combined with the bulk DOS's obtained in step four to yield the DOS, electron transmission probabilities and *I-V* characteristics of the molecule.

In this procedure, the self-consistent treatment given to the influence of the applied bias electric field on the extended molecule ensures that the chemistry of the molecule is not lost throughout the calculations. The coupling between the metal

electrodes, Au and Pd, and the molecule can be represented by the mixing matrix as previously described in the introduction:

$$\sum_i = H_{M_i} g_i H_{iM} \tag{14}$$

The 'H' matrices represent the complex molecular Hamiltonians while 'g_i' is the complex Green function. This "mixing" matrix must be accounted for in the molecular Hamiltonian due to the electrode effects on the molecule. The modified molecular Hamiltonian is now represented as thus:

$$H_e = \begin{bmatrix} H_{11} & H_{1M} & H_{12} \\ H_{M1} & H_{MM} + \sum_1 + \sum_2 & H_{M2} \\ H_{21} & H_{2M} & H_{22} \end{bmatrix} \tag{15}$$

where '1' is the atoms of the electrode on one end, '2' is the atoms of the electrode on the other end, "M" is the molecule itself, and $\sum_i$ is the mixing term described in equation (9). However, this Hamiltonian matrix is not orthogonalized and must be transformed properly with the overlap matrix. After the transformation, the submatrix representing the molecule's Hamiltonian can be extracted to determine the Green's function using the Hamiltonian, H, and overlap, S, matrices.

$$G_M(E) = [ES_{MM} - H_{MM} - \Sigma_L(E) - \Sigma_R(E)]^{-1} \tag{16}$$

$$\Sigma_X(E) = (ES_{MX} - H_{MX}) g_X (ES_{XM} - H_{XM}), \quad X = L, R \tag{17}$$

where subscripts X and Y in H_{XY} and S_{XY} (submatrices of H and S, respectively) refer to the molecule (M), left contact (L) and right contact (R). The self-energy function $\sum_x$ accounts for the coupling between contact X and the standalone molecule; it contributes to the shifting and broadening of the molecular levels and depends on the Green's function of the contact, g_X, which is given by

$$g_X(E) = \pi i \times \begin{bmatrix} g_{X1} & \cdots & 0 \\ \vdots & \ddots & \vdots \\ 0 & \cdots & g_{XN_X} \end{bmatrix} \tag{18}$$

$$g_{XK}(E) = \begin{bmatrix} (Ds)_{XK}(E) & 0 & 0 & 0 \\ 0 & (Dp)_{XK}(E) & 0 & 0 \\ 0 & 0 & (Dd_{t_{2g}})_{XK}(E) & 0 \\ 0 & 0 & 0 & (Dd_{e_g})_{XK}(E) \end{bmatrix} \quad (19)$$

The diagonal entries of $g_{XK}(E)$, from top to bottom, give the *s*, *p*, $d_{t_{2g}}$, and d_{e_g} contributions to the DOS of contact-atom *K*. The number of contact-atoms is such that the size of $g_x(E)$ equals the number of columns (rows) of the coupling matrix H_{MK} (H_{KM}). The transmission function (T) and the DOS are obtained from the relations

$$T(E) = \text{Trace}\,(\Gamma_L(E) G_M(E) \Gamma_R(E) G_M^+(E)) \quad (20)$$

$$D(E) = \text{Trace}\,(i(G_M(E) - G_M^+(E))S), \quad (21)$$

where $\Gamma_X(E) = i(\sum_X(E) - \sum_X^+(E))$. $T(E)$ is the sum of the transmission probabilities from each of the channels available at energy *E*.

In consequence**,** the current $I(V)$ at a bias voltage *V* is obtained from

$$I(V) = \frac{2e}{h} \int_{-\infty}^{\infty} dE\, T(E)(f_L(E - eV/2) - f_R(E + eV/2)) \quad (22)$$

with f_x denoting the Fermi-Dirac function at contact *X*.

Gaussian ’03 and MoCAF were the software used to calculate the Green’s function, and the subsequent I-V curves. Gaussian ’03 was used to calculate the modified Hamiltonians from equation (10), while MoCAF was used to extract the transmission function, DOS and I-V curves from equations (15) through (17). The process is as follows, first a Fortran-created program called ‘ROTA’ is used to align the Oligoaniline system, metal contacts and molecule, along the Z-axis using the log files of the optimized geometries. Second, Gaussian ’03 is used to calculate the modified Hamiltonians with a tight SCF convergence criteria under electric fields ranging from (-50 to 50) * 10^{-4} atomic units along the Z-axis, in steps of 2. The Oligoaniline system,

metal contacts and molecule, was first rotated so that the overall orientation was along the Z-axis. Third, the data for the modified molecular Hamiltonian was extracted and then used as input for the MoCAF program, which yielded the results pertaining to equations (15)-(17). The input files used to run the Gaussian batch job and MoCAF are included in the appendix.

CHAPTER IV

MOLECULAR ANALYSIS

In this chapter, the molecular structures of the Oligoaniline obtained by use of *ab initio* calculation are reported. First, the characteristics and equilibrium distributions of the conformations of Oligoaniline **1** will be reported at each stage of the optimization hierarchy**.** For each of these conformations, details of its electronic structures including the molecular orbital energies and degree of localization will be given. Likewise, the same analysis will be performed on the molecular junction formed by attaching molecule **2** between two metallic electrodes made of Pd or Au. For the sake of practical solvability, the molecular junctions are approximated by the extended molecules **3**, **4**, and **5** as shown in scheme **1**, in which the electrodes are simulated by clusters of sizes of up to three Pd or Au atoms. This is a reasonable approximation since the values of a molecular junction's parameters converge well when about four metallic end atoms are used in the calculations. This is followed by a thorough analysis of their infrared and Raman spectra. The extended molecules are then coupled at each of their ends with semi-infinite metallic leads: the Pd-atom-end with the Pd-lead and the Au-atom-end with the Au-lead. Similar results pertaining to the charged states of Oligoaniline systems with anti-symmetric metal ends will also be reported here with subsequent discussions.

4.1 Oligoaniline Conformations

Four distinctive conformational isomers of the Oligoaniline **1** were found. They were named the Alpha, Beta, Gamma, and Delta conformation based on the orientation of the Methyl Groups with respect to the Benzene Ring, and the dihedral angle between the rings on the side and the ring in the middle. Their typical geometrical parameters in terms of bond lengths, bond angles and dihedral angles are listed in Table I, with Figure 10 serving as a label reference. Bond lengths represent the distance between the specified atoms and are listed in Angstroms, bond angles represent the angle created

using three specified atoms as points, and the dihedral angle is the angle between two planes that are defined by three atoms each.

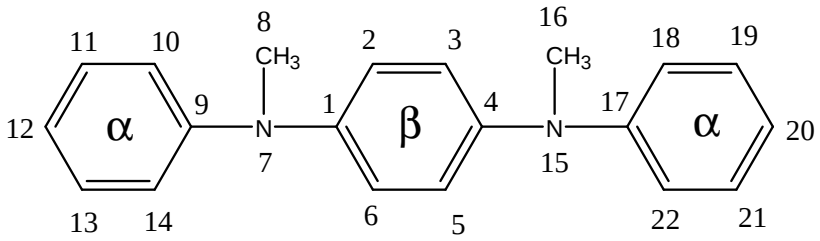

Figure 10. Typical oligoaniline molecule with labeled atoms

Table I. Dimensions of optimized oligoaniline isomers

	α	β	γ	δ
		Bond Length		
H14 – H6	2.824	2.818	2.765	2.782
H5-H22	2.823	2.818	2.873	2.781
C9-N7	1.399	1.416	1.418	1.398
C1-N7	1.419	1.405	1.398	1.418
C8-N7	1.452	1.452	1.452	1.452
C12-C20	12.431	12.430	11.645	11.370
		Bond Angle		
C9-N7-C8	118.9	117.4	117.5	118.9
C1-N7-C8	117.2	118.3	118.7	117.3
C9-N7-C1	121.0	120.7	121.3	121.2
C4-N15-C16	117.2	118.3	116.9	117.3
C17-N15-C16	118.9	117.4	119.2	118.9
C4-N15-C17	121.0	120.7	121.0	121.2
		Dihedral Angle		
C10-C9-N7-C8	-8.8	58.2	-58.9	-8.7
C14-C9-N7-C8	168.3	-120.8	119.7	168.5
C2-C1-N7-C8	-61.7	12.9	-10.3	-61.0
C6-C1-N7-C8	116.6	-163.9	166.7	117.2
C3-C4-N15-C16	61.7	-12.9	-67.3	-60.9
C5-C4-N15-C16	-116.6	164.0	110.6	117.3
C18-C17-N15-C16	8.8	-58.2	-5.3	-8.7
C22-C17-N15-C16	-168.3	120.8	172.2	168.4

From the table, it can be observed that the bond angles between the methyl carbons and adjoining nitrogen groups are quite similar, around 120 degrees. The value of 117 degrees could correspond to the uncertainties obtained from using the basis set or the fact that the hybridization of the nitrogen and carbon orbitals is a mix of sp^2 and sp^3. In an aniline monomer, due to the interaction between the nitrogen p-orbital and the phenyl pi-orbital, the nitrogen exhibits more sp^2 hybridization tendencies than sp^3 hybridization as expected in a lipid amine, resulting in the aniline molecule being almost coplanar. Both of the hydrogen atoms slightly stretched from the molecular plane in an angle of ~25.2^o as shown by our calculation at B3PW91/cc-pVTZ level of theory which is consistent with experimental results. When one of the hydrogen atoms is substituted by a second methyl group, the dihedral angle between the H-atom and the phenyl decrease to 19.8^o and that between the methyl C-atom and phenyl group is 14.5^o. When both of the amine H-atoms are substituted by a methyl and a phenyl, the dihedral angles between the methyl C-atom and phenyl groups are 10.2^o and 58.0^o, respectively (we shall call the methyl is in coplanar conformation if its dihedral angle with a phenyl ring at about 10^o and less). And the two phenyl rings can't be coplanar due to the strong repulsion between the neighboring phenyl H-atoms, a dihedral of 61.5^o is observed between these two phenyl groups. Although these substitutions don't cause conformational isomerization due to the symmetry of the molecule; they do cause conformational isomerization in Oligoaniline **1**. The atomic representation of the aniline, N-methyl substituted aniline and the N-methyl-N-phenyl aniline are presented below in Figure 11.

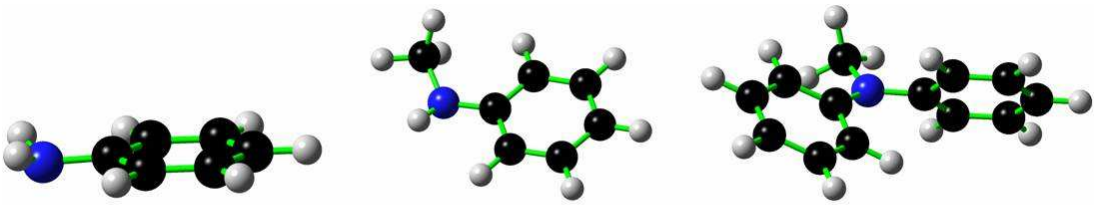

Figure 11. Conformation of aniline and its derivatives: (a) aniline, (b) N-methyl aniline and (c) N-methyl-N-phenyl aniline

In the Oligoaniline, the two phenyls bonded to the same nitrogen are in a dihedral angle of about 61^{o}, and the methyl is in coplanar conformation with either of the phenyls. Therefore, the naming of the conformations corresponds to whether the methyl groups are in coplanar conformation with the α phenyls or β phenyls, with each isomer being labeled the α or β conformation respectively. The isomer is called the γ conformation if one methyl is coplanar with the α phenyl and the other is coplanar β phenyl. The fourth conformation, δ, entails the methyl groups being coplanar with the α phenyls, but is dissimilar in that the α phenyls are not parallel and the dihedral angles are essentially reversed for one of the α phenyls, as can be seen from Table 1.

The calculations show that α conformation has the lowest conformational energy (0 meV) and the β conformation has the highest conformational energy (54 meV). The γ conformation is only slightly unstable (1 meV) than the α conformation. The conformation is than the α conformation. Using simple statistics mechanics calculation, it could be predicted that there are 33.3%, 4.0%, 31.4%, and 31.3% of the molecules in the α, β, γ, and δ conformation, respectively, when equilibrium is reached at room temperature (25 ^{o}C). Figures 12-15 show the four optimized conformations of the Oligoaniline molecule itself.

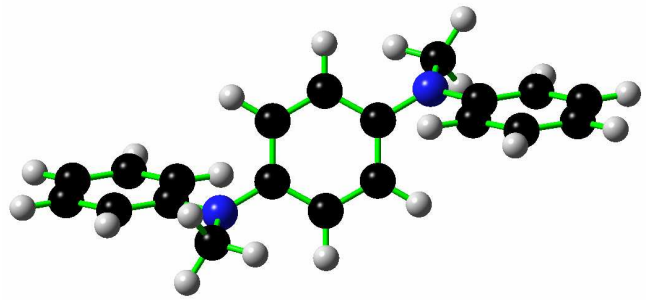

Figure 12. Alpha conformation

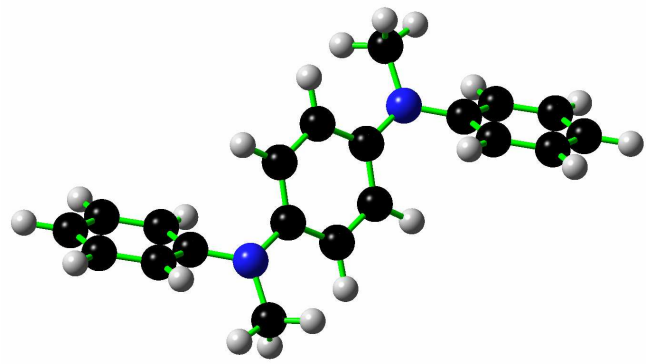

Figure 13. Beta conformation

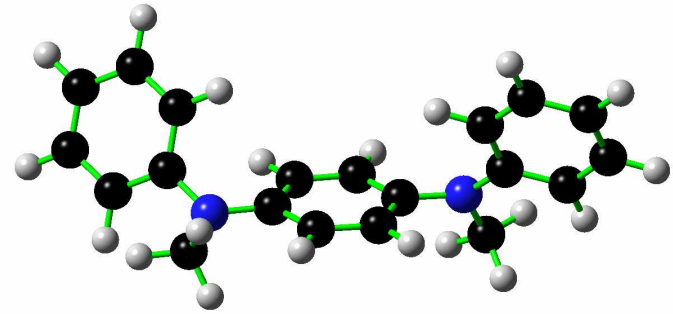

Figure 14. Gamma conformation

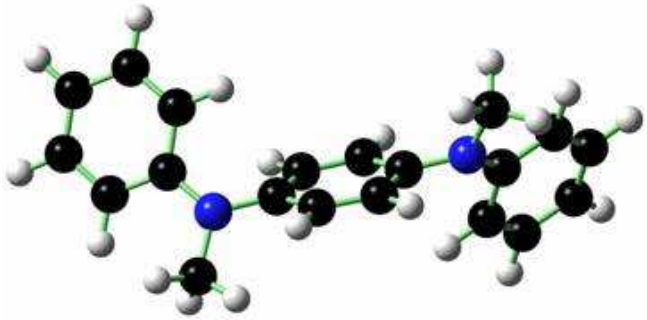

Figure 15. Delta conformation

From Figures 12 to 15, it can be seen that in terms of orientation of the alpha phenyl rings with respect to the beta phenyl ring, that the α and β conformations are similar while the conformations of δ and γ are more alike. The alpha phenyl rings in the α and β conformations are exactly parallel to each other, with the notable differences being the orientation of the methyl groups and the dissimilar dihedral angles between the alpha and beta phenyl rings. The δ and γ conformations are distinct from the α and β conformations in that the alpha phenyls are skewed with respect to each other, most likely in an effort to minimize the interaction between the phenyl hydrogens. However, upon observing Table 1, it can be seen that the dihedral angles for one of the δ conformation alpha rings is essentially the reverse for one of the α conformation alpha rings. In addition, the methyl groups for the δ conformation is oriented in the same manner as the α conformation, which is being aligned with the alpha phenyls. It is possible then, that perhaps the α conformation is more similar to the δ conformation than the β conformation in terms of electrical structure thought initially, and will be analyzed on a more detailed basis later. Although this similarity was observed for the α and δ conformations, no type of resemblance could be observed for the β and γ conformation. These similarities and differences leads to the notion that perhaps the conformations are mainly dependant only on the orientation of the methyl groups with respect to the phenyl rings.

Conformational differences have a large effect on the electron transport properties of molecular junctions, and conformational changes have been used to explain some of the bistable (or switching) molecular junctions. Since the conformational energy of the Oligoaniline is only a few meV, an external electric field induced by the bias voltage can easily cause conformational changes and affect its conformational distribution. Next the different molecular orbitals that arise from the different conformations will be looked at with more detail.

4.2 MO Analysis of Neutral Oligoaniline Systems

4.2-1 Standalone Oligoaniline Molecule

Figure 16 and 17 presents the molecular orbital diagrams for the four conformations of the standalone Oligoaniline molecule.

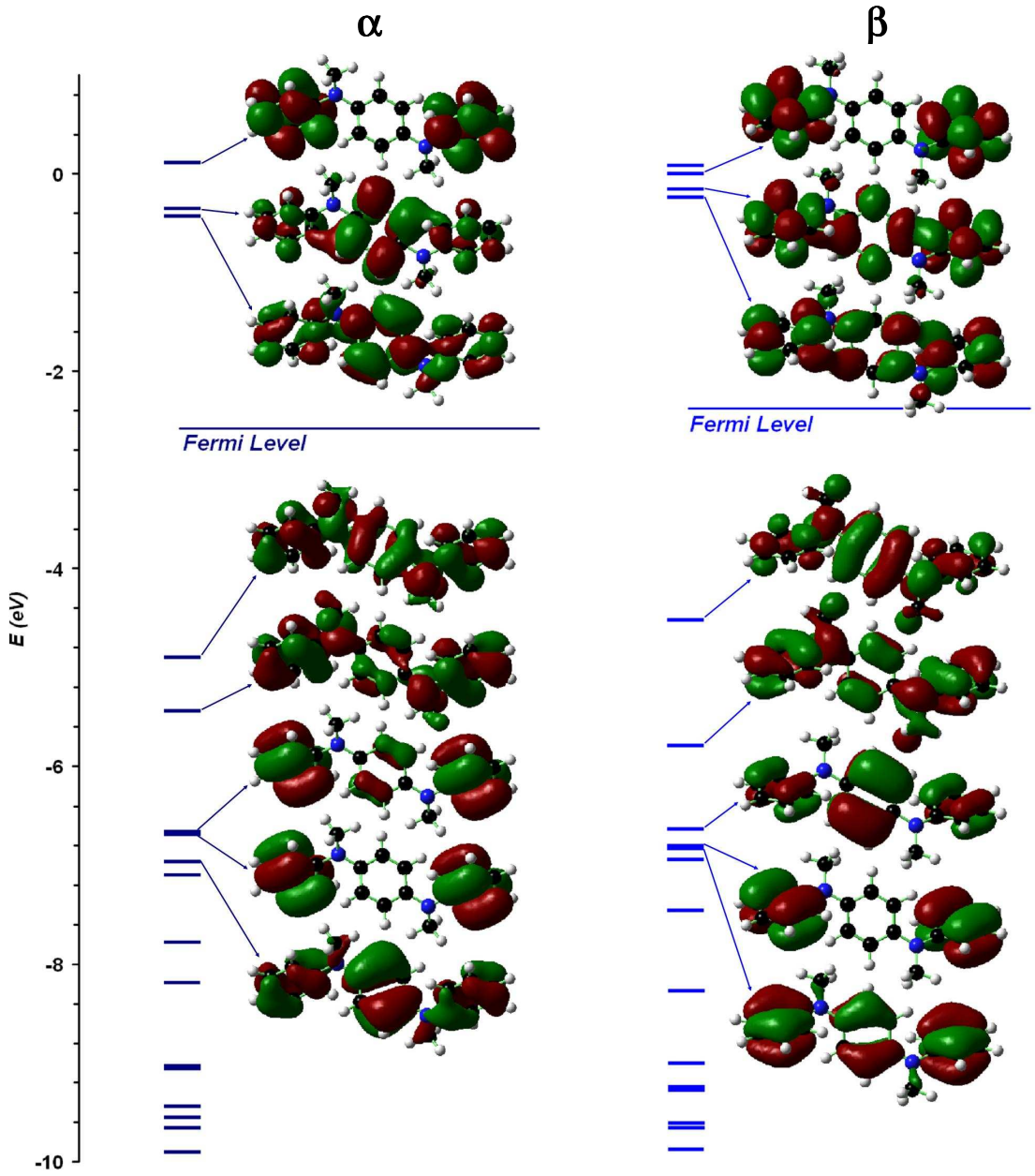

Figure 16. Molecular orbital diagram of the standalone α and β conformations

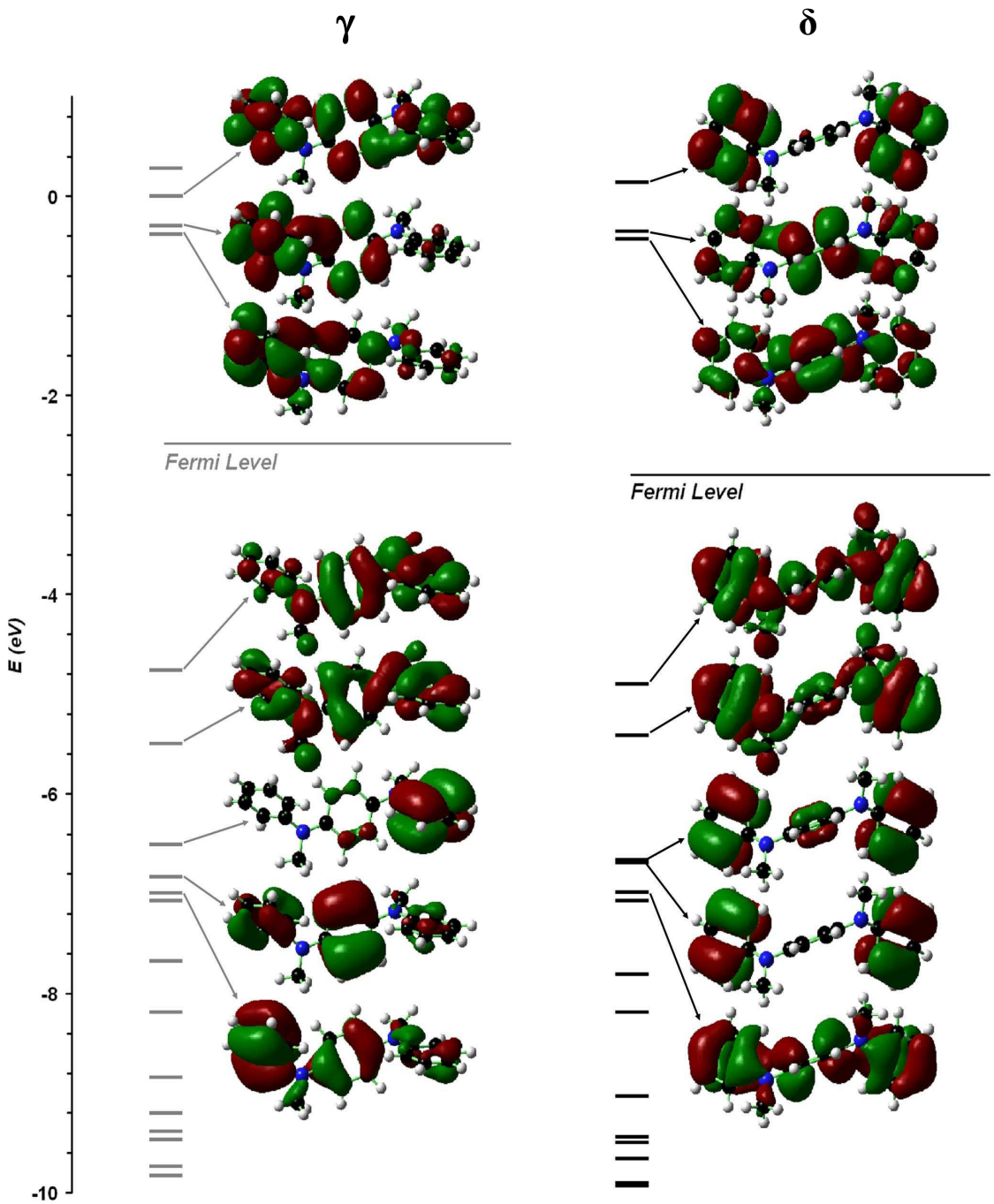

Figure 17. Molecular orbital diagram of the standalone γ and δ conformations

The Fermi level, or the ionization potential, is defined here as the energy situated between the HOMO and LUMO gap. The green and red solid regions represent molecular orbitals with completely opposite phases. The more the molecular orbitals are spread out, the more delocalized it is, signifying areas of electron flow, or conductivity. The lone molecular orbital above the Fermi level is the lowest unoccupied molecular orbital (LUMO) and can be seen that the molecule is quite delocalized equally for all conformations except for the γ conformation where the left portion is more delocalized than the right. The fact that the γ conformation is the only conformation that has each of the methyl groups oriented differently may be a factor, but nothing can be confirmed at this point, especially when the metal contacts aren't even implemented yet. The molecular orbital right under the Fermi level is the highest occupied molecular orbital and can be seen that the electron density is delocalized equally throughout the entire molecule for all conformations. The most relevant energy levels for conduction involve the HOMO and LUMO energy levels, but molecular orbitals at energy levels far away from the Fermi level can still contribute to the conductivity, just to a lesser extent. If the LUMO is delocalized, the molecule can serve as a electron transfer device and if the HOMO is delocalized, the molecule can serve as a hole transfer device. Since all of the conformations exhibit a high degree of delocalization, there is no insulating state for the molecule to convert to, which suggests that the coupling to metal electrodes brings about the insulating behavior, or one conformation exhibits a notable increase in conductivity over another one.

Going back to the possibility that the α conformation is more similar to the γ conformation, it was found that the Fermi level for both conformations were exactly the same at -2.67 eV with the same bandgap length, which further lends credence that the methyl groups are the deciding factor in determining the electronic structure for the molecule. The β and γ conformations had Fermi energies of -2.38 eV and -2.57 eV respectively, providing further support that the different energy levels are based on the orientation of the methyl groups. Next, the electronic structure of the sulfur terminated Oligoaniline molecule will be analyzed.

4.2-2 Thiol-Terminated Oligoaniline

Incorporating S-H thiol ends to the molecule does not change the original geometries, inducing only insignificant changes to the bond lengths, angles and dihedrals. The geometrical parameters are presented below in Table II:

Table II. Dimensions of thiol-terminated oligoaniline isomers

	α	β	γ	δ
		Bond Length		
S-C	1.784	1.805	1.775	1.785
S-H	1.348	1.348	1.348	1.348
S-C *	1.785	1.805	1.769	1.784
S-H *	1.348	1.348	1.348	1.348
		Bond Angle		
H-S-C	97.8	104.0	106.5	97.8
H-S-C *	97.8	104.0	104.9	97.7
		Dihedral Angle		
$H\text{-}S\text{-}C\text{-}C^{1}$	-80.0	-135.4	-151.2	-87.0
$H\text{-}S\text{-}C\text{-}C^{2}$	103.4	45.9	30.0	95.8
$H\text{-}S\text{-}C\text{-}C^{1*}$	95.5	-45.9	-141.2	-109.3
$H\text{-}S\text{-}C\text{-}C^{2*}$	-87.3	-135.4	39.96	74.2

'*' refers to a different alpha ring, subscript '1' and '2' refer to different Sulfur-Carbon dihedrals

Upon attaching the sulfurs, the Fermi Levels for the α, β, γ, and δ conformations are -3.22 eV, -2.93 eV, -2.93 eV, and -3.20 eV respectively. Interestingly, the Fermi energies for the β and γ conformations are now equal, but examination of the molecular orbitals illustrated in Figures 18 and 19 shows that the geometry of the orbitals near the HOMO and LUMO levels are quite dissimilar with notably different energy levels also. However, looking at the α and δ conformations, it can be seen that the orbital shapes are quite similar at comparable energy levels. The incorporation of the sulfur atoms does not affect the existing energy levels of the molecule but instead adds additional energy states, as can be seen in figures 16-17 and 18-19 and also shifts the Fermi Level downwards. Figures 18 and 19 present the molecular orbital diagrams for the four conformations of the thiol-terminated Oligoaniline molecule.

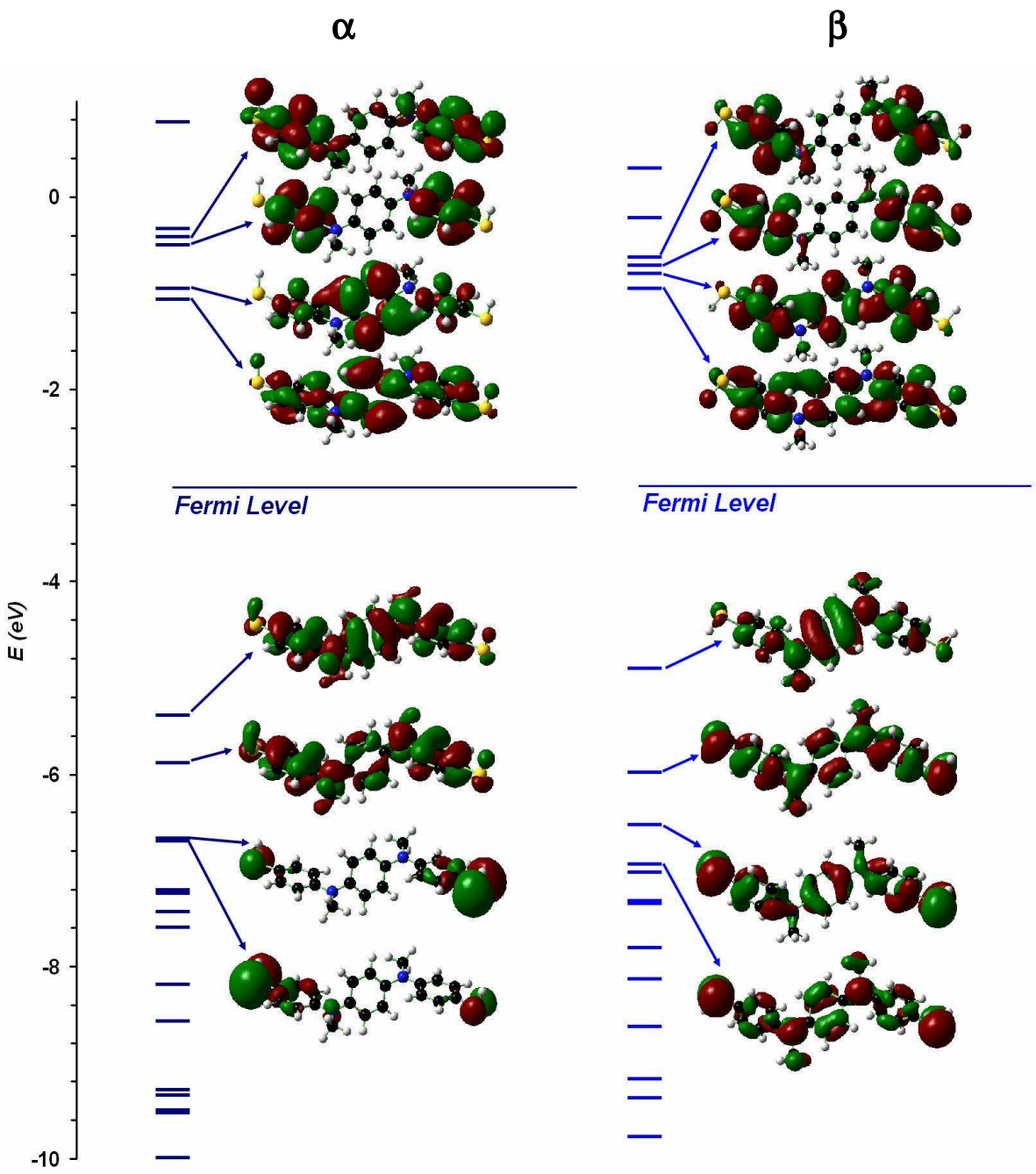

Figure 18. Molecular orbital diagram of the thiol-terminated α and β conformations

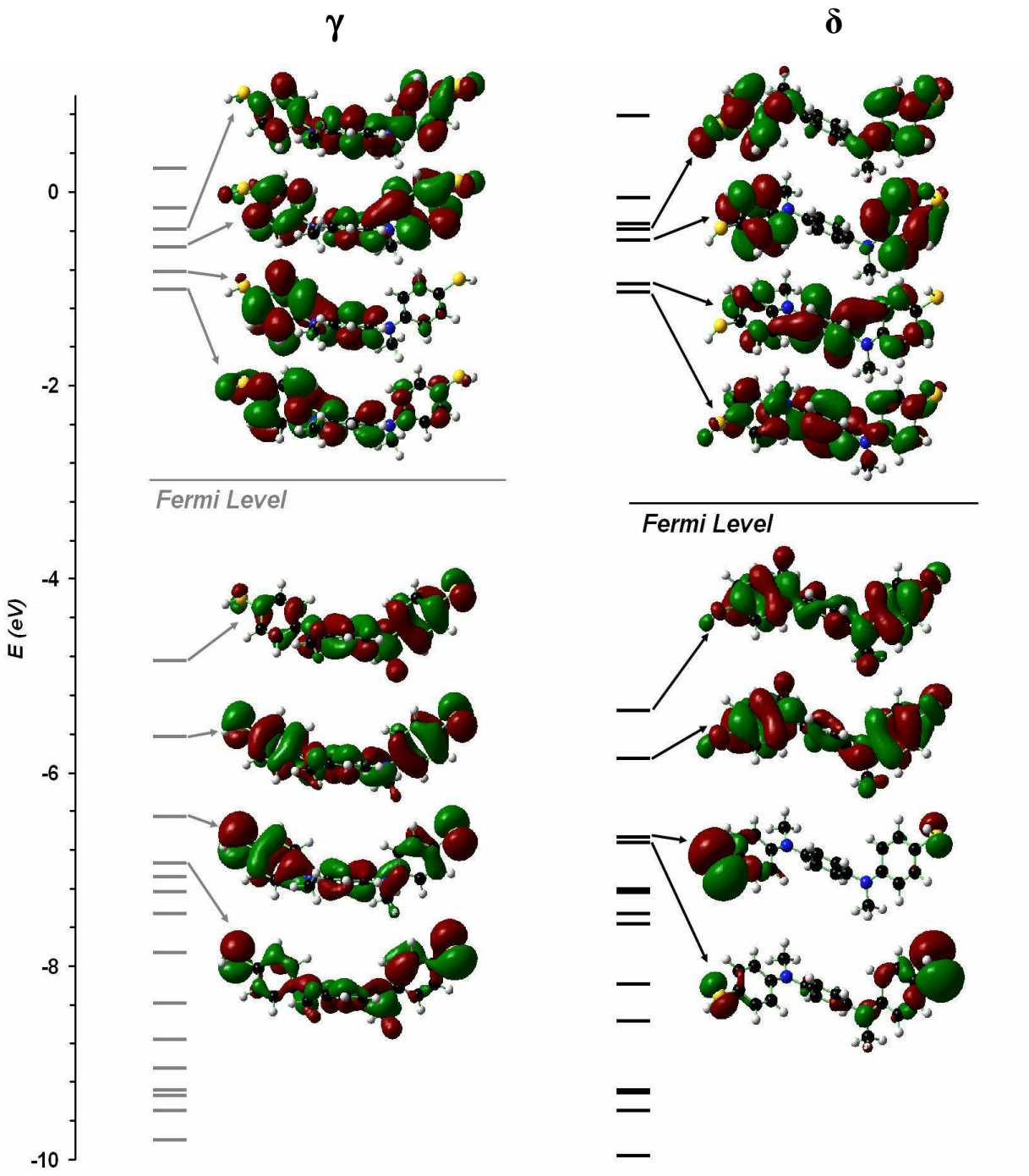

Figure 19. Molecular orbital diagram of the thiol-terminated γ and δ conformations

4.2-3 Oligoaniline with Single Atom Gold Contacts

Like the sulfur atom, incorporating one gold atom contact to the molecule does not change the original geometries, inducing only insignificant changes to the bond lengths, angles and dihedrals. The relevant dimensions of the single gold atom terminated molecule are presented below in Table III:

Table III. Dimensions of oligoaniline isomers with single Au contacts

	α	β	γ	δ
		Bond Length		
Au-S	2.384	2.383	2.386	2.384
Au-S *	2.385	2.383	2.381	2.385
		Bond Angle		
Au-S-C	104.1	103.3	103.5	103.7
Au-S-C *	103.6	103.3	103.1	103.8
		Dihedral Angle		
Au-S-C-C ^{1}	92.5	-91.9	91.4	91.5
Au-S-C-C ^{2}	-92.1	91.9	-91.8	-92.3
Au-S-C-C ^{1*}	-91.1	-92.0	90.7	-88.7
Au-S-C-C ^{2*}	92.4	-91.8	-93.5	94.9

'*' refers to a different alpha ring, subscript '1' and '2' refer to different Au-Sulfur dihedrals

While it is true that one gold atom doesn't represent bulk behavior for the electrode very well, the presence of only one atom still allows a good insight on the general electrical characteristics of the molecule. In addition, one gold atom allows for relatively easy optimization for the molecule geometry. Figures 20 and 21 below present the molecular orbital diagrams for the four conformations of the Oligoaniline molecule attached to single gold atom contacts at the ends.

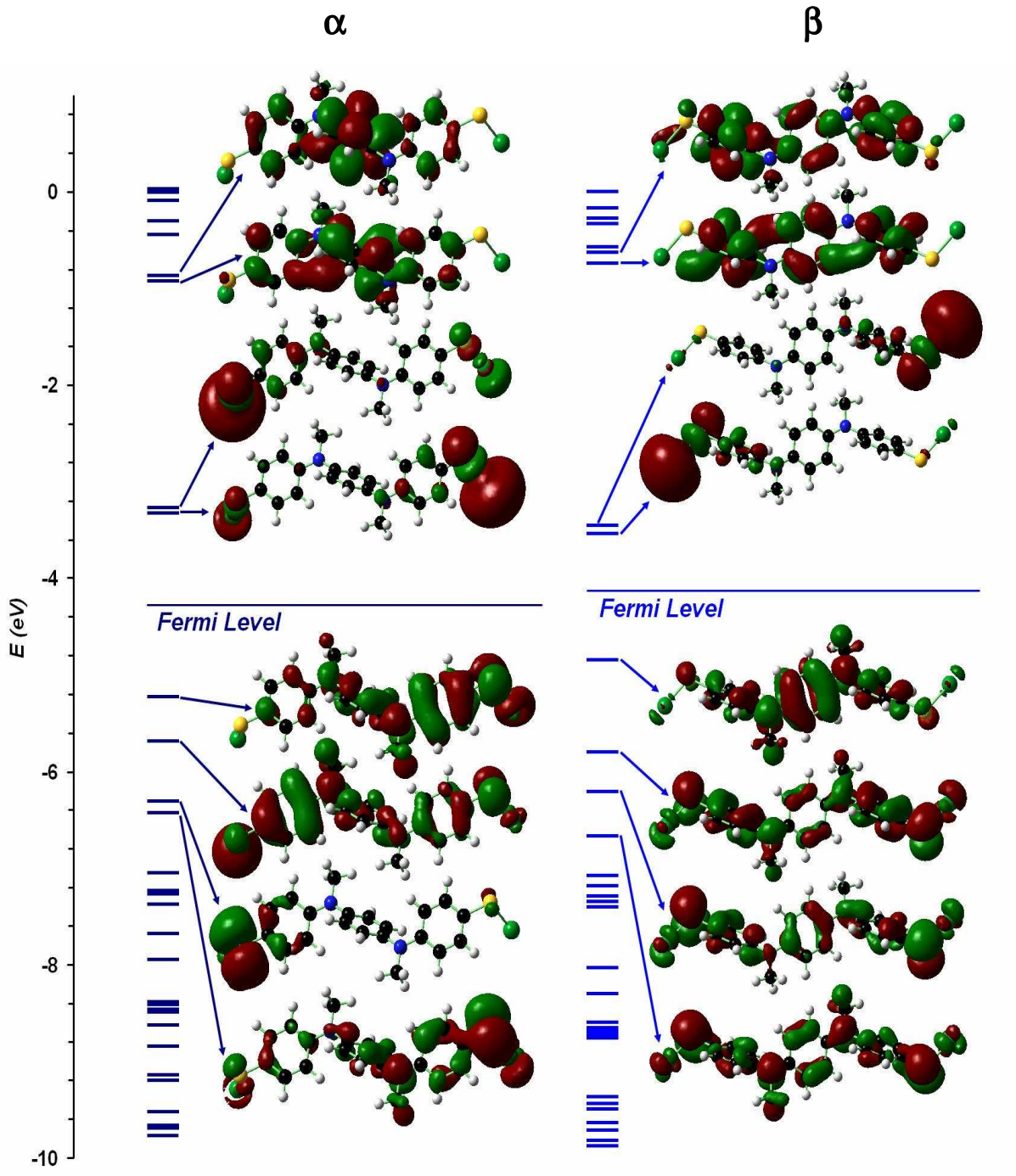

Figure 20. MO diagrams of symmetric single Au atom contact system for α and β

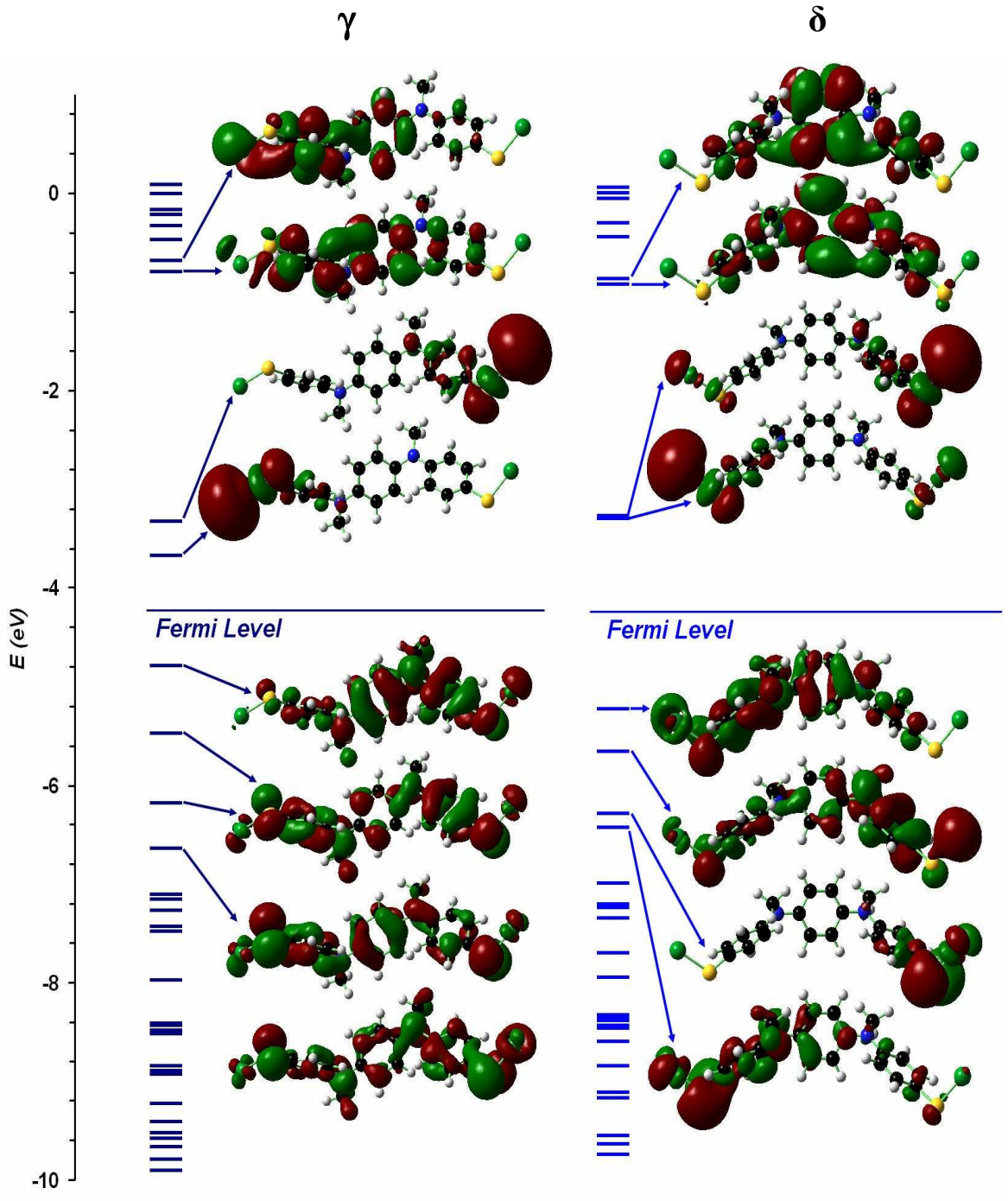

Figure 21. MO diagrams of symmetric single Au atom contact system for γ and δ

Upon attaching the gold atoms, the Fermi levels for the α, β, γ, and δ conformations are -4.27 eV, -4.19 eV, -4.23 eV, and -4.26 eV respectively. The similarity of allowable energy states between the α and δ conformations are also observed again. The incorporation of the gold atoms shifts the existing energy levels of the molecule by a small amount and adds additional energy states, as can be seen in the previous figures. The gold atom also shifts the Fermi Level downwards, not because it is an electron withdrawing group like the sulfur atoms but because of the mixing of allowable energy states between the metal atoms and the molecule as mentioned in the introduction. After coming to equilibrium, a single Fermi level will form, representative of the standalone molecule's "Fermi level" and the Fermi level of gold, which is -5.31 eV. This mixing of energy states also contributes to the slight shifting of the molecule's energy states.

Due to the discontinuity of allowable energy states at the molecule-metal interface, a barrier forms at the gold-sulfur Junction that electrons must tunnel through. For the symmetric single Au-Au atom contact case, a significant increase in localization can be observed for LUMO orbitals above relative to the previous molecules lacking the metal contacts. The delocalization that is present for the HOMO orbitals but not for the LUMO orbitals suggests that the conduction mechanism for this system is by hole transport rather than electron transport.

4.2-4 Oligoaniline with Single Atom Palladium Contacts

Similar to the gold atom, incorporating one palladium atom attachments to the molecule does not change the original geometries, inducing only insignificant changes to the bond lengths, angles and dihedrals. The relevant dimensions of the single palladium contact terminated molecule are presented in Table IV:

Table IV. Dimensions of oligoaniline isomers with single Pd contacts

	α	β	γ	δ
		Bond Length		
Pd-S	2.347	2.348	2.346	2.344
Pd-S *	2.347	2.348	2.344	2.344
		Bond Angle		
Pd-S-C	103.9	104.6	106.1	105.5
Pd-S-C *	103.9	104.6	104.5	105.5
		Dihedral Angle		
Pd-S-C-C ^{1}	-44.6	-140.5	-150.1	-144.3
Pd-S-C-C ^{2}	136.5	41.0	31.1	36.8
Pd-S-C-C ^{1*}	44.6	140.5	-140.6	-144.3
Pd-S-C-C ^{2*}	-136.5.	-41.0	40.3	36.8

'*' refers to a different alpha ring, subscript '1' and '2' refer to different Pd-Sulfur dihedrals

Upon attaching the palladium atoms, the Fermi levels for the α, β, γ, and δ conformations are -4.33 eV, -4.42 eV, -4.41 eV, and -4.27 eV respectively. Just like gold atoms, the incorporation of the palladium atoms shifts the existing energy levels of the molecule slightly and adds additional energy states, although not as much as gold, which has more core electrons. From the below figures, it can be seen that the orbitals are much less delocalized than the symmetric gold-molecule-gold system's, suggesting a lower conductivity. Unlike the metal-molecule interface analysis performed by Seminario, Cruz and Derosa,[28] the Au-thiol group here exhibits a lower barrier to conduction compared to the Pd-thiol group, implying that the Oligoaniline has a better coupling to the Au atoms. This result could help explain why the similarity of allowable energy states between the α and δ conformations are not observed, unlike the gold-molecule-gold system. Since the coupling of the molecule to the Pd electrode is considerably worse, the difference in dihedral angles with respect to the Pd atoms will be more of a factor in determining conductivity. Figures 22 and 23 below present the molecular orbital diagrams for the four conformations of the Oligoaniline molecule attached to single Pd atom contacts at the ends.

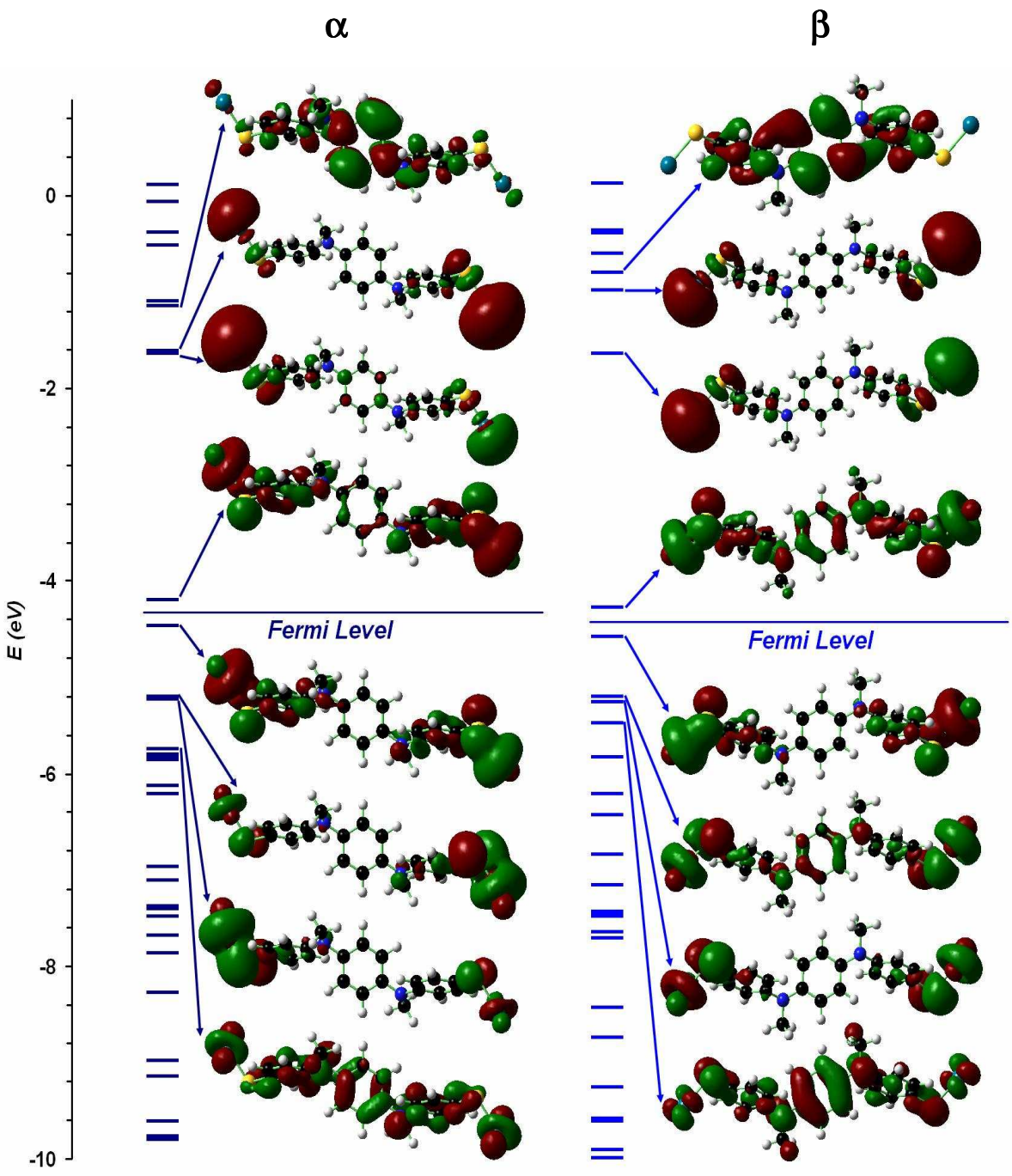

Figure 22. MO diagrams of oligoaniline with single Pd atom contacts for α and β

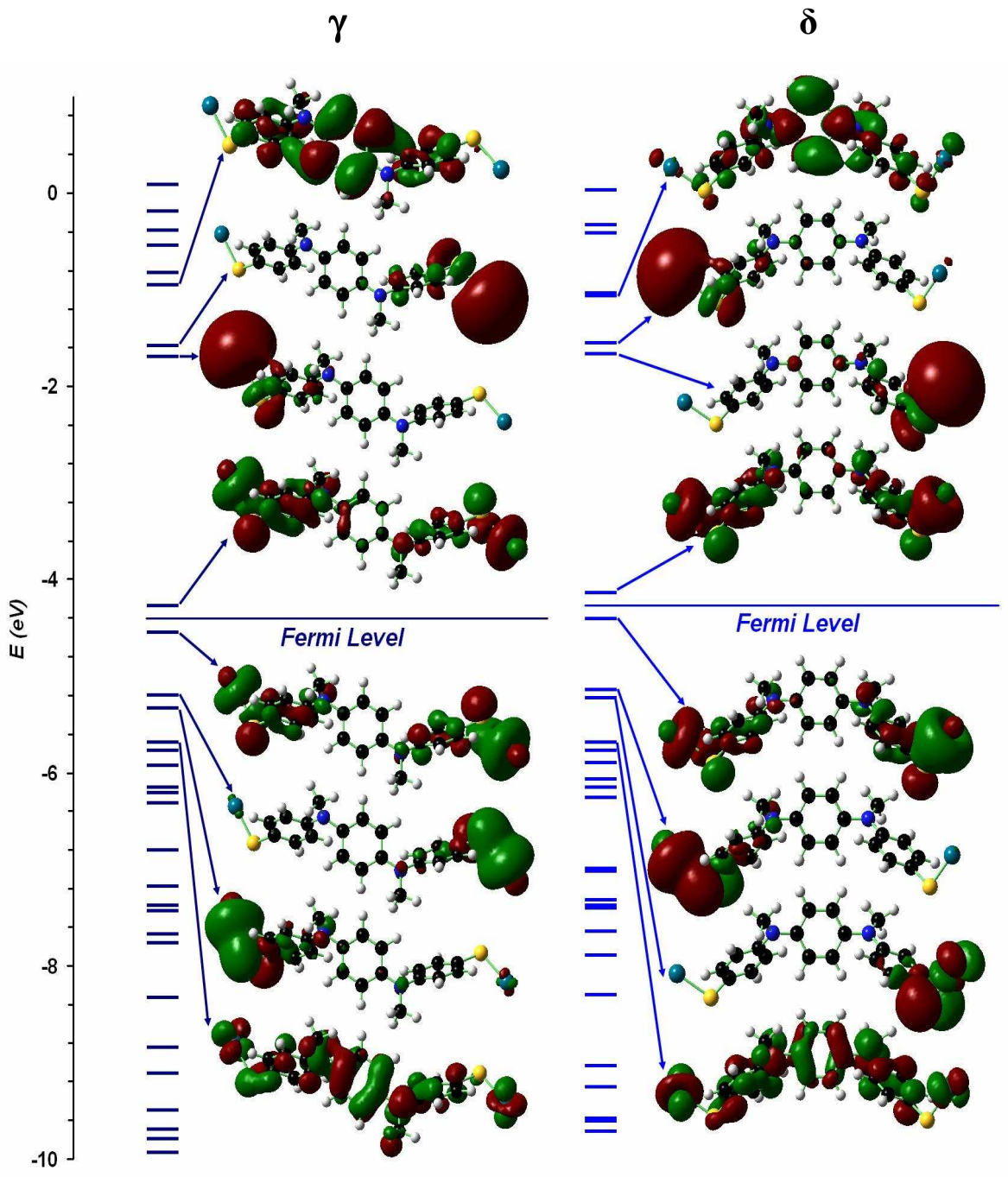

Figure 23. MO diagrams of oligoaniline with single Pd atom contacts for γ and δ

4.2-5 Oligoaniline with Single Atom Pd and Au Contacts

Similar to the symmetric metal-molecule-metal systems, incorporating one palladium atom at one side and a gold atom at the other side of the molecule does not change the original geometries, inducing only insignificant changes to the bond lengths, angles and dihedrals. The relevant dimensions of the single Pd-Au atom contact system are presented in Table V:

Table V. Dimensions of oligoaniline isomers with single Pd-Au contacts

	α	β	γ	δ
		Bond Length		
Pd-S	2.345	2.340	2.341	2.343
Au-S	2.381	2.384	2.381	2.385
		Bond Angle		
Pd-S-C	101.0	103.7	102.3	102.0
Au-S-C	103.7	103.3	103.1	103.6
		Dihedral Angle		
Pd-S-C-C ^{1}	-120.2	141.9	48.1	-127.1
Pd-S-C-C ^{2}	62.3	-39.5	-133.2	54.8
Au-S-C-C ^{1}	94.4	90.8	92.4	90.6
Au-S-C-C ^{2}	-89.4	-92.9	-91.7	-92.7

superscripts '1' and '2' refer to different Pd/Au - Sulfur dihedrals

The Fermi levels for the antisymmetric single atom contact α, β, γ, and δ conformations are -4.20 eV, -4.37 eV, -4.25 eV, and -4.15 eV respectively. The anti-symmetric system is different from the previous symmetric systems in the regard that the number of total electrons is odd, leading to a multiplicity of 2. The 2n multiplicity corresponds to multiple spin states, alpha and beta that are indistinguishable from each other and cannot be treated separately. From the molecular orbitals shown below, it can be seen that the delocalization is now very limited, implying a low conductivity relative to the symmetric systems, which was also observed for the anti-symmetric system in the experiment.[17] For all of the conformations except for α and δ, the HOMO is much more delocalized,

implying that α and δ may be the low conducting state. Figures 24 through 26 below show the energy levels and some of the associated molecular orbitals.

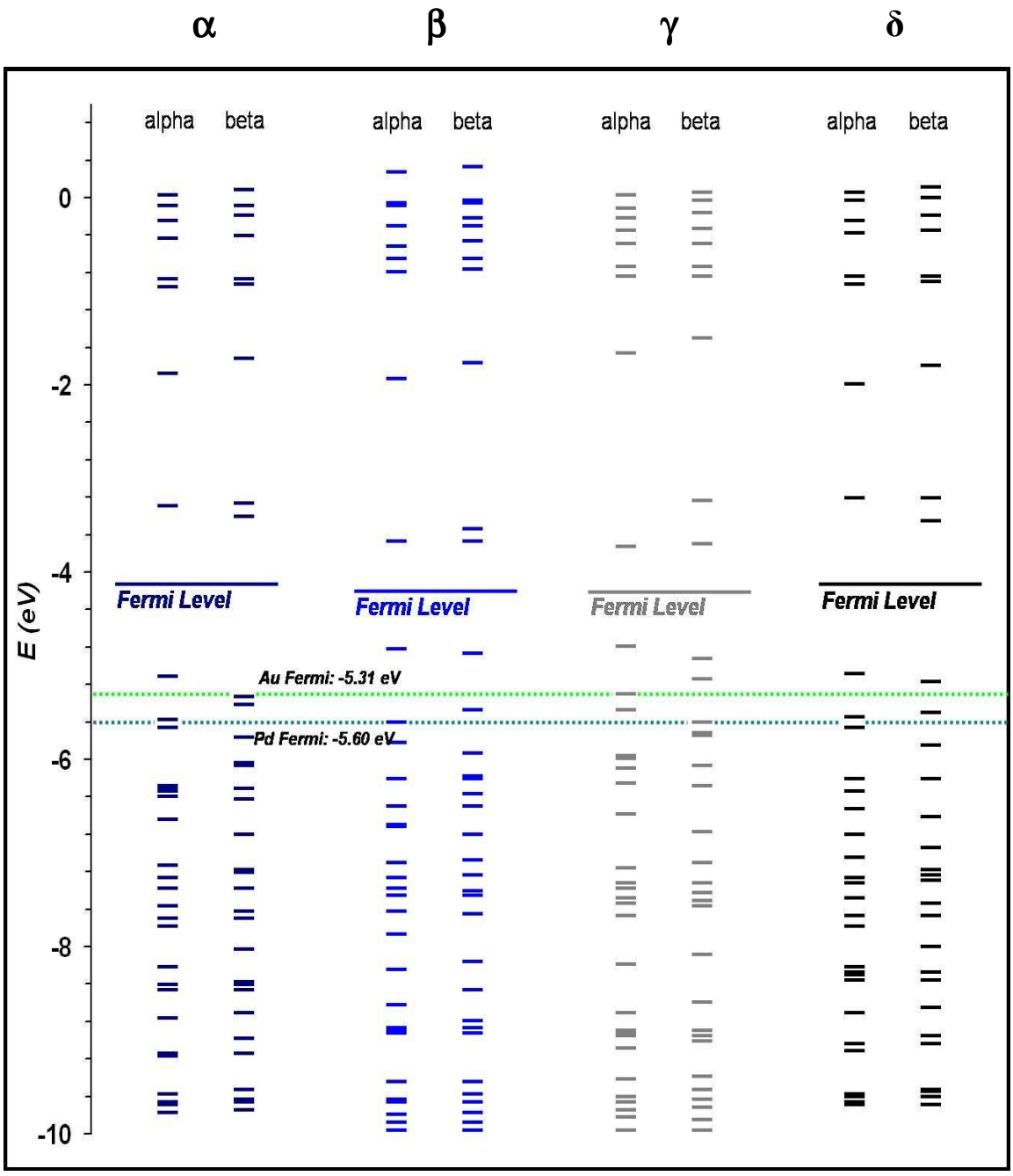

Figure 24. Allowable energy levels for the single Pd-Au atom contact system

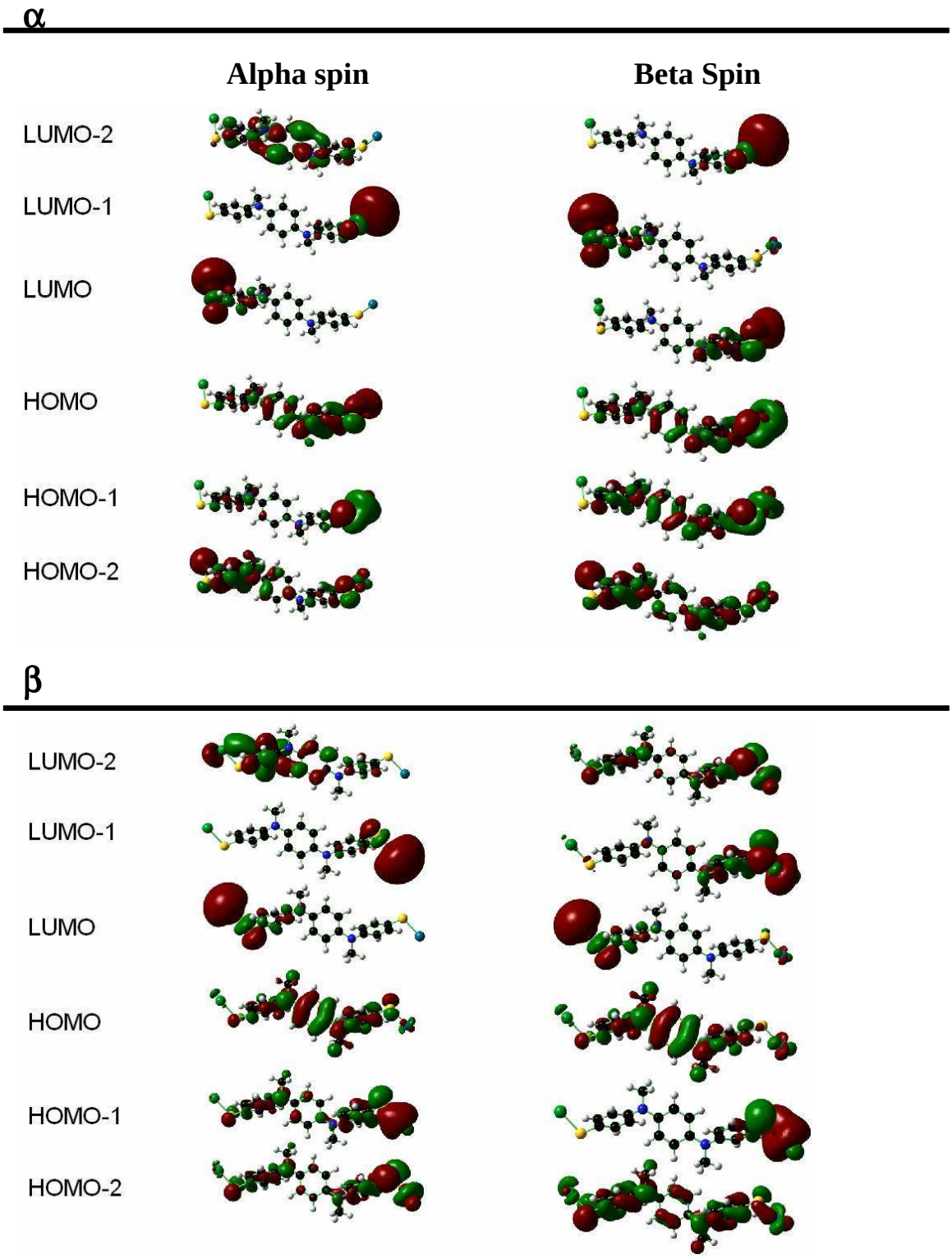

Figure 25. Molecular orbitals for the single Pd-Au atom contact system for α and β

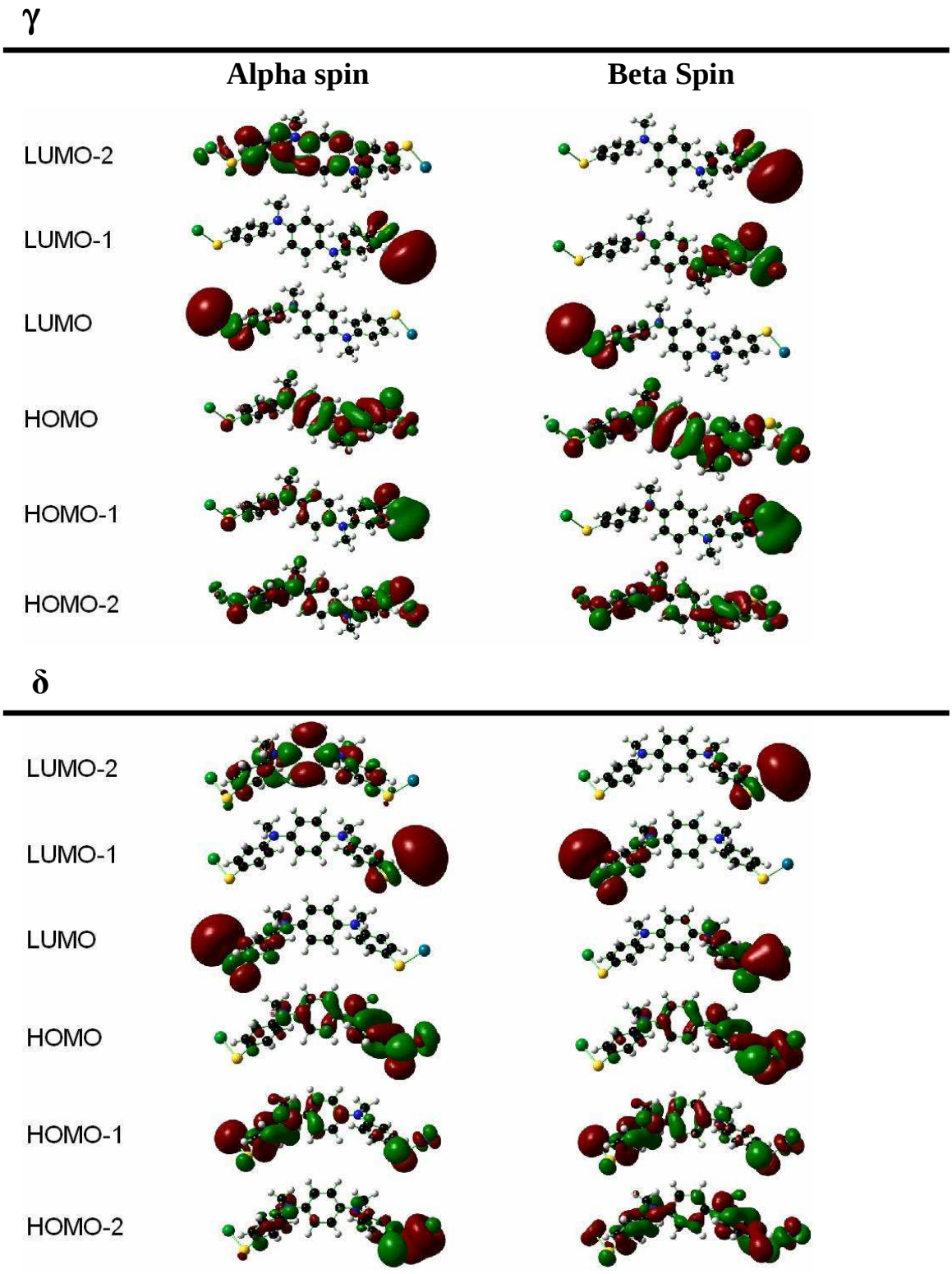

Figure 26. Molecular orbitals for the single Pd-Au atom contact system for γ and δ

4.2-6 Oligoaniline with Pd and Au Trimer Contacts

In order to generate a more representative system of the antisymmetric Au-Pd system, three contact atoms were implemented and subsequently analyzed. Three atoms could hardly be constituted as a continuum, but for the scope of this work, this system should suffice as a reasonable estimate. Unlike the single Pd-Au atom contact system, three late transition metals at each end of the molecule complicates the calculations considerably. Therefore, in order to obtain a reasonable geometry, a certain procedure was needed. First, since the geometrical parameters of the molecule stayed relatively the same, only the geometry of three metal contacts and the molecule point of contact was optimized. However, even the optimization calculation of only the three metal contacts and the molecule point of contact proved to be a difficult task, as many candidate geometries were rejected (nonconvergence). After numerous runs, a consistent pattern was observed that eventually lead to the convergence of the subsystem. Figure 27 shows the optimized geometries of the three metal contact atoms and the molecule point of contact. The relevant dimensions are presented in Table VI.

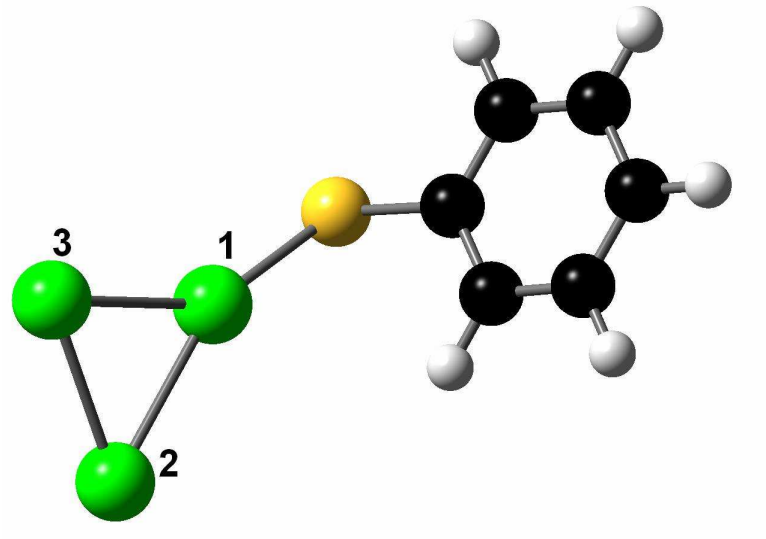

Figure 27. Optimized structure of trimer Au-S-benzene subsystem

Table VI. Dimensions of the trimer Au-S-benzene subsystem

	Bond Length
Au1-Au2	2.723
Au1-Au3	2.705
Au2-Au3	2.640
S-Au1	2.370
	Bond Angle
Au3-Au1-S	148.7
Au2-Au1-S	153.1
Au1-S-C	103.8
	Dihedral Angle
Au3-Au1-S-C	93.6
Au2-Au1-S-C	-92.1

The optimization calculations for the gold subsystems was relatively easier than the palladium subsystems due to the fact that the palladium system had a multiplicity of 2. Nevertheless, the same optimization procedure was followed. Figure 28 shows the optimized geometries of the three metal contact atoms and the molecule point of contact. The relevant dimensions are presented in Table VII.

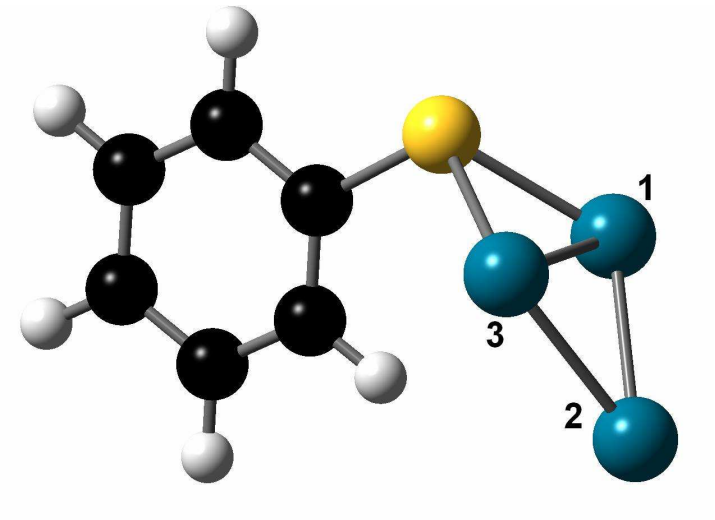

Figure 28. Optimized structure of trimer Pd-S-benzene subsystem

Table VII. Dimensions of the trimer Pd-S-benzene subsystem

	Bond Length
Pd1-Pd2	2.640
Pd1-Pd3	2.660
Pd2-Pd3	2.641
Pd1-S	2.392
Pd3-S	2.392
	Bond Angle
Pd1-S-C	107.0
Pd3-S-C	107.0
Pd2-Pd1-S	111.9
Pd2-Pd3-S	111.8
	Dihedral Angle
Pd2-Pd1-S-C	-78.9
Pd2-Pd3-S-C	78.9

After the optimized geometries were found for the two subsystems, the bond lengths, angles and dihedrals of each contact were noted and were then manually inputted to the thiol-terminated Oligoaniline. A single point calculation (no optimization) was then performed on the system to obtain the wavefunction data.

The Fermi Levels for the trimer metal atom antisymmetric α, β, γ, and δ conformations are -4.45 eV, -5.09 eV, -4.56 eV, and -4.44 eV respectively. The Fermi levels for the three contact atoms are shifted downwards relative to the Fermi levels for the single contact atom scenario, and can be attributed to Sanderson's principle of electronegativity equalization, where the chemical potential will align more towards the metal Fermi level as more atoms are added.[29] From the molecular orbitals shown below, it can be seen that the delocalization is now even more limited, especially around the metal contacts, compared to the system with a single atom contact, implying that the molecule-metal interface barrier is increased. The fact that the HOMO is much more delocalized than the LUMO implies that conductivity is dominated by hole transport. Figures 29 through 31 below show the energy levels and some of the associated molecular orbitals.

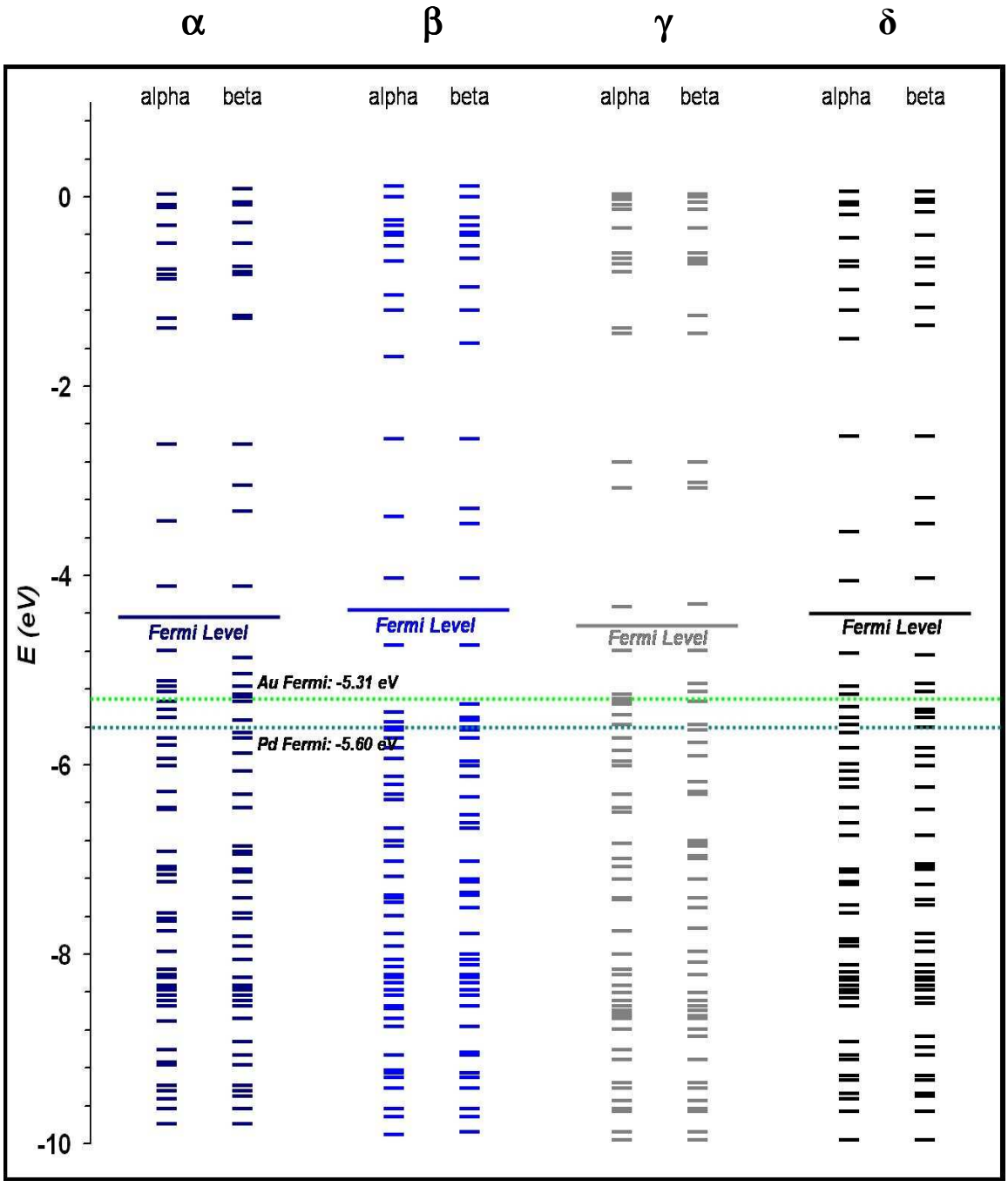

Figure 29. Allowable energy levels for the trimer Pd - oligoaniline - Au system

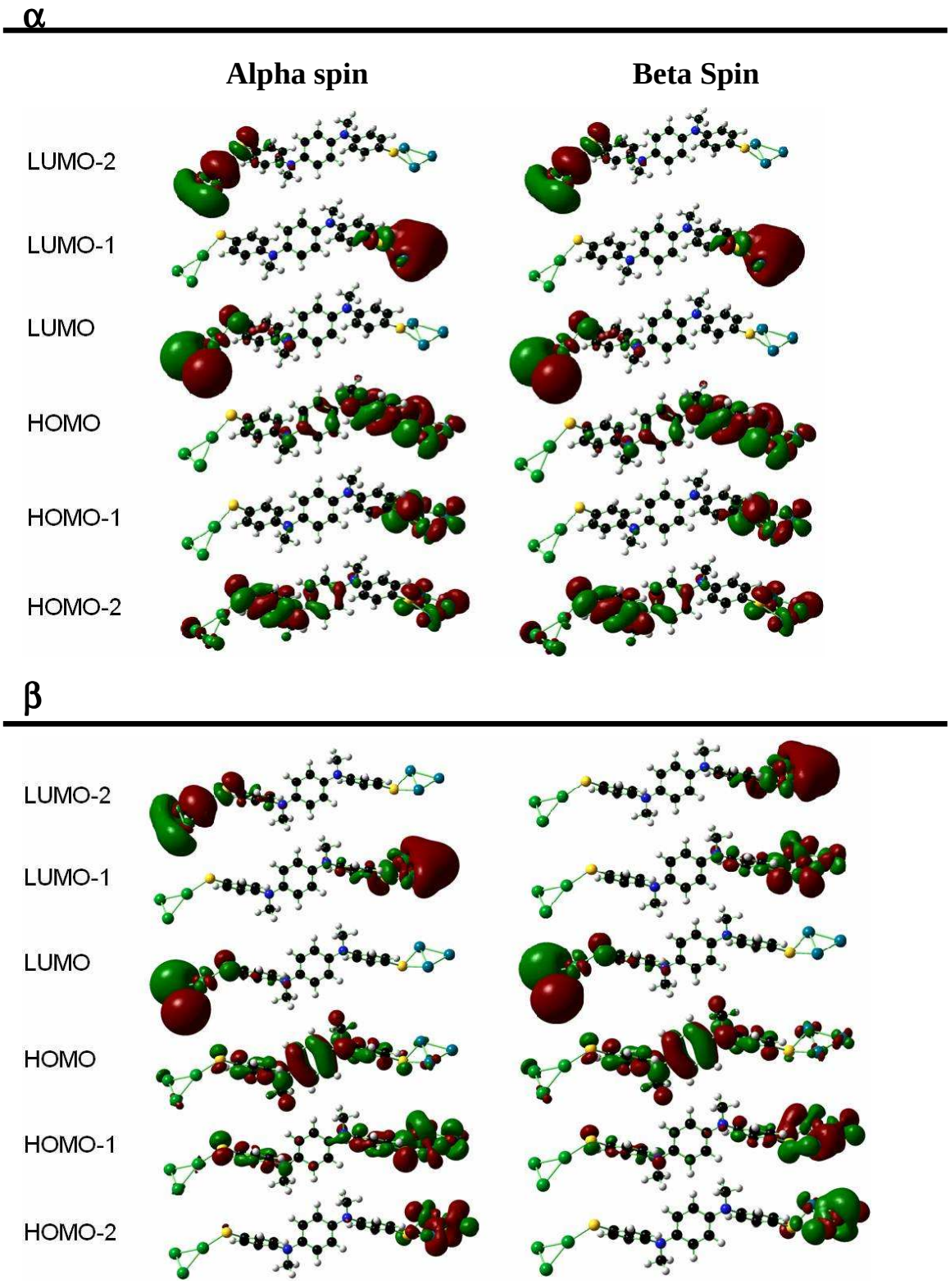

Figure 30. Molecular orbitals for the trimer Pd - Au system for α and β

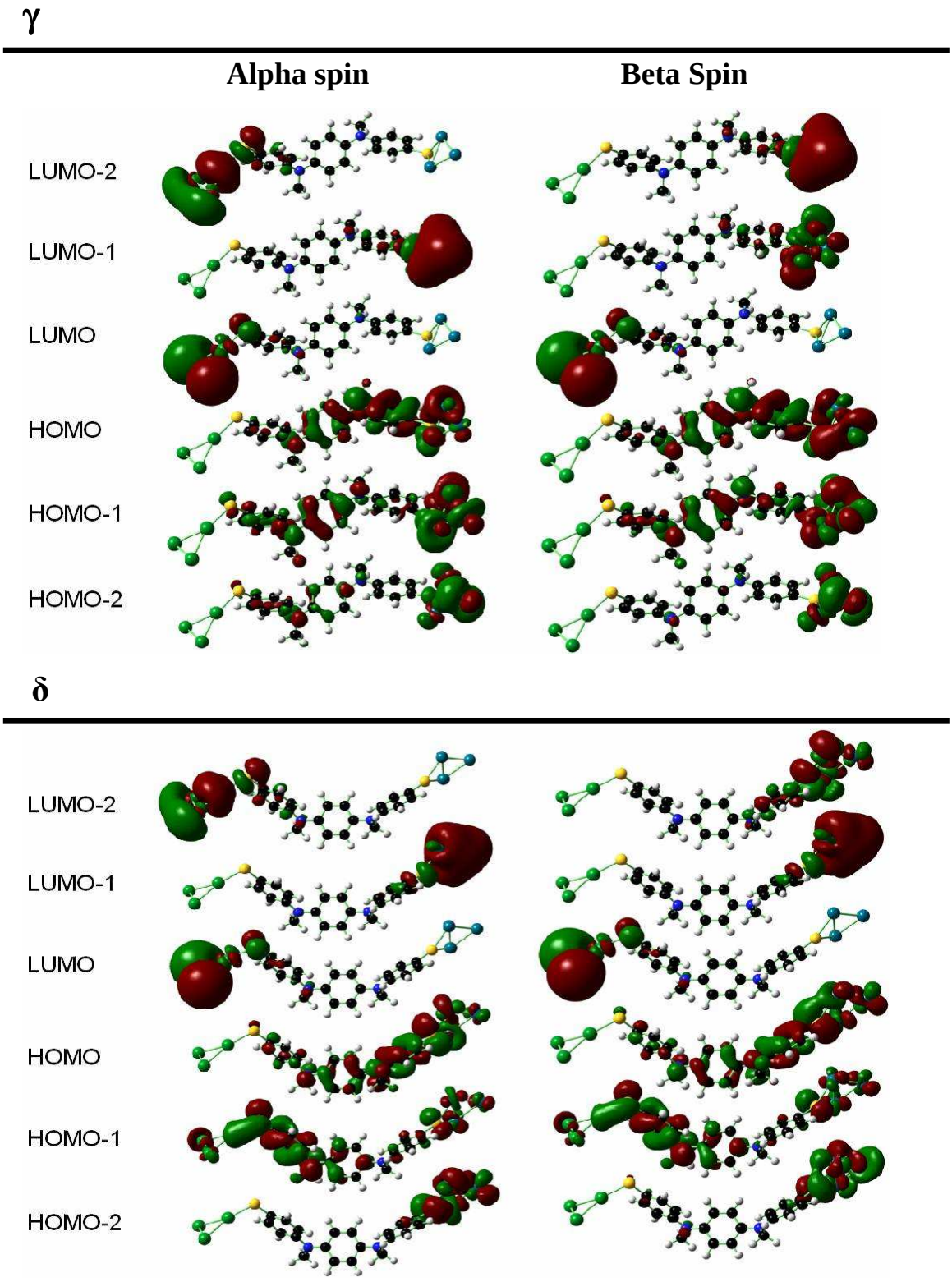

Figure 31. Molecular orbitals for the trimer Pd - Au system for γ and δ

4.3 MO Analysis of Ionized Oligoaniline Systems

4.3-1 -1 Charge Molecule

There is the possibility that when a bias is applied, the Oligoaniline system could get negatively charged due to the relatively long residential time spent by electrons moving through the molecule. The investigation of charged possibilities was also inspired by the experiment[14] where the molecule-metal junction exhibited NDR behavior and increased conductivity upon acquiring one extra electron from the passing current. Since there are only a few works that treat charged systems with ab initio methods, the Fermi level, required for the I-V calculations, was characterized in the same way as the ab initio analysis of the dinitro device,[16] where it was taken to be the center of the HOMO-LUMO gap. The antisymmetric system with only single Pd and Au contacts were analyzed due to convergence issues. In order to have a general idea on how the charge was distributed throughout the molecule, a Mulliken analysis was performed, with the values presented in Table VIII. The molecular orbitals are displayed in Figures 32 and 33.

Table VIII. Mulliken population analysis of the oligoaniline anion

	α	β	γ	δ
	Relative Charge Population			
Au	-0.30	0.02	-0.51	-0.29
S(Au)	0.04	0.11	-0.05	0.05
Pd	-0.31	-0.50	-0.14	-0.33
S(Pd)	-0.07	-0.16	0.02	-0.07
N^{1}	-0.30	-0.31	-0.32	-0.30
N^{2}	-0.30	-0.31	-0.31	-0.30
$CH_3{}^{1}$	0.04	0.02	0.05	0.03
$CH_3{}^{2}$	0.02	0.02	0.03	0.02

'1' refers to the gold side '2' refers to the palladium side

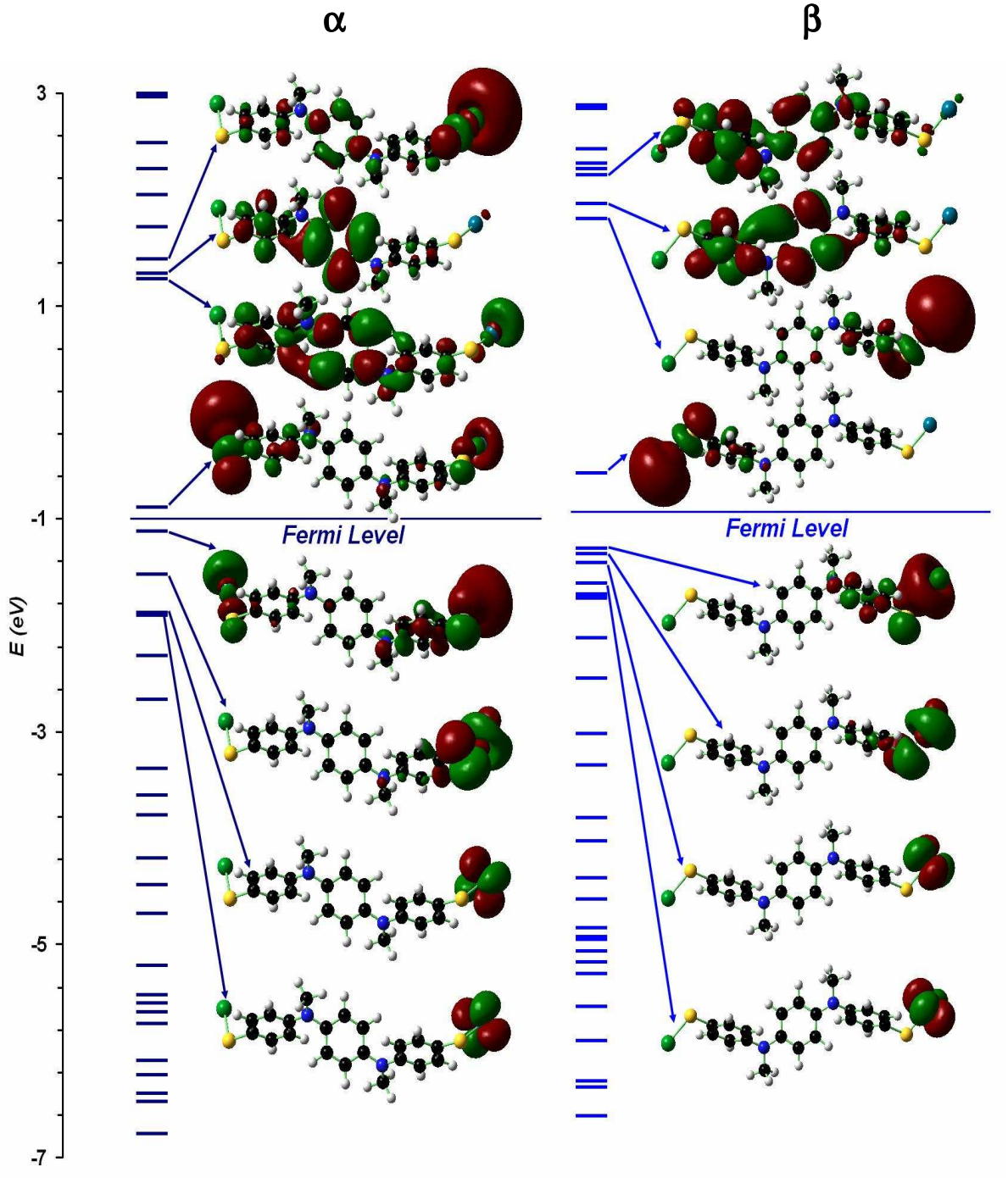

Figure 32. MO diagrams of the -1 charged antisymmetric system for α and β

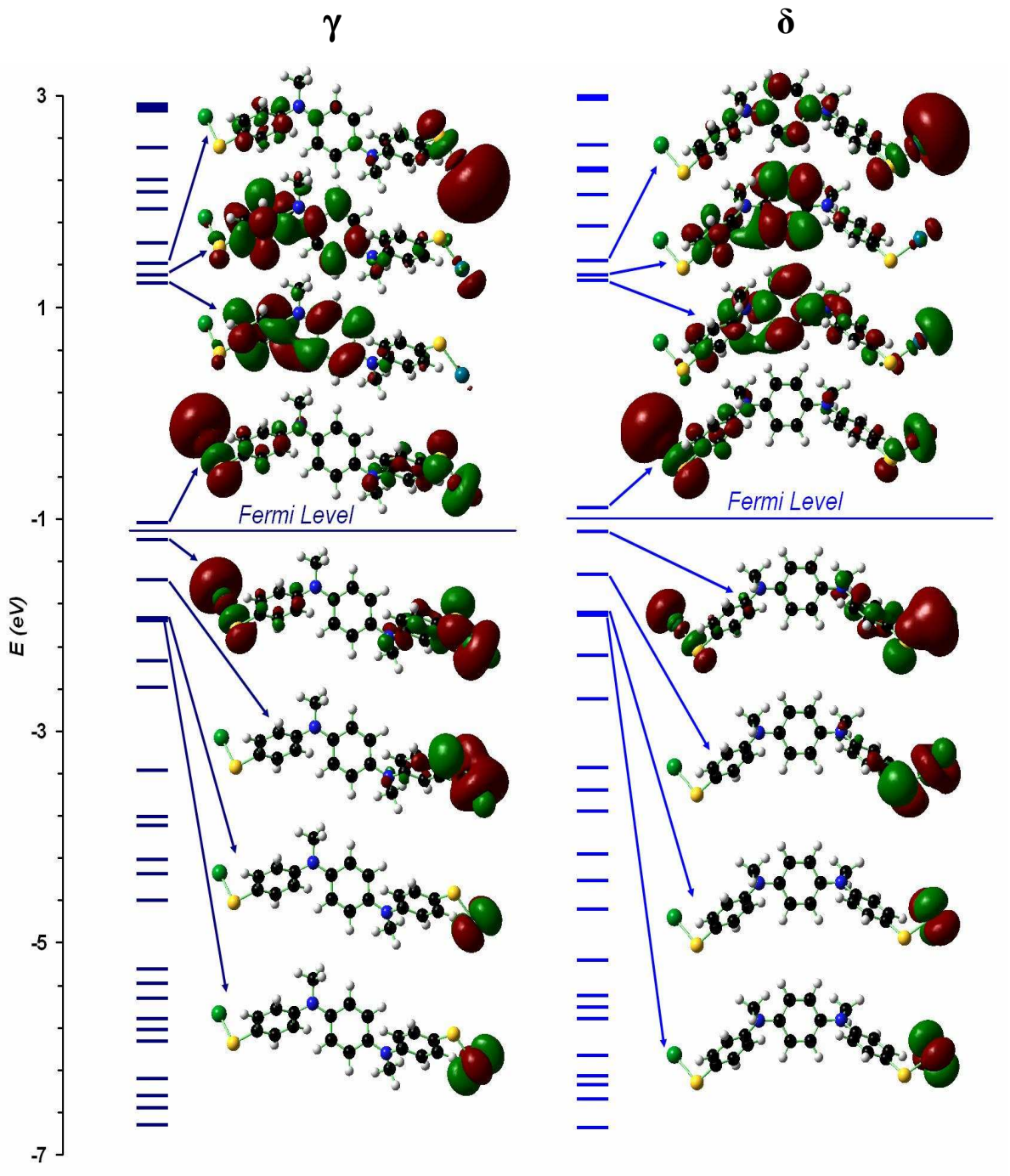

Figure 33. MO diagrams of the -1 charged antisymmetric system for γ and δ

The Fermi levels for the -1 charged antisymmetric α, β, γ, and δ conformations are -1.01 eV, -0.93 eV, 1.17 eV, and 1.01 eV respectively. The drastic upshift in Fermi level is due to the -1 state since the molecule has an extra electron in its outer shell now. Since the Fermi level represents the ionization potential to acquire one electron from the molecule, it should be lower now since the extra electron is not tightly bound. From the two figures above, it can be seen that the delocalization is extremely limited to the LUMO side, implying that the extra charge could induce the molecule to act as an insulator due to the Coulomb Blockade effect.

4.3-2 +1 Charge Molecule

There is the additional possibility that when a bias is applied, one electron from the HOMO goes to the positive electrode, leaving a hole in the molecule, which will then be subsequently filled by one electron from the negative electrode. In effect, it will appear that a positive charge, known as a "positive quasiparticle" is moving in the opposite direction of the electron. Again, only the antisymmetric system with only single Pd and 1 Au contacts were analyzed due to convergence issues. In order to have a general idea on how the charge was distributed throughout the molecule, a Muliken analysis was performed, with the values presented in Table IX. The molecular orbitals are displayed in Figures 34 and 35.

Table IX. Muliken population analysis of the oligoaniline cation

	α	**β**	**γ**	**δ**
	Relative Charge Population			
Au	0.02	0.03	0.02	0.01
S(Au)	0.15	0.14	0.13	0.15
Pd	0.15	0.13	0.13	0.15
S(Pd)	0.18	0.14	0.17	0.18
N^{1}	-0.28	-0.27	-0.30	-0.28
N^{2}	-0.26	-0.26	-0.28	-0.26
CH_3 ^{1}	0.10	0.10	0.12	0.10
CH_3 ^{2}	0.12	0.12	0.14	0.12

'1' refers to the gold side '2' refers to the palladium side

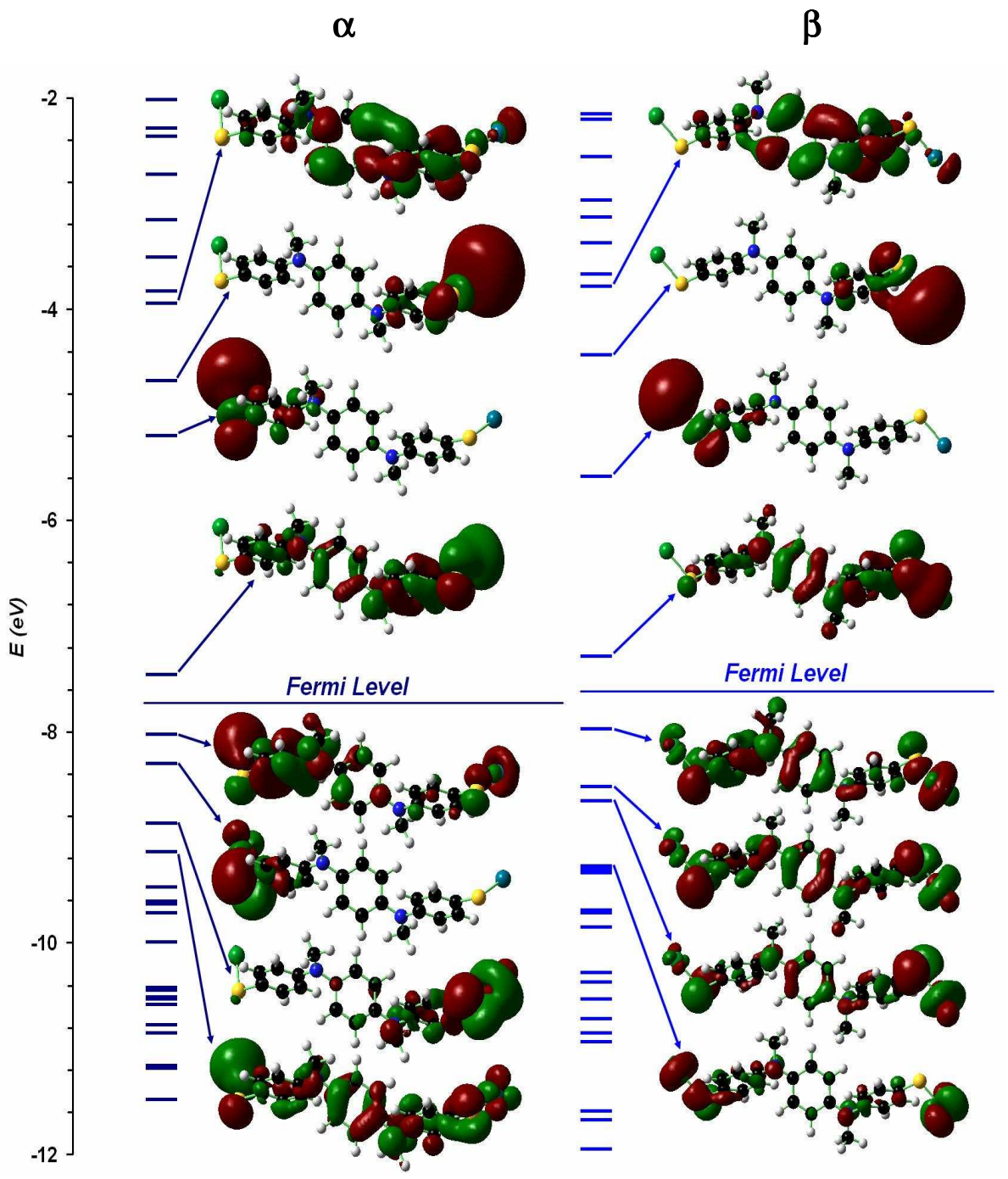

Figure 34. MO diagrams of the +1 charged antisymmetric system for α and β

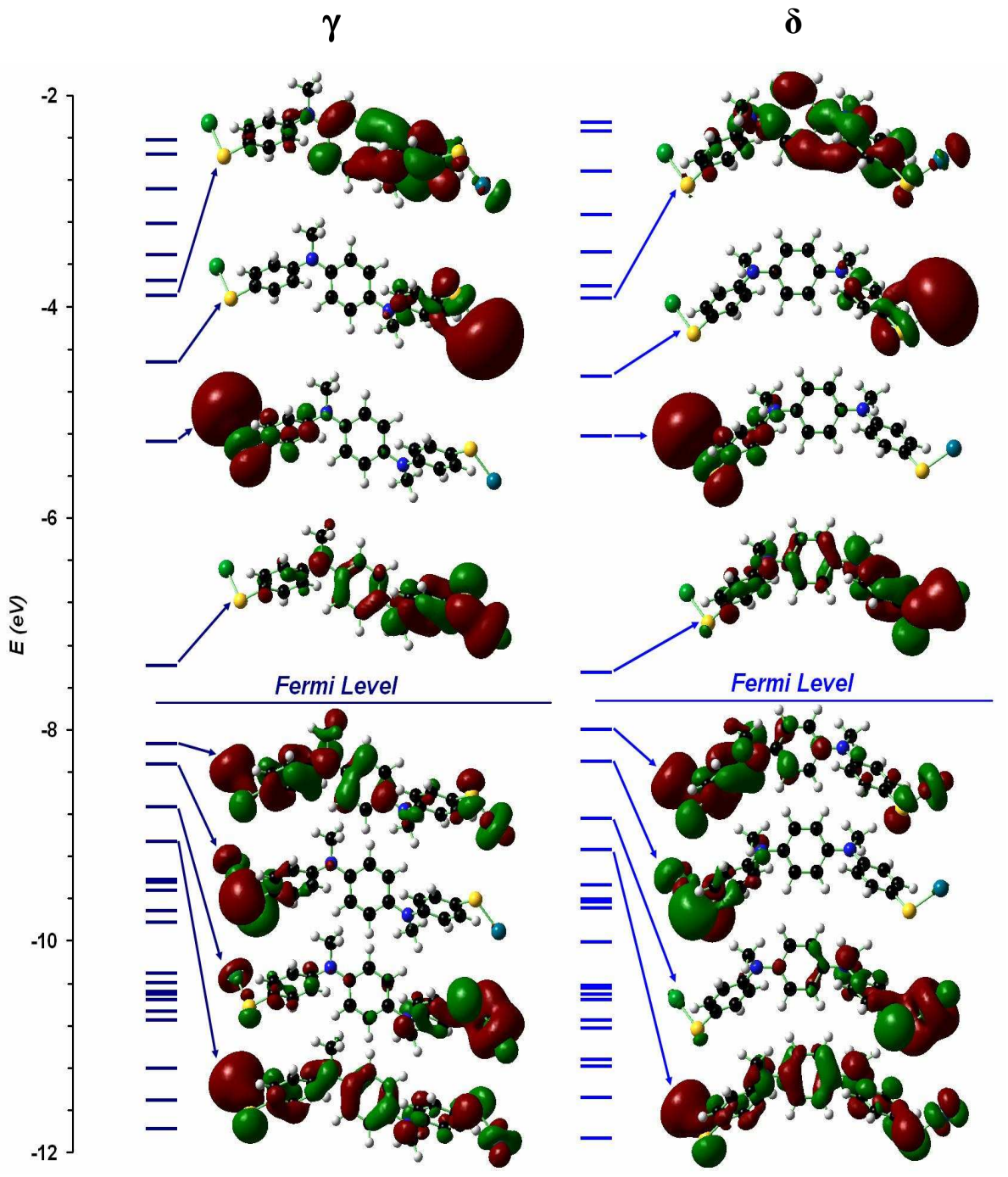

Figure 35. MO diagrams of the +1 charged antisymmetric system for γ and δ

The Fermi Levels for the +1 charged antisymmetric α, β, γ, and δ conformations are -7.74 eV, -7.63 eV, 7.77 eV, and 7.73 eV respectively. The drastic downshift in Fermi level is due to the +1 state since the molecule has lost extra electron in its outer shell. The lower Fermi level reflects how more energy is required to acquire a second electron from the valence orbital. From the two figures above, it can be seen that the degree of delocalization for the +1 state HOMO and LUMO orbitals is a little more extended than the orbitals of the neutral state, suggesting that the +1 charged molecule may possess higher conductivity.

4.4 Inelastic Tunneling Spectroscopy Analysis

When electrons are injected into a metal-device-metal system, the atoms of the bridging material may absorb energy through momentum transfer from the tunneling electrons. At the molecular level, the energy that results from the inelastic collisions is quantized with discrete amounts, termed "phonons", analogous to photons. Upon absorbing phonons, the nuclei of the atoms will undergo different vibrational modes depending on how the electrons traverse through the molecule. Inelastic electron tunneling spectroscopy (IETS) provides for a way to analyze the effects of these vibronic interactions on the charge transfer process. An IETS analysis is conducted through IR and Raman frequency runs for the standalone Oligoaniline molecule, the antisymmetric Oligoaniline system with three contact atoms, and the ionized Oligoaniline involving the antisymmetric Oligoaniline system with one contact atom. The IR and Raman spectrum of the different conformations are compared in hopes that the high and low conducting state can be distinguished as in the experiment,[18] where it was found that the low conductivity state exhibited a different frequency spectrum than the high conductivity state.

4.4.1 Standalone Oligoaniline IET Spectrum

Figures 36 and 37 below present the IR and Raman spectrum for the standalone Oligoaniline molecule.

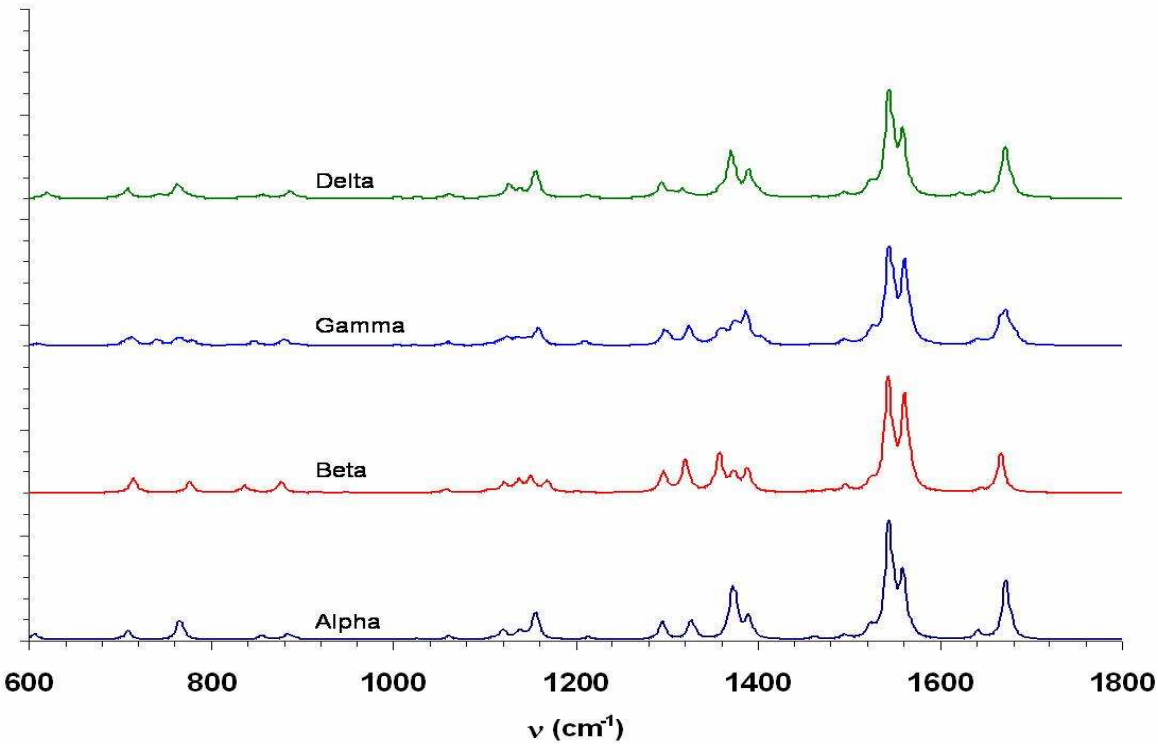

Figure 36. IR spectrum of standalone oligoaniline

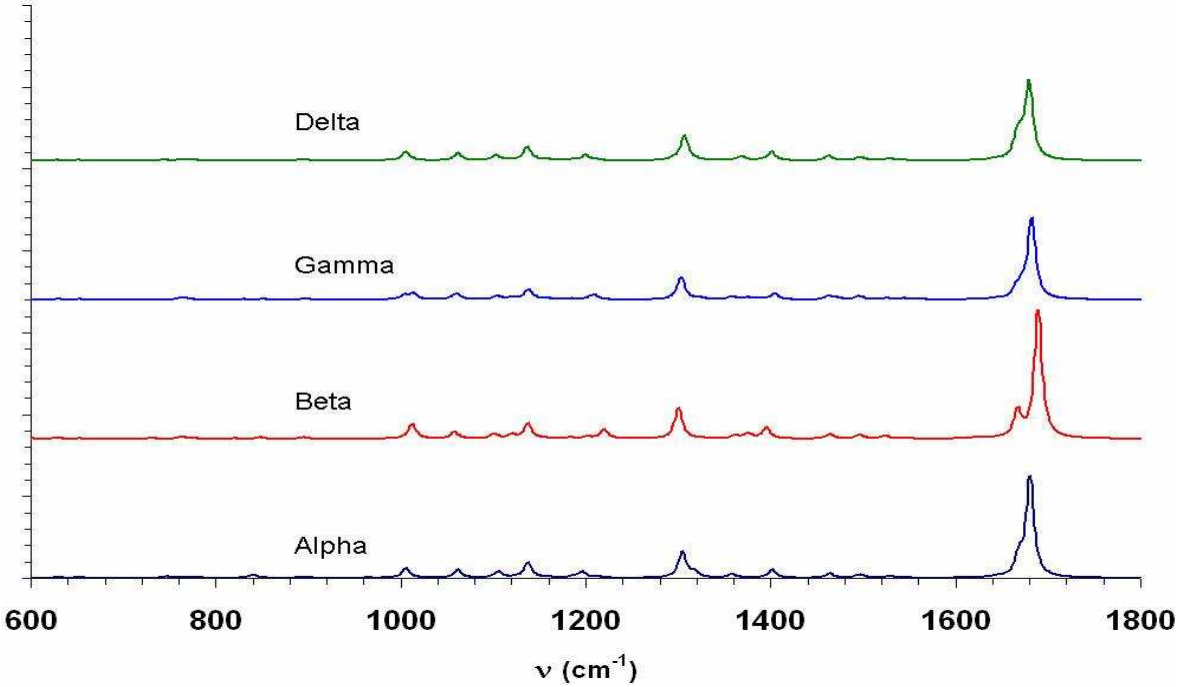

Figure 37. Raman spectrum of standalone oligoaniline

From the figures, it can be seen that the spectrums of all the conformations are similar in terms of peak location and intensity. Some of the minor differences include the presence of the triple peaks at 1360 to 1400 cm^{-1} for the Beta and Gamma formation compared to the double peaks for Alpha and Delta. Also, an additional smaller peak for the Beta conformation at around 1565 cm^{-1} is observed for the Raman spectra. The vibrational modes of antisymmetric stretching and scissoring are both observed, but the peaks at 1360-1400 cm^{-1} correspond more to the Nitrogen group scissoring with respect to the benzene carbons while the peaks at 1520 to 1560 cm^{-1} correspond more to the nitrogen group stretching with either the alpha or beta benzene ring. The Raman peak at 1690 cm^{-1} corresponds to the entire center benzene ring being distorted while being stretched antisymmetrically with both of the nitrogen groups. At this point the frequencies are too similar to distinguish a high conductivity state and a low conductivity state from the different conformations.

4.4.2 IET Spectrum of Oligoaniline with Trimer Contacts

The IET spectrum of the Oligoaniline system with three contact atom attachments should be similar in terms of peak location to the standalone Oligoaniline IET spectrum from the fact that the presence of contact electrodes won't affect the nuclear motion of the individual molecular atoms. However, the metal electrodes provide an extra source of electrons that would affect the intensity, most likely exaggerating the previous peaks found for the standalone Oligoaniline. Figure 7 exhibits a peak at around 1480 cm^{-1} for the low conducting state, which distinguishes it from the high conducting state where the lone peak is split into two peaks at 1450 and 1550 cm^{-1} for the high conducting state. These peaks correspond to the C-N stretching and a resonant C=N mode; it was claimed that the peak splitting was due to an extended delocalization between the nitrogen group and the benzene carbon. Figures 38 and 39 below present the IET spectra for the trimer contact Oligoaniline system and will help determine whether switching behavior is present.

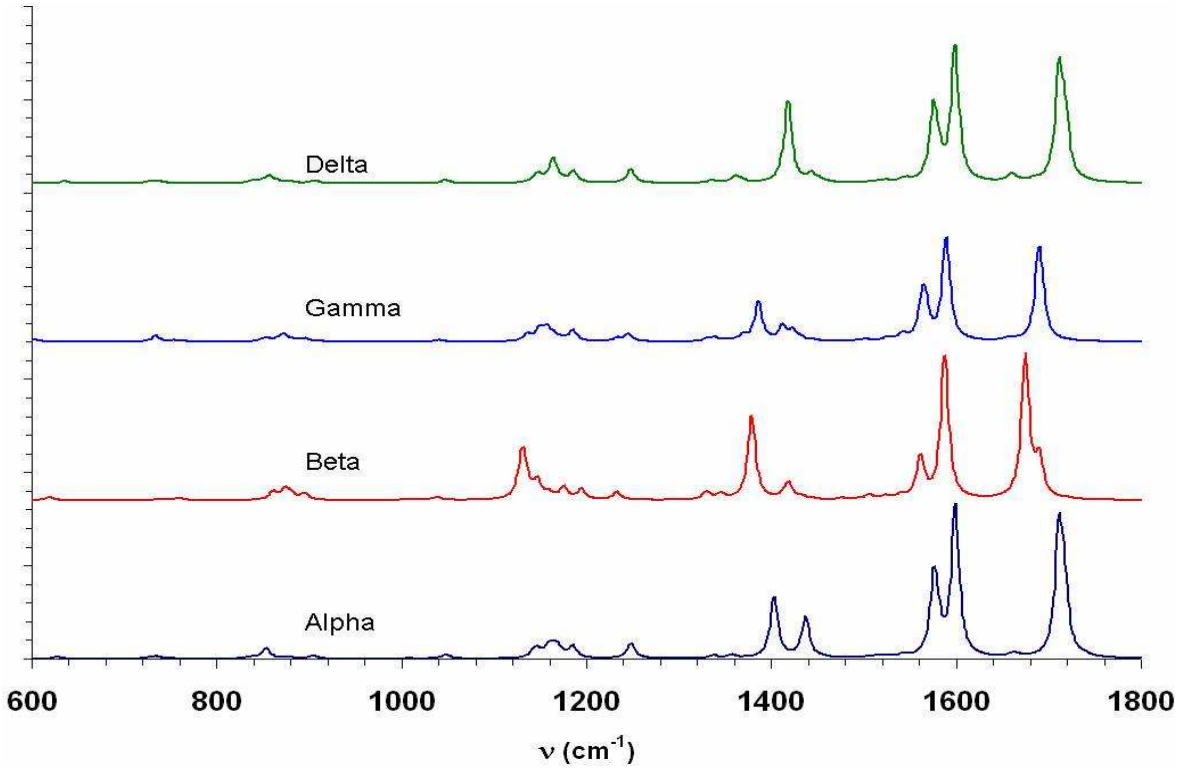

Figure 38. IR spectrum of oligoaniline with trimer contact atoms

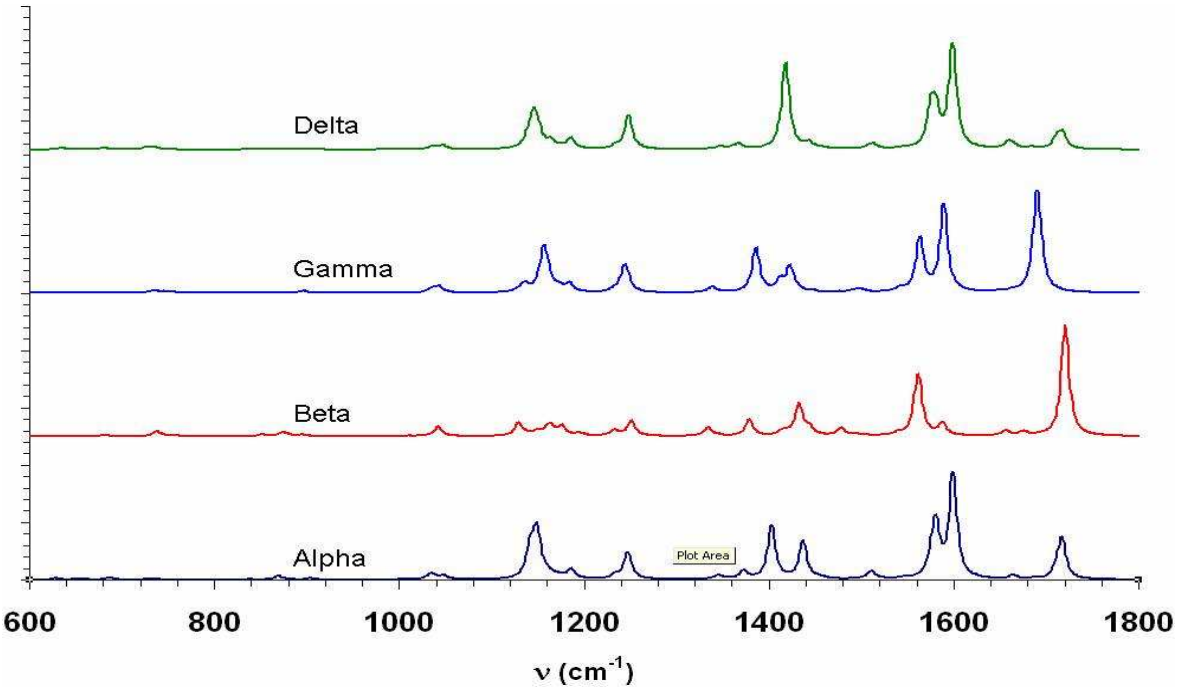

Figure 39. Raman spectrum of oligoaniline with trimer contact atoms

From the figures, it can be seen that the shape of the all the IR spectrums have similar shapes, but some of the peak locations have shifted. As expected, the relative intensity of the peaks increase, most likely due to the presence of the electrodes. However, the prominent peak found experimentally at 1480 cm^{-1} for the low conducting state is not observed in the figures above, nor the double peaks at 1450 and 1550 cm^{-1} for the high conducting state. The vibrational modes of antisymmetric stretching and scissoring are both observed again, with the peaks at 1360-1440 cm^{-1} corresponding more to the Nitrogen group scissoring with respect to the Benzene Carbons while the peaks at 1560 to 1600 cm^{-1} correspond more to the Nitrogen group stretching with either the alpha or beta benzene ring. The Raman spectrum shows some notable differences for the different conformations, such as the peaks at 1360-1440 cm^{-1} present for the alpha conformation, but is much less defined for the Beta conformation, and combined into a single peak for the Delta conformation. These modes correspond to all of the benzene rings bending symmetrically with respect to the nitrogen groups. The prominent peak at 1560 to 1600 cm^{-1} is associated with the entire center benzene ring being distorted by being stretched antisymmetrically with both of the nitrogen groups. From the results presented above, it appears that different molecular conformations are not the driving force behind the switching behavior observed experimentally. Other factors such as charging effects might play a more determining role in changing the conductivities of the molecule.

4.4.3 IET Spectrum of Ionized Oligoaniline with Single Atom Pd and Au Contacts

Upon charging the molecule, the IET characteristics of each conformation shouldn't bear any resemblance to the IET spectrum of the neutral Oligoaniline systems due to the shifting of electronic states. Additional factors that will influence the conductivity include the Coulomb Blockade phenomena induced by the -1 Charged state, where electrons are prevented from tunneling into the molecule reducing the relative intensities. Figures 40 to 43 below present the IR and Raman spectrum for the negative and positive ionized Oligoaniline molecule with a single contact atom.

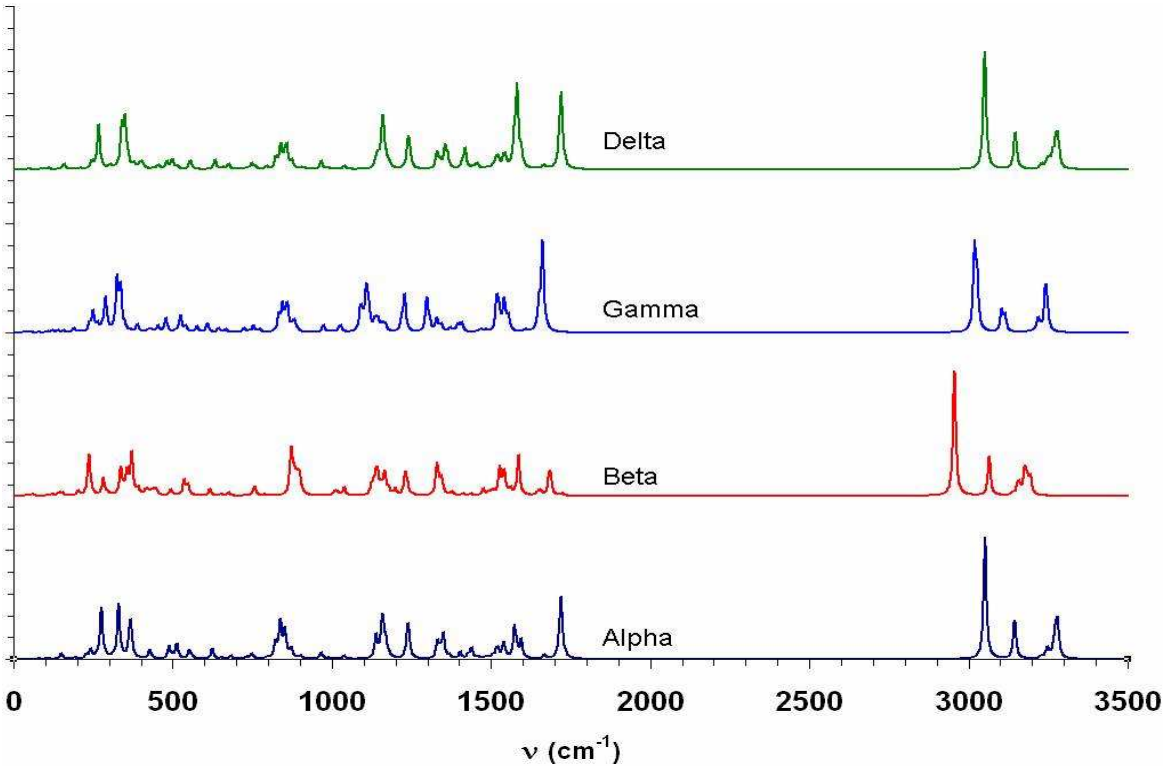

Figure 40. IR spectrum of single Pd-Au antisymmetric oligoaniline anion

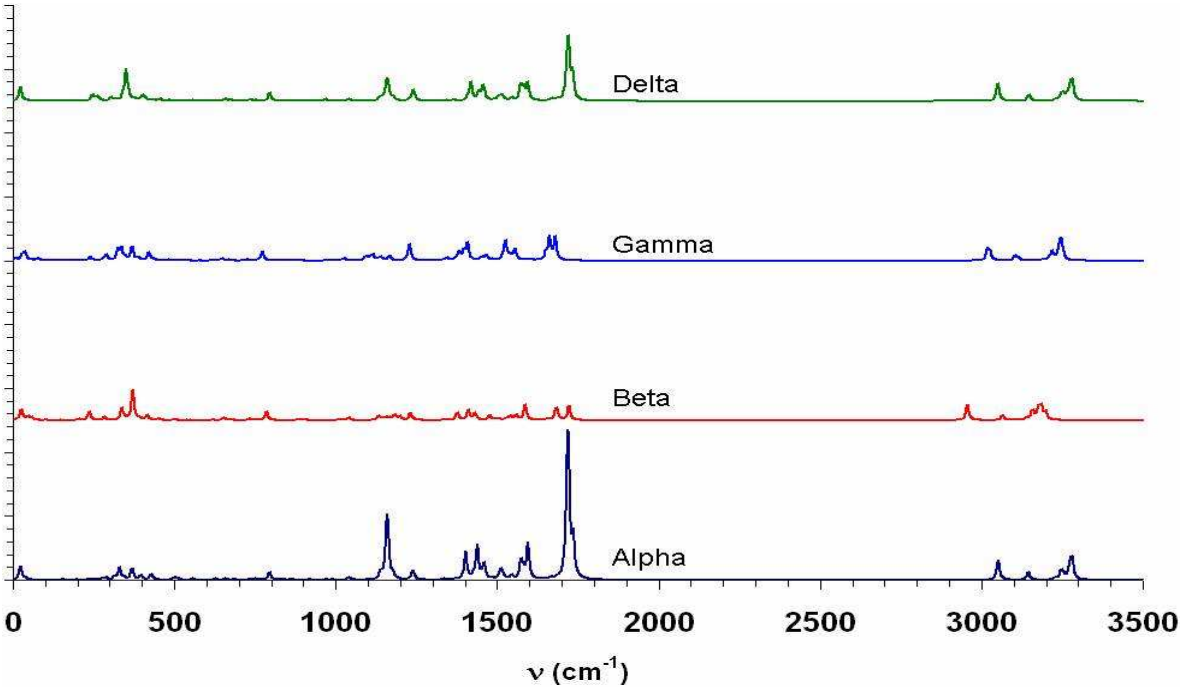

Figure 41. Raman spectrum of single Pd-Au antisymmetric oligoaniline anion

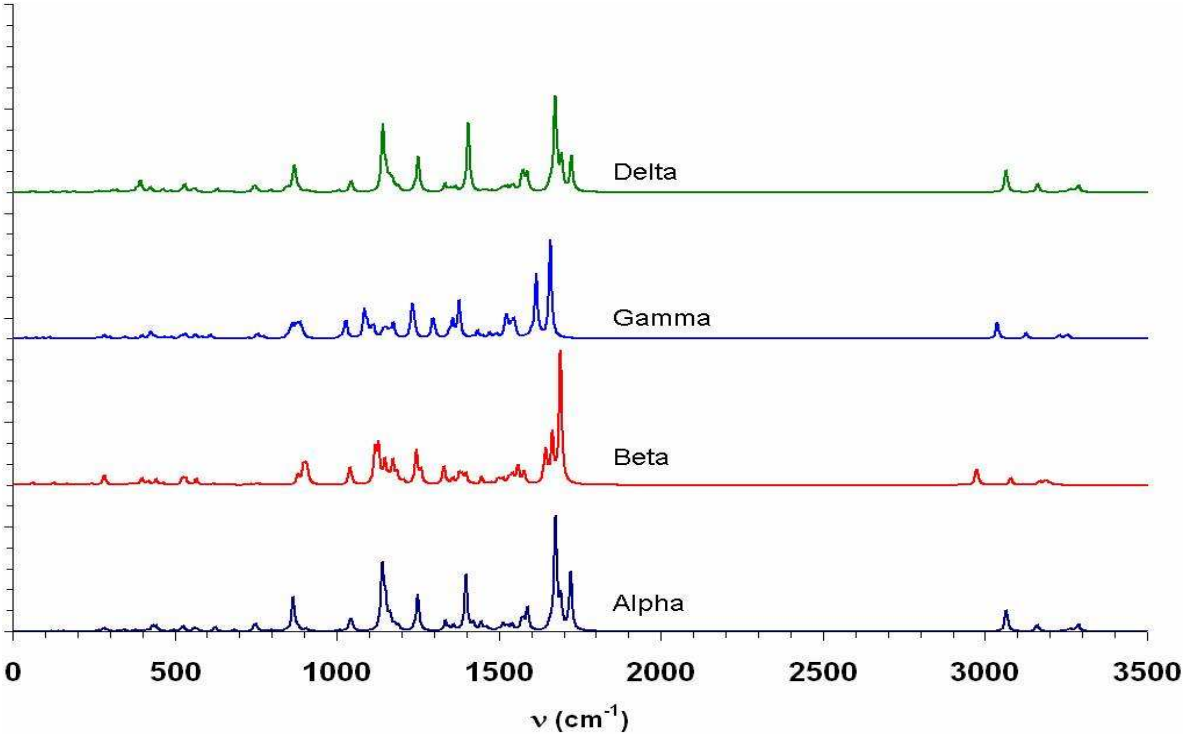

Figure 42. IR spectrum of single Pd-Au antisymmetric oligoaniline cation

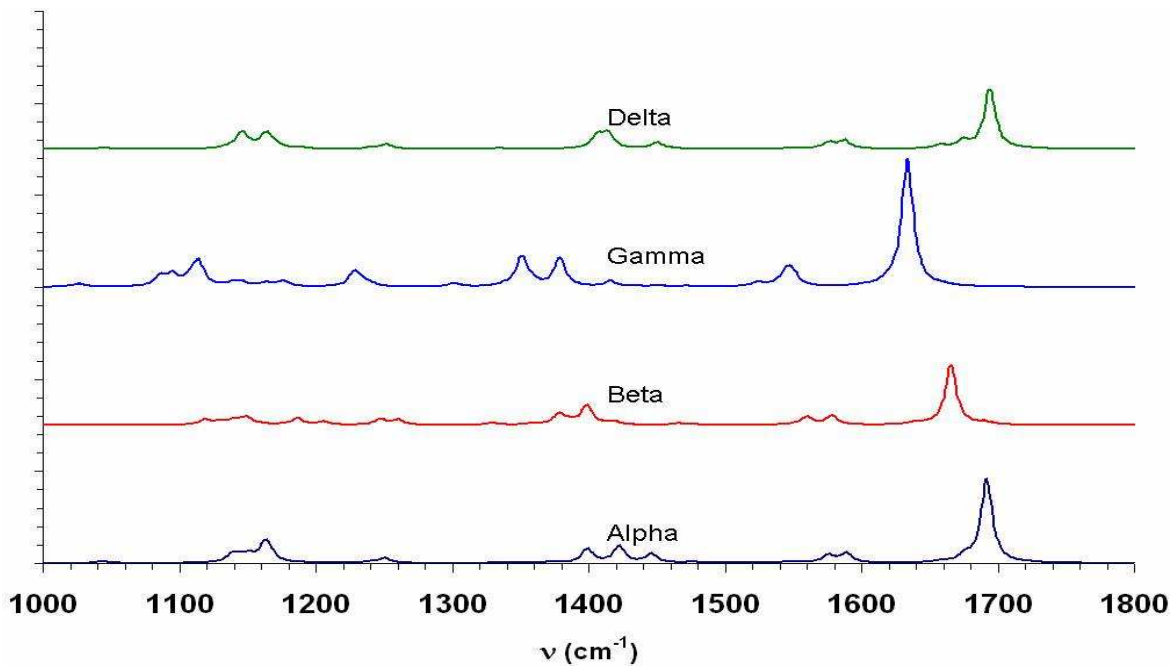

Figure 43. Raman spectrum of single Pd-Au antisymmetric oligoaniline cation

From the figures above, it can be seen that the IET spectra of each conformation start to deviate from each other.

For the anion Oligoaniline, the prominent peak around 1700 cm^{-1} is not present for the Beta conformation. The intensity of that peak is much lower than for the other conformations, suggesting a lower relative delocalization around the center benzene ring. The wavenumber of 1600 cm^{-1} corresponds to the carbon-nitrogen double bond, which leads to a conjugated bond between the nitrogen group and the benzenes. This is consistent with the MO diagrams for the -1 ionized Oligoaniline system, where the Beta conformation demonstrated the least delocalization while the Alpha and Delta conformation were the most delocalized. The peaks around 850 cm^{-1}, or 900 cm^{-1} for the Beta conformation correspond to symmetrical out-of-plane bending for the benzene hydrogens for the gold side. The peaks around 1150 cm^{-1} are associated with the symmetric scissoring of the benzene hydrogens for each side, with a little out-of-plane symmetric bending from the nitrogen group. The peaks around 1700 cm^{-1} correspond to the in-plane symmetrical bending of all the benzene hydrogens.

For the cation Oligoaniline, the delocalization behavior is essentially reversed for that of the anion. This time, the Beta conformation exhibits the highest relative intensity peak around 1600 cm-1, implying the highest delocalization, which matches the results from the +1 Beta MOs. It can be seen that the Alpha, Delta and Gamma peak at around 1670 cm^{-1} splits into two peaks for the Beta conformation, but cannot be constituted as evidence for the switching behavior. The peaks around 1150 cm^{-1} are associated with the slight out-of-plane bending for the nitrogen methyl group on the gold side. The 1250 cm^{-1} peak corresponds to the in plane scissoring of the benzene hydrogens for the alpha benzenes only, and the stretching of the nitrogen methyl group on the palladium side. The peak at 1400 cm^{-1} corresponds to the nitrogen stretching with the alpha benzene carbons. The Raman peak around 1680 is associated with the antisymmetrical benzene carbon stretching for only the center ring and the gold side ring. The cation Oligoaniline exhibits much more nitro group activity than the anion, implying more delocalization.

4.5 Dynamical Behavior under Bias

From the results of the MO diagrams and the IET spectrums for each conformation, the basis of the switching behavior in the Oligoaniline molecule is likely rooted in the change in charge delocalization coupled with different ionization states as the applied voltage exceeds a critical threshold value.[18] This postulation is a reasonable assumption only if the molecules are able to exhibit the established conformational changes under different biases, demonstrating physical switching behavior. In order to test this dynamic behavior, ab initio methods were again used to conduct conformational optimization for the Oligoaniline molecule under different fields. Outlined previously in the Methodology section in Chapter III, only the anti-symmetric single contact atom system is treated. The molecule corresponding to different conformations is rotated parallel to the Z-axis, and then geometry optimizations of the molecule is performed in the presence of varying electric fields to test the stability of each of the conformations. The contact atoms are not fixed in position since it is presumed that the adjacent contact area moves slightly to accommodate the molecular movements. If the contacts were truly fixed, the conformations will not be able to switch to the other conformations due to the different molecule lengths. Please refer to section 3.3 for more details. Table X summarizes the results for the neutral molecule, the numbers correspond to the field applied in atomic units, which results in different voltage for different Fermi levels and molecule lengths.

Table X – Conformational changes under bias for the neutral oligoaniline

-35	-30	-25	-20	-10	0	10	20	25	30	35
δ	δ	δ	α	α	α	α	α	δ	δ	δ
α	α	γ	β	β	β	β	γ	γ	α	α
α	α	α	δ	γ	γ	γ	δ	α	α	α
α	α	δ	δ	δ	δ	δ	δ	α	α	α

The results show that that the molecule can change from one geometry to another, supporting the possibility that conformational changes do play a part in the switching mechanism. However, within the range of bias voltages investigated, the results yield that the α conformation is the most stable, consistent with it being the conformation with lowest total energy. Upon being subjected to the field, it appears that every conformation converts to an alpha configuration after a threshold voltage of approximately 1.8 V, though β switches (to a γ) even before 1 V. The alpha configuration stays unchanged until around 2.5 V where it then converts to a delta configuration. In order for a conformation to serve as a conducting state, it must retain its geometry under the applied bias until the threshold voltage is reached, where it then switches to the other state, which should also be stable for a range of voltages. The alpha and delta conformations exhibit this characteristic, but the previous MO analysis suggest that the conductivities of the two conformations should be quite similar.

To study the effect of charge on the dynamic field behavior, the molecule for each conformation are either charged with or stripped of one electron and subjected to the same treatment, where the geometries are optimized in the presence of an electric field {calculation in progress}. A major downfall in this method is that the calculations involve static charge behavior for each molecule. What this means is that it cannot account for scenarios where the molecule is initially neutral and then is ionized in the middle of the run. In other words, the molecule must be either neutral or charged from the initial setup of the run. From Table XI, the molecule does not exhibit any switching behavior at all when positively charged, implying no conformational effects at all.

Table XI – Conformational changes under bias for the oligoaniline cation

-35	-30	-25	-20	-10	0	10	20	25	30	35
γ	γ	γ	γ	γ	α	γ	γ	γ	γ	γ
γ	γ	γ	γ	γ	β	γ	γ	γ	γ	γ
γ	γ	γ	γ	γ	γ	γ	γ	γ	γ	γ
γ	γ	γ	γ	γ	δ	γ	γ	γ	γ	γ

4.6 Chapter IV Summary

The first section of this chapter covered the MO diagrams of the molecule and was shown that the molecule without contact atoms is fully delocalized around the HOMO and LUMO. Upon attaching contact atoms, the delocalization decreased due to the barrier induced by the discontinuous metal-molecule interface. The symmetric Gold-molecule-Gold system showed a better coupling and delocalization than the symmetric Palladium-molecule-Palladium system. Another dissimilarity between the two systems is that the predominant charge carrier for the Gold system is holes while electron transport govern the conduction process for the Palladium system. The anti-symmetric case exhibited an even more limited delocalization, perhaps due to the antisymmetry of the two contact ends. The Beta conformation was shown to exhibit the highest delocalization around the HOMO out of the four conformations, suggesting a hole transport mechanism for conduction.

The second part of this chapter covered the MO diagrams of the anion and cation states of the molecule to see how charge effects will affect the conductivity. Results showed that the delocalization for -1 charged molecule was severely reduced, an effect similar to the Coulomb Blockade Effect where the extra electron prevents electrode electron from tunneling into the molecule. Here it was found that the Alpha and Delta conformation had a higher delocalization than the Beta one, an occurrence that was not observed for any of the neutral Oligoaniline systems. On the contrary, results for the +1 charged molecule demonstrated a much higher delocalization, especially for the Beta conformation.

The third segment of this chapter covers the IET spectroscopy analysis for the standalone molecule, the trimer contact atom system, and the ionized states of the molecule. The IR and Raman spectrums for the neutral systems were all found to be quite similar but the switching behavior found in the experimental IET was not observed for the neutral systems. The results for the ionized states provided some supporting evidence for the switching behavior, but were not definite enough draw any appropriate conclusions.

The last section of this chapter analyzes the dynamical behavior of the molecule under various biases to test whether conformational changes plays any part in the switching behavior. It was found that that all the conformation states convert to the Alpha state at the threshold voltage of about 1.8 V, except for the Alpha conformation, which switches to a Delta conformation at about 2.5 V.

These 4 factors just listed are important in providing information on how conformational changes and charge states are related to the conductivity, but some of the results have been speculative so far. For example, delocalization for the MOs signify conductivity, but how much does each MO contribute to the electrical current when different fields are applied? In order to develop a more quantitative treatment for the effects of conformational changes on conductivity, an electrical analysis will be necessary to complement the results from this chapter.

CHAPTER V

ELECTRICAL ANALYSIS

In order to have a more quantitative analysis on the molecule's conductivity, I-V plots are essential in making definite comparisons between the different conformations and ionization states. MO diagrams give a general idea on whether the molecule will be a good conductor or insulator but does not give information regarding the effects of the molecular orbitals on the magnitude of the current. There are three main factors that determine the contribution of a MO to the current: (1) its energy position relative to the Fermi energy of the molecule, (2) its degree of delocalization, and (3) its coupling to the contacts. As mentioned in the Methodology section, the current is calculated by integrating the Transmission probability function relative to the Fermi Level, which is directly related to the degree of delocalization of the MO at a particular energy level. The Transmission probability function represents the probability that an electron will traverse from the electrode, past the molecule-metal interface and through the molecule. This probability arises from the metal-molecule interface, which forces the semi-infinite number of nodes of conduction in the electrode to redistribute themselves with respect to the discrete number of conduction nodes for the standalone molecule. Another means of analyzing the effects of the MO's on the current is the density of states (DOS), which refers to the quantized energy levels of the standalone molecule resulting from the shifting and overlapping effects of the metal contacts. The DOS also represents the state energies that the electrons are allowed to occupy, usually a small number due to the mismatch between the energy states of the molecule and metal.

In this chapter, the I-V curves, DOS and Transmission probability functions are calculated for the Oligoaniline systems #3-#5. An additional analysis is performed on the ionized states of the Oligoaniline molecule in the same manner. Characteristics in the I-V curve are explained through the DOS and Transmission plots with references to the MO diagrams.

5.1 Symmetric Single Atom Contact Pd System

The I-V analysis of the symmetric single Pd atom system for the four conformations are shown below in Figure 44.

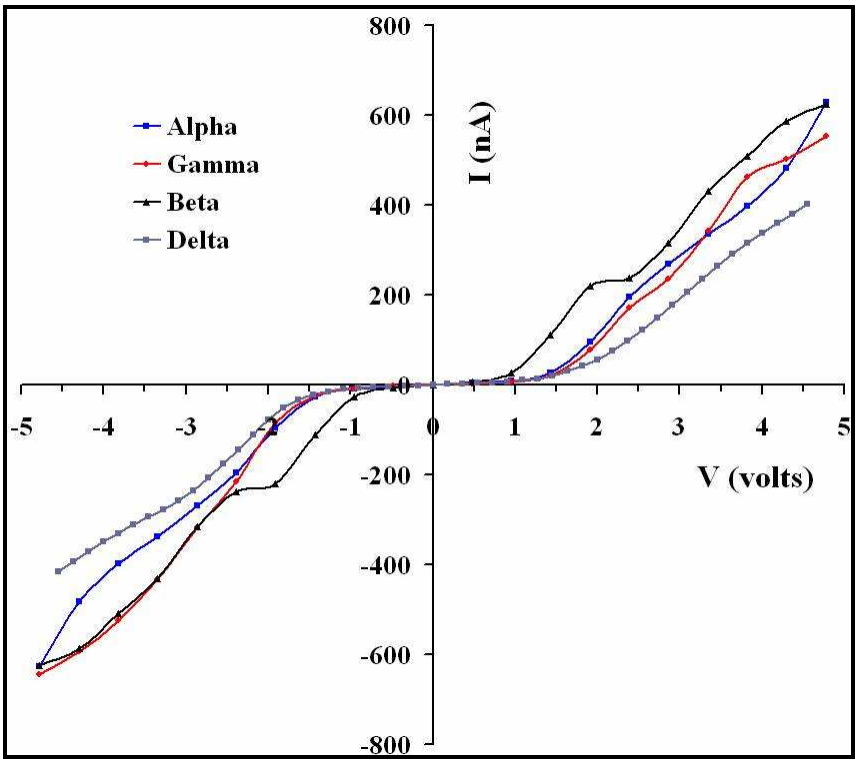

Figure 44. IV for symmetric single Pd atom contact system

As expected, the Beta conformation exhibits the highest conductivity, while the other conformations have lower, similar conductivities, as represented by the MO diagrams. The Beta curve shows traits of the hysteresis curve observed experimentally at around the range of -2 to 2 volts but the magnitude of the observed current is several times smaller than the experimental values. If it wasn't for the molecular analysis in the previous chapter, it would have been thought that the switching behavior was between the Beta conformation with the Alpha conformation. Another key observation is that the Alpha and Delta conformations deviate starting at 1.5 and -1.5 V, which follows from

the different energy states observed in the molecular orbital analysis for the symmetric Pd contact system. A possible reason for the difference in conductivities could be that the orientation effects of the side benzene rings are now more sensitive to the palladium metal – molecule coupling.

The current of all four conformations first increases sharply at around 1 V, shown by the broad peak in the transmission function at about 1 eV from the Fermi Level in Figures 45 to 48. The second increase occurs at about 2.5 eV from the Fermi Level. From the Beta MO diagrams for the single Pd contact atoms, it can be seen that the molecule starts to exhibit delocalization around -5.7 eV, where is there is a small noticeable peak in the DOS. It is at this point too that the Transmission function starts increasing, as seen in the figures. As mentioned in the Methodology section, the current is calculated directly from the integration of the Transmission function shifted around the Fermi level. The sharp narrow peaks for the Transmission function at around -7.5 eV and -9.5 eV correspond to bad coupling regions due to the presence of both the thin Transmission peak and the DOS peak. This is because the rise of additional states is associated with only a small increase in the area under the Transmission curve. However, there is a good coupling region in the Alpha and Gamma conformation at around -9 eV that is not present in the Beta conformation. The sharp DOS peaks at around -7.25 and -7.5 refer to fully delocalized MOs. The location of the DOS peaks for the Alpha and Delta conformations are similar except at around -9.75 eV, where the lone DOS peak for Alpha is split into two peaks for the Delta conformations seen in Figures 45 and 48. The magnitudes of the DOS peaks for both conformations are also quite different, but the main difference lies in the DOS peak at -9 eV, which corresponds to a large, broad peak in the Transmission function. Although the shape of the Transmission function around this point is similar for both conformations, the peak for the Alpha is much higher and broader, which corresponds to the higher current starting from 1.5 V on the IV plot.

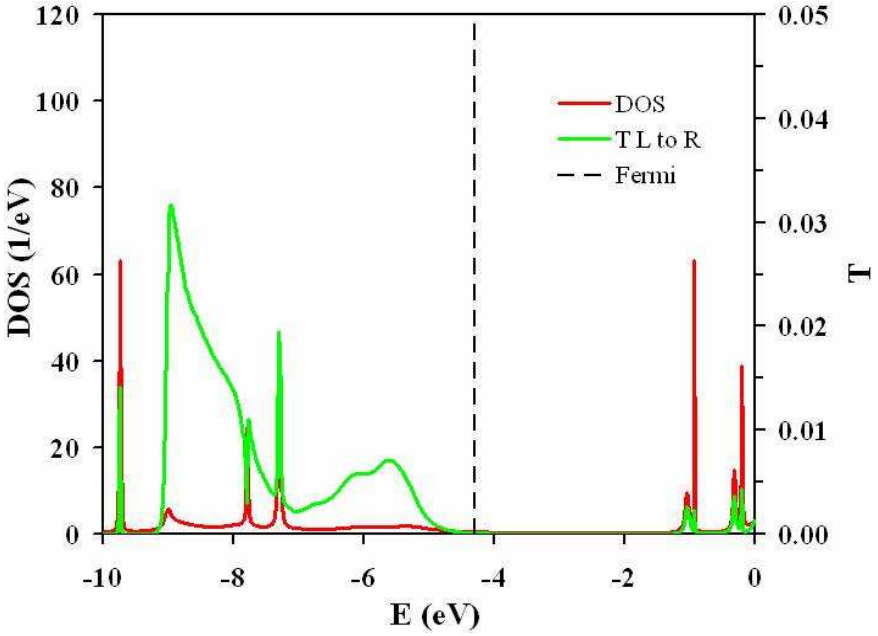

Figure 45. Single Pd atom contact system DOS/TR for alpha

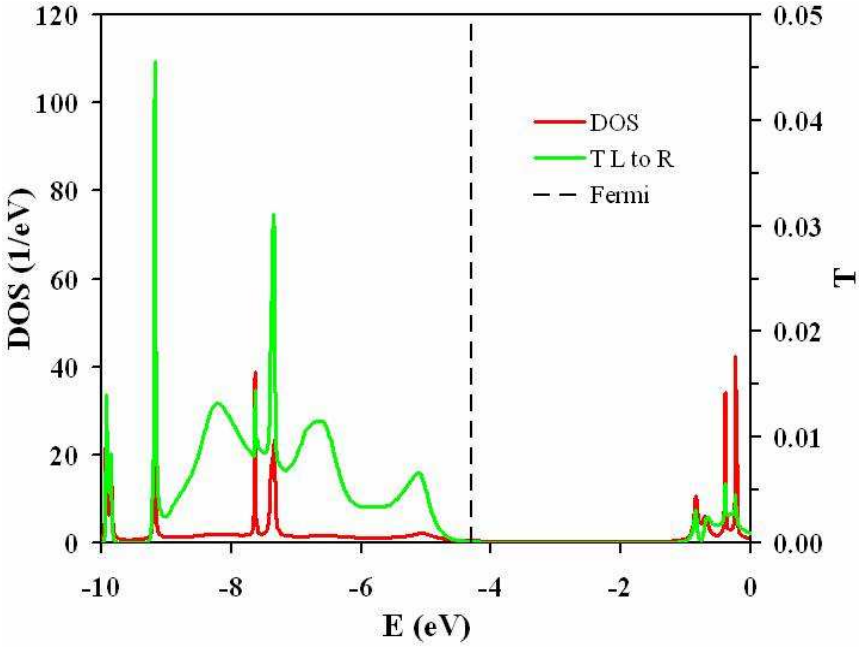

Figure 46. Single Pd atom contact system DOS/TR for beta

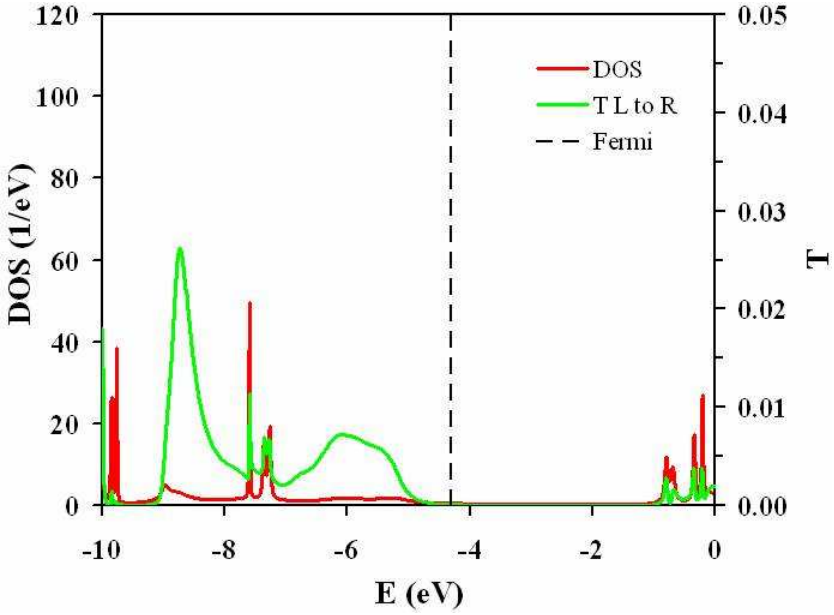

Figure 47. Single Pd atom contact system DOS/TR for gamma

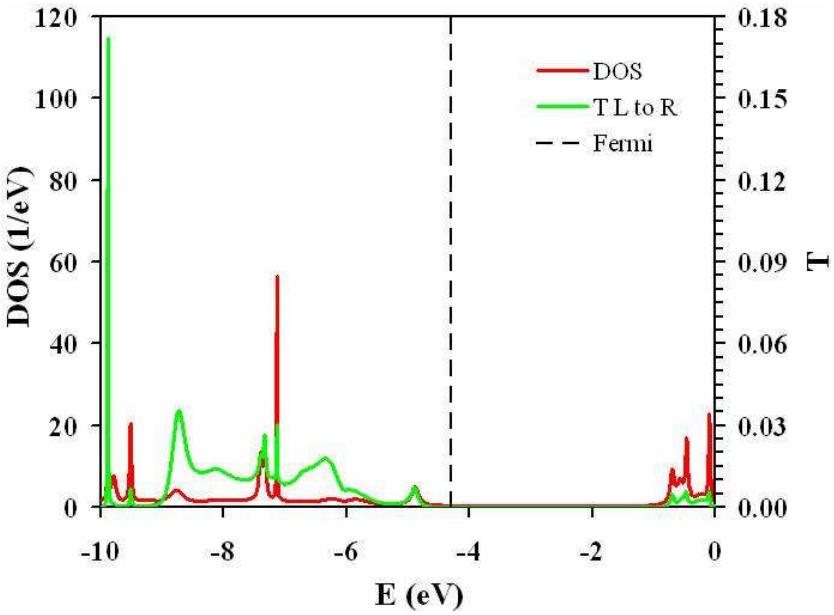

Figure 48. Single Pd atom contact system DOS/TR for delta

5.2 Symmetric Single Atom Contact Au System

The I-V plots of the symmetric single Pd atom system for the four conformations are shown below in Figure 49.

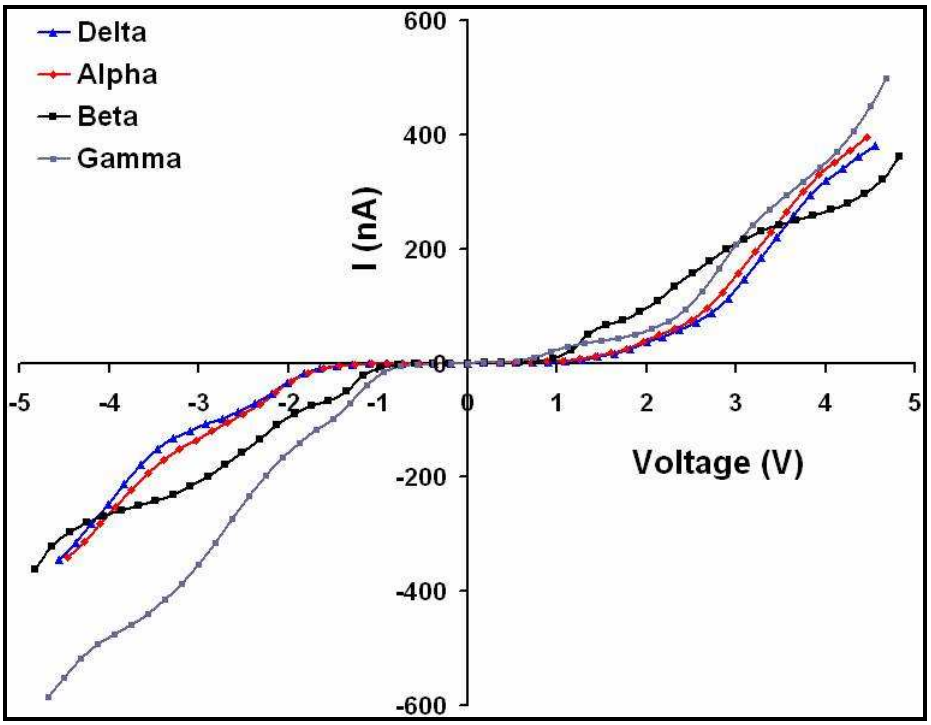

Figure 49. IV for symmetric single Au atom contact system

In the symmetric system for the single Au contact atom system, the Beta conformation exhibits the highest current up to around 2.8 V, whereupon the current of the Gamma conformation overtakes the current of the Beta conformation. The current for the Delta and Alpha conformation are quite similar for negative and positive voltages, consistent with the similar energy levels found in the MO analysis. It can also be seen that the current for this system doesn't increase as fast for the symmetric palladium system; the current for the palladium system at 3 V is already over 200 nA whereas the current for the gold system just reaches 200 nA. This answers the question presented previously in

the MO analysis of whether the contact resistance between the palladium contact atoms and the molecule is less than the gold contacts.

The current of all four conformations first increases sharply at around 1 V, shown by the broad peak in the Transmission function at about 1 eV from the Fermi Level. The second increase occurs at about 2.5 eV from the Fermi Level, shown by the increased slope in the current around 2.5 V. The Gamma conformation exhibits a peak around -5.5 eV not seen for the other conformations, which translates to a more drastic increase in the current as seen in the I-V plot at 2.5 V. A narrow peak in the Transmission function around -7.25 eV is observed for all of the conformations, denoting an area of bad coupling. However, the narrow Transmission peak found at -7.5 eV for the Alpha and Delta conformation starts to broaden for the Gamma and Beta conformations. The broad peak around -8.5 eV for the Alpha and Delta conformation is narrowed for the Beta conformation, leading to a smaller current than the Alpha and Delta conformation. The aforementioned observations can be seen in Figure 50-53.

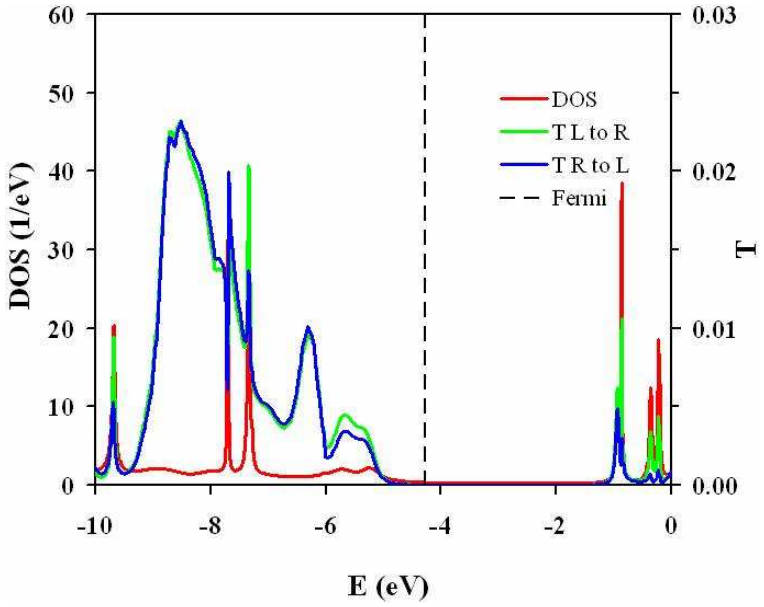

Figure 50. Single Au atom contact system DOS/TR for alpha

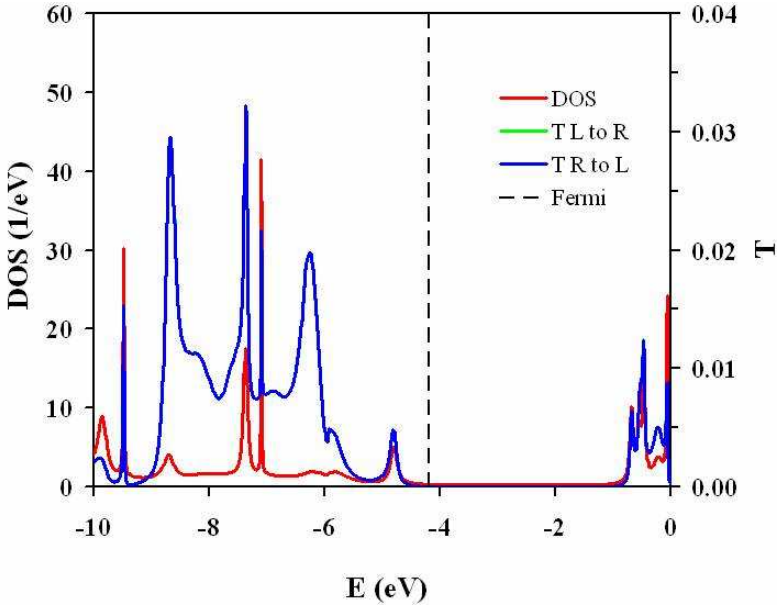

Figure 51. Single Au atom contact system DOS/TR for beta

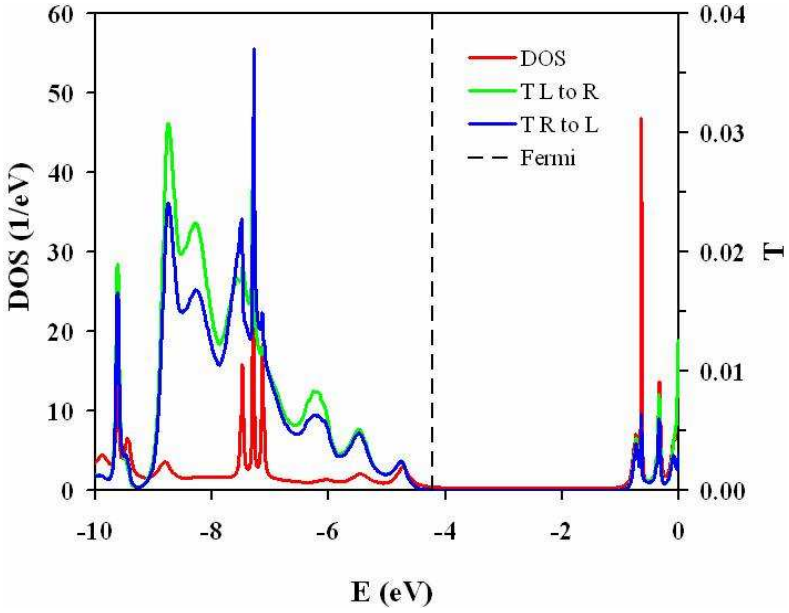

Figure 52. Single Au atom contact system DOS/TR for gamma

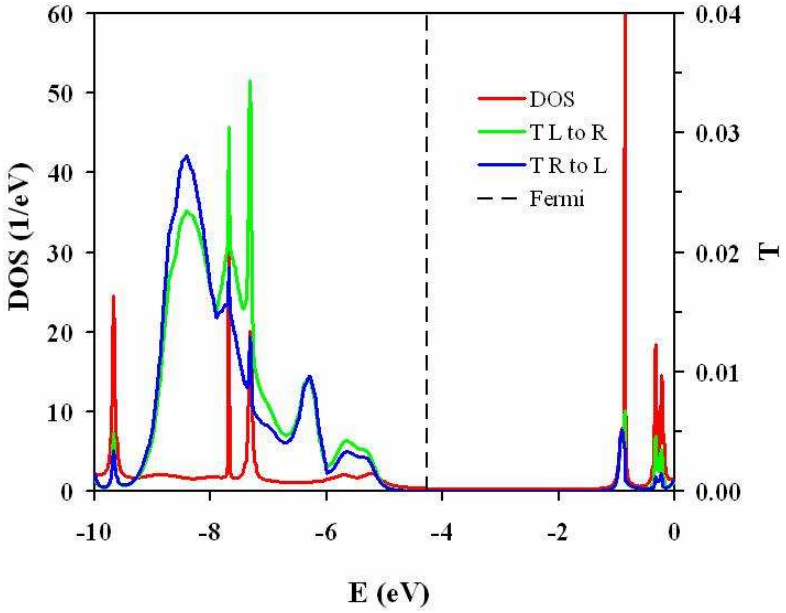

Figure 53. Single Au atom contact system DOS/TR for delta

5.3 Antisymmetric Au-Pd Contact System

The I-V plots of the antisymmetric Au and Pd contact(s) system for the four conformations are shown below in Figures 54 and 55.

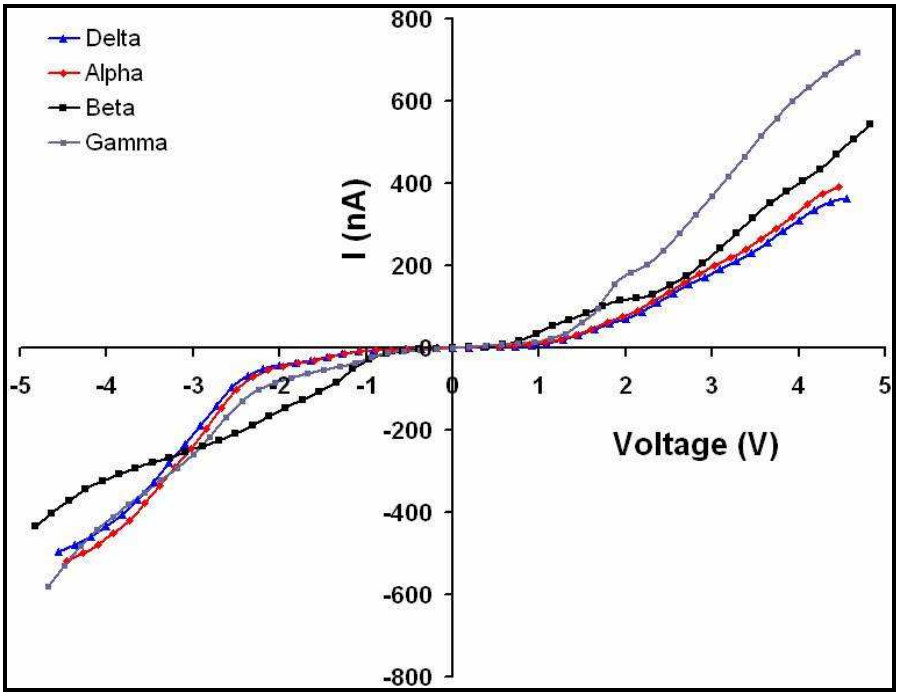

Figure 54. IV for antisymmetric single Pd-Au contact atom system

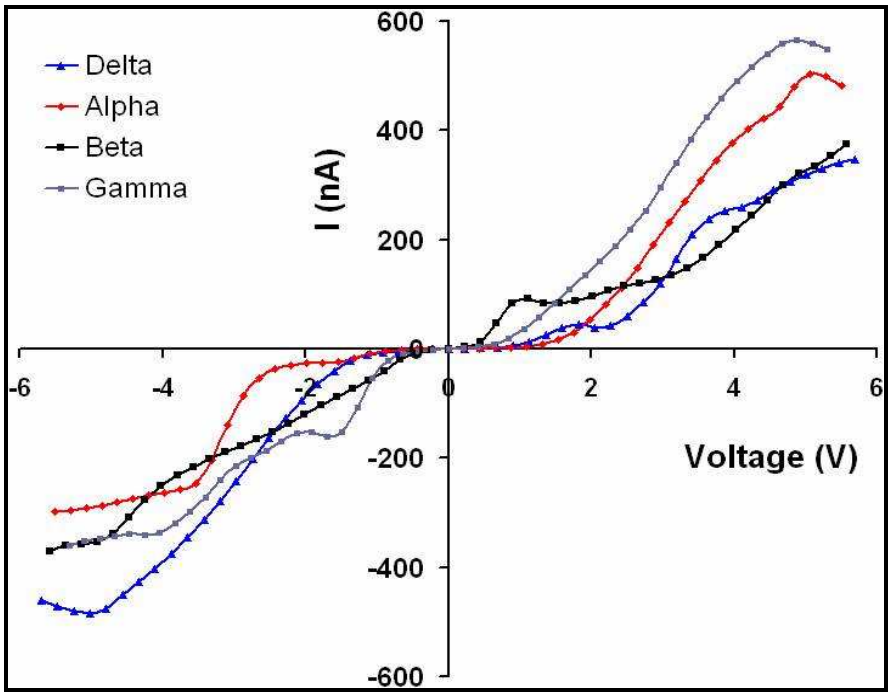

Figure 55. IV for antisymmetric trimer Pd-Au contact atom system

From the figures above it can be seen that the Beta conformation still exhibits the highest conductivity in the 2.5 V and -2.5 V range. The plot shapes of the current for all of the conformations are retained, except for the Gamma configuration that experiences a boost in the current. As the number of contact atoms is changed from one to three, the current starts to take on NDR characteristics, which is likely the representation of a true infinite contact system. The magnitude of the observed current for this system is on the same magnitude for the symmetric single Pd contact system which warrants concern since the experiment[18] yielded results that were almost forty times that of the antisymmetric system. A possible explanation could be that the antisymmetric system shown here is not the I-V associated with the true switching behavior. Another key observation to make note of is that the Alpha and Delta conformations exhibit relatively the same conductivities for the single contact atom system, but shows a significant deviation at 2V for the trimer contact atom system. There is no clear explanation for this observation, but using the results for the symmetric Pd atom contact system, it can be speculated that perhaps additional Pd atoms increases the sensitivity of the orientation effects of the side benzene rings.

Relative to the symmetric single Pd contact system, the DOS for the antisymmetric Pd Au trimer contact system decreases dramatically except for an extremely high peak at around -7.5 eV. Since the contacts are now antisymmetric, the Transmission function from right to left should be different than left to right, as shown below, where gold serves as the left electrode and palladium the right electrode. The broad peak in the Transmission function at about -5.5 eV corresponds to the current increase for all of the conformations at about 1 V. The Transmission function peaks of -7.5 eV and -9.5 eV found in the symmetric Pd system are also present here, except the Transmission peaks are much broader, corresponding to two separate increases in the current. The location of the DOS and Transmission peaks for the Alpha and Delta conformations are similar, but again have significant differences in the magnitudes of the peaks, corresponding to different currents. The aforementioned observations can be seen in Figures 56 through 59.

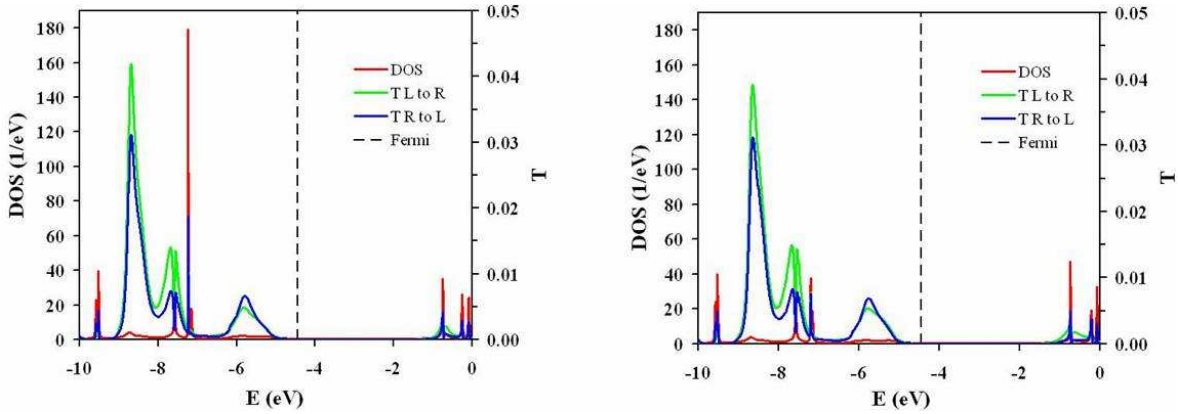

Figure 56. TR/DOS for the alpha(left) and beta(right) states for alpha with trimer atoms

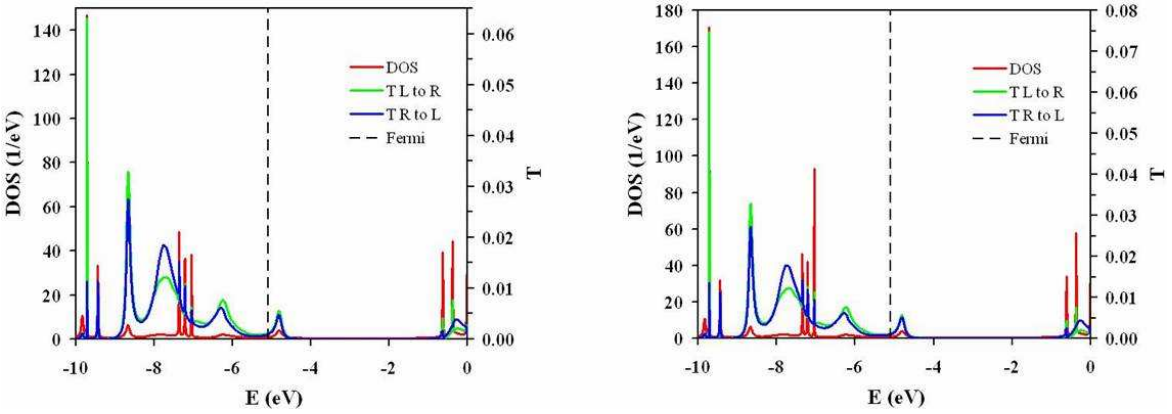

Figure 57. TR/DOS for the alpha and beta states for beta with trimer atoms

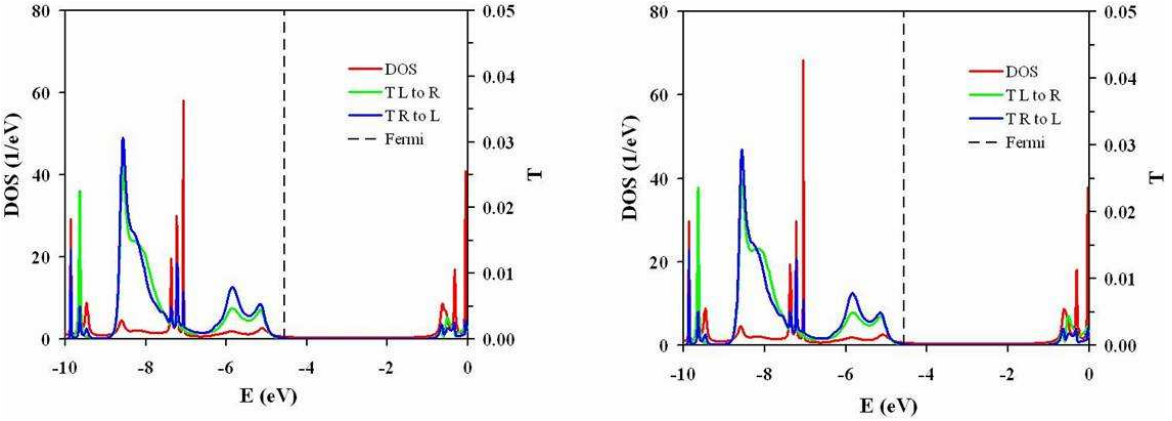

Figure 58. TR/DOS for the alpha and beta states for gamma with trimer atoms

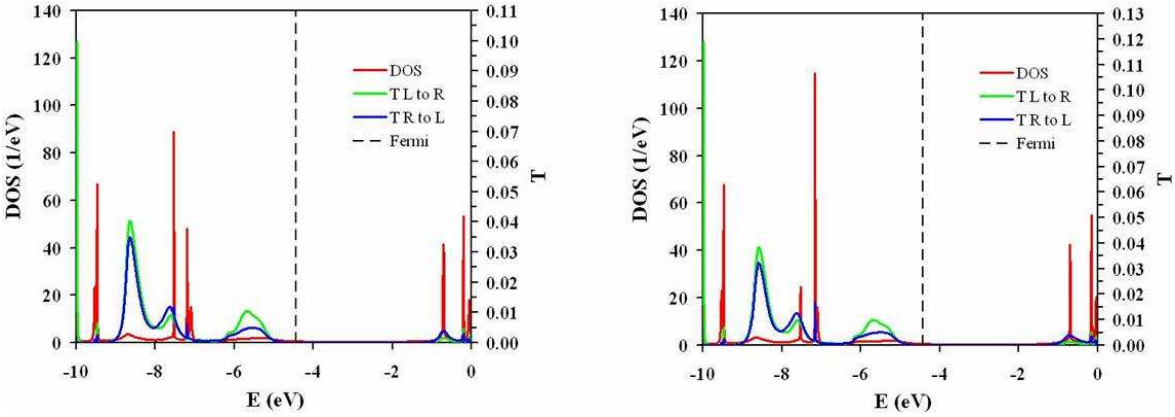

Figure 59. TR/DOS for the alpha and beta states for delta with trimer atoms

5.4 Ionized Alpha Conformation

The I-V plot of the anti-symmetric ionized single Au-Pd system for the Alpha conformations is shown below in Figure 60.

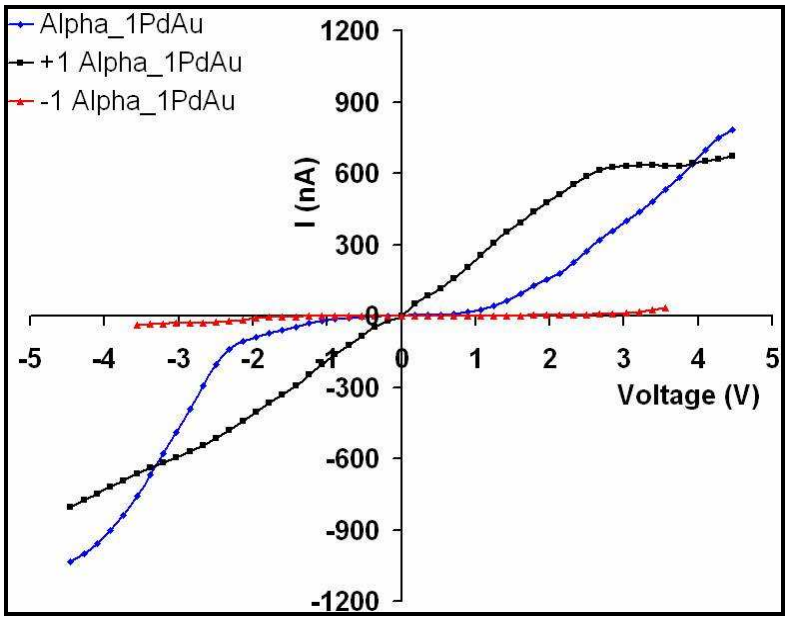

Figure 60. IV for antisymmetric single Pd-Au contact ionized alpha system

The Alpha anion shows almost no current activity, as expected from the MO analysis. As mentioned previously, this behavior most likely results where the extra electron charge prevents additional electrons from tunneling into the molecule. The Alpha cation shows appreciable current activity, and demonstrates characteristics similar to the hysteresis curve.

The number of DOS at different energies and the number of Transmission peaks increases for the Alpha anion as seen in Figure 61, but the fact that the Fermi Level is shifted considerably to the right renders a poor conductivity. This supports the Coulomb Blockade Theory, where a significant amount of energy is needed to surpass the higher barrier induced by the negative charge (shifting in the TR). For the Alpha cation, the Fermi Level is shifted to a region of low DOS states but high Transmission as shown in Figure 62, which explains the higher conductivity.

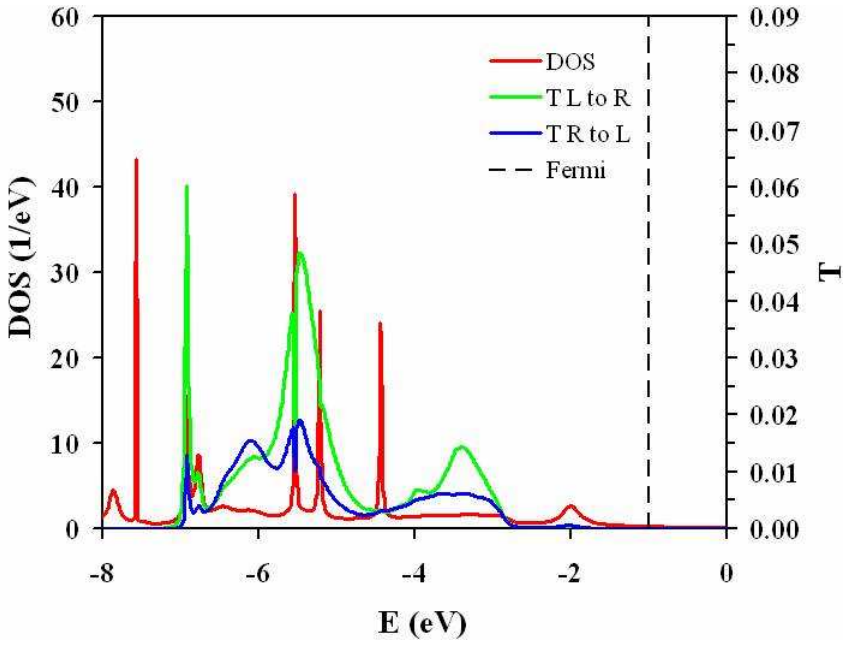

Figure 61. TR/DOS for alpha anion

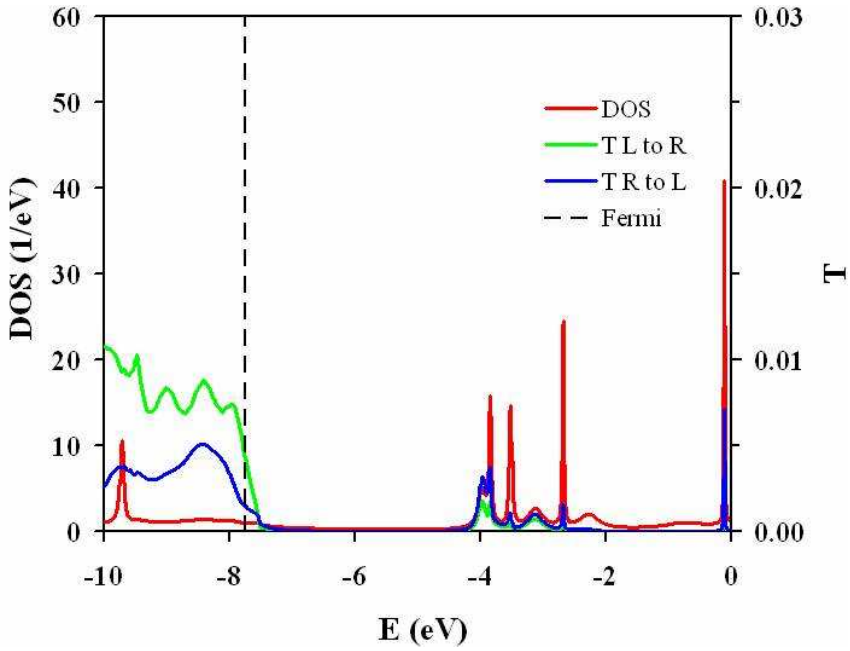

Figure 62. TR/DOS for alpha cation

5.5 Ionized Beta Conformation

The I-V plot of the anti-symmetric ionized single Au-Pd contact system for the Beta conformations is shown below in Figure 63.

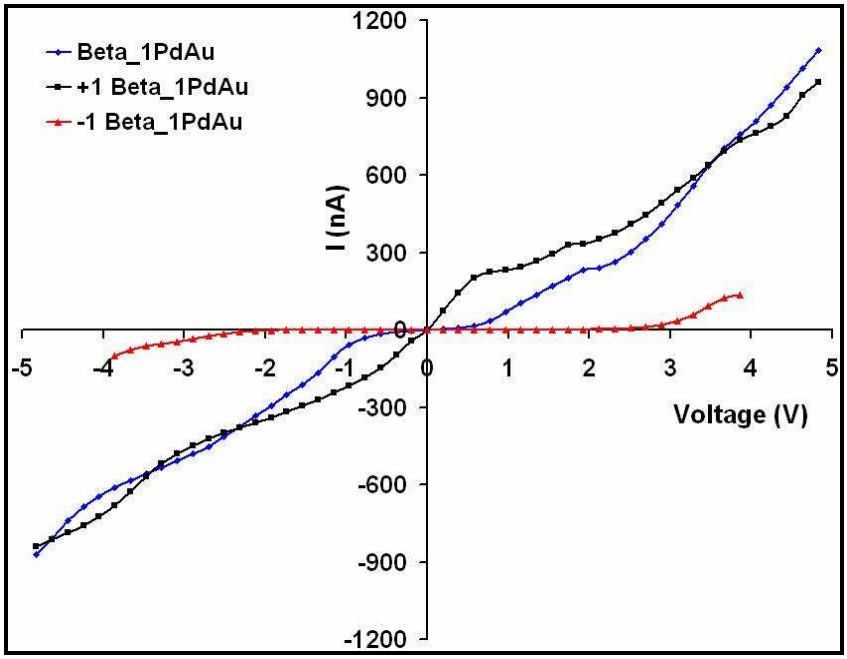

Figure 63. IV for antisymmetric single Pd-Au contact ionized beta system

The Beta anion shows almost no current activity in Figure 64, as expected from the MO analysis. As mentioned previously, this behavior most likely results from the Coulomb Blockade, where the extra negative charge prevents additional electrons from tunneling into the molecule. The Beta cation shows appreciable current activity also, and demonstrates characteristics similar to the hysteresis curve, although with more peaks and dips.

The number of DOS at different energies is higher for the ionized Beta conformation than for the ionized Alpha conformation, but the magnitudes of the Transmission peak are much lower than the Alpha conformation, which is consistent with the MO analysis. For the Beta cation, an additional DOS peak is observed, corresponding to a relatively broad Transmission peak, as shown in Figure 65. The peak at -10 eV is also higher than that for other cation conformations, leading to a higher conductivity.

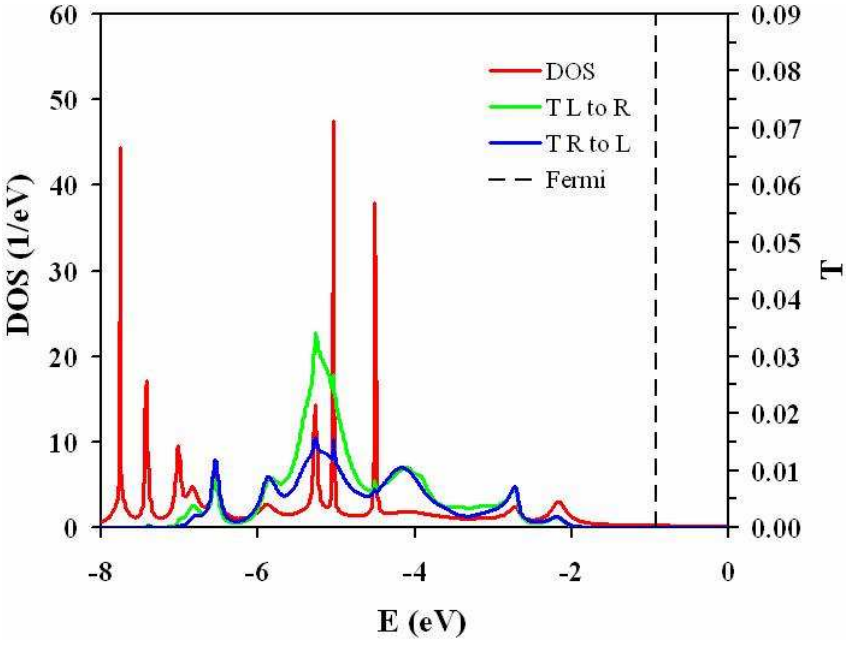

Figure 64. TR/DOS for beta anion

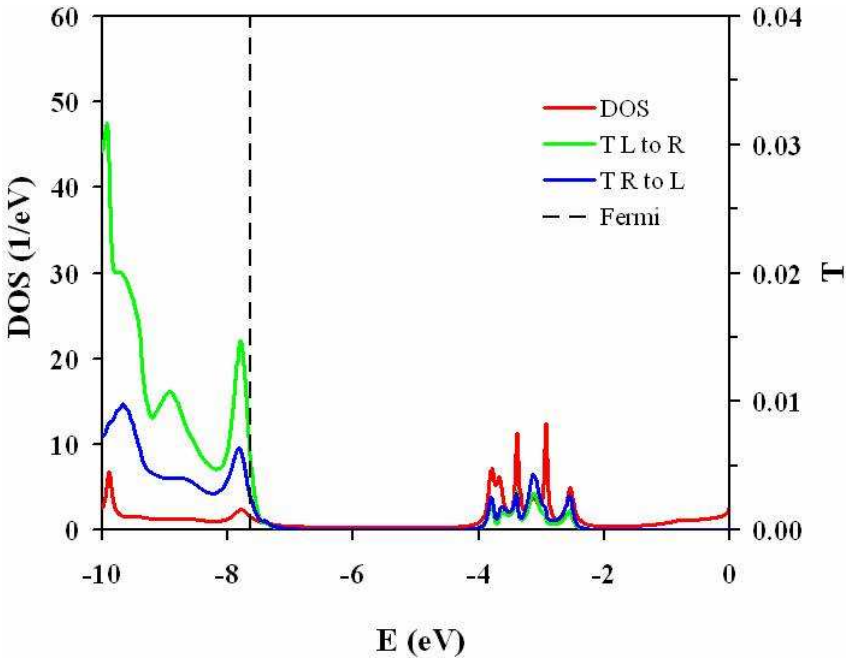

Figure 65. TR/DOS for beta cation

5.6 Ionized Gamma Conformation

The I-V plot of the anti-symmetric ionized single Au-Pd system for the Gamma conformations is shown below in Figure 66.

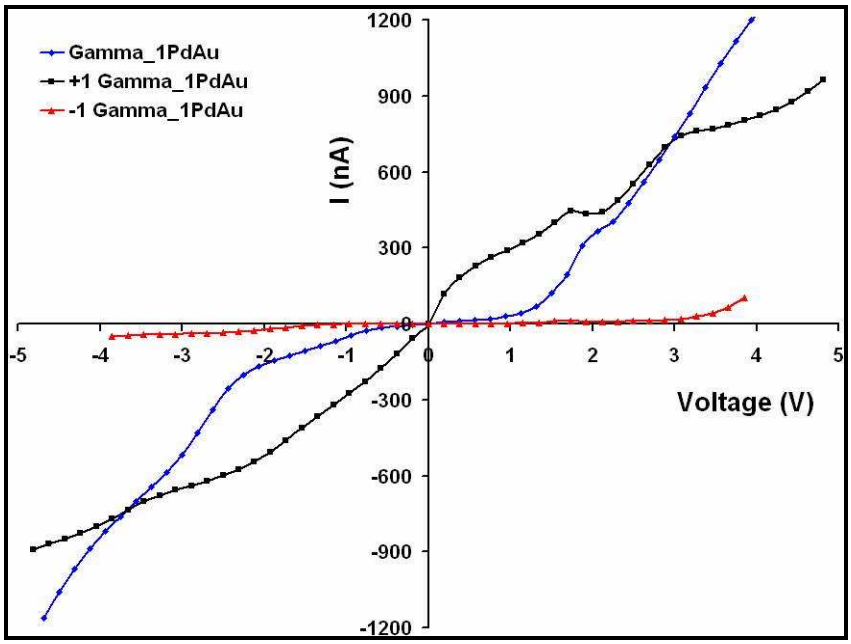

Figure 66. IV for antisymmetric single Pd-Au contact ionized gamma system

The Gamma anion shows almost no current activity in Figure 67, as expected from the MO analysis. The Gamma cation shows appreciable current activity also, and demonstrates characteristics similar to the hysteresis curve, although this current exhibits the most peaks and dips out of all the conformations.

The number of DOS at different energies is higher for the Gamma anion than for the other anion conformations, and a new Transmission peak is observed at approximately -7 eV. For the Gamma cation, one sharp DOS peak is observed around -9.5 eV in Figure 68, which doesn't correlate to any Transmission peaks, implying bad coupling.

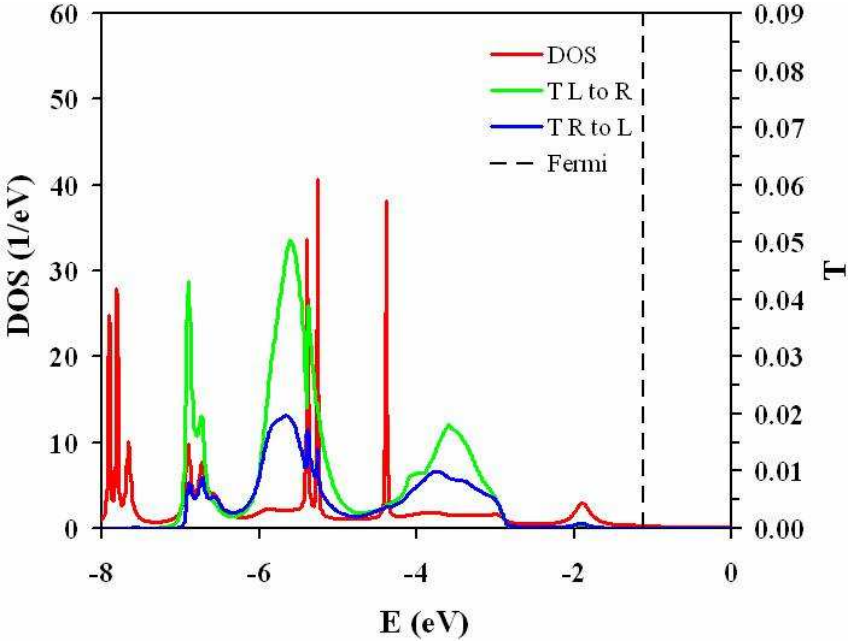

Figure 67. TR/DOS for gamma anion

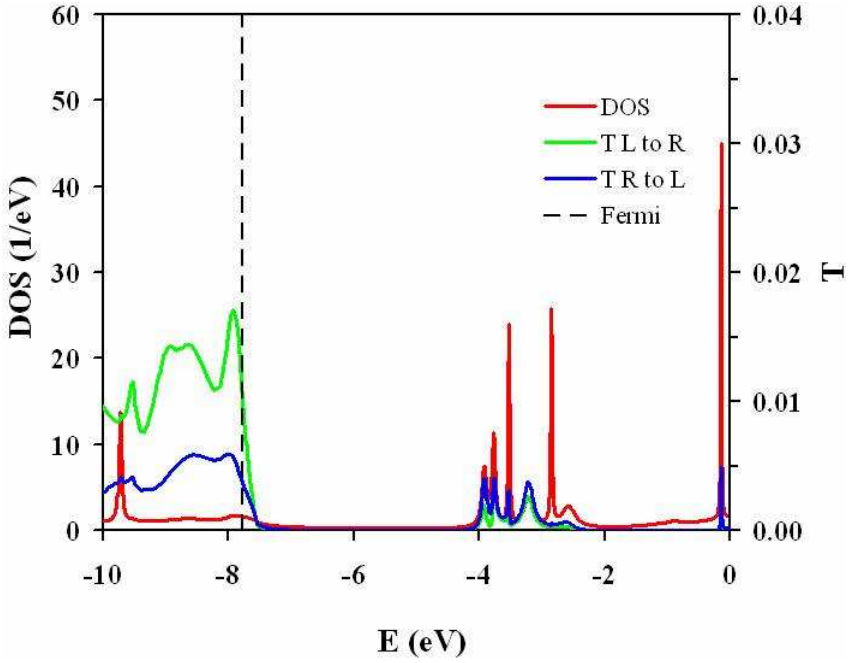

Figure 68. TR/DOS for gamma cation

5.7 Ionized Delta Conformation

The I-V plot of the anti-symmetric ionized single Au-Pd system for the Gamma conformations is shown below in Figure 69.

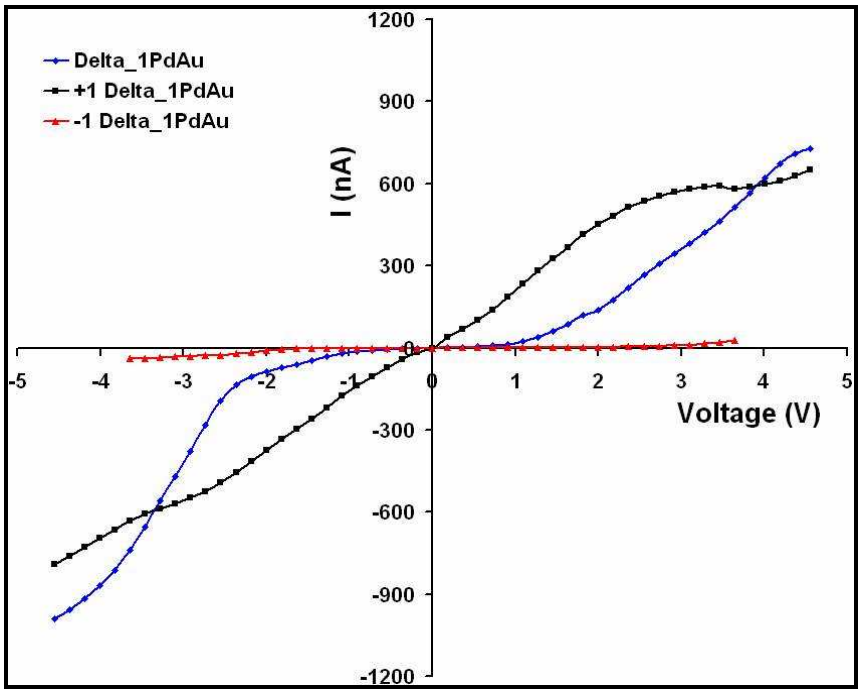

Figure 69. IV for antisymmetric single Pd-Au contact ionized delta system

The ionized Delta conformation shows similar current behavior as the ionized Alpha conformation, as expected from the MO analysis. The "well-behaved" hysteresis curve exhibited by the cation is retained, intersecting the current of the neutral molecule at the same location at about -3.9 eV

The Transmission function exhibits the same two broad peaks at -3.5 eV and -5.5 eV. The number of DOS states at different energies increases for the anion in Figure 70, most likely due to the differences in the dihedral angles of one of the alpha benzene rings. This difference in the DOS is not observed for the cation however, where there is only one lone peak at -9.5 eV for both conformations, which can be seen in Figure 71.

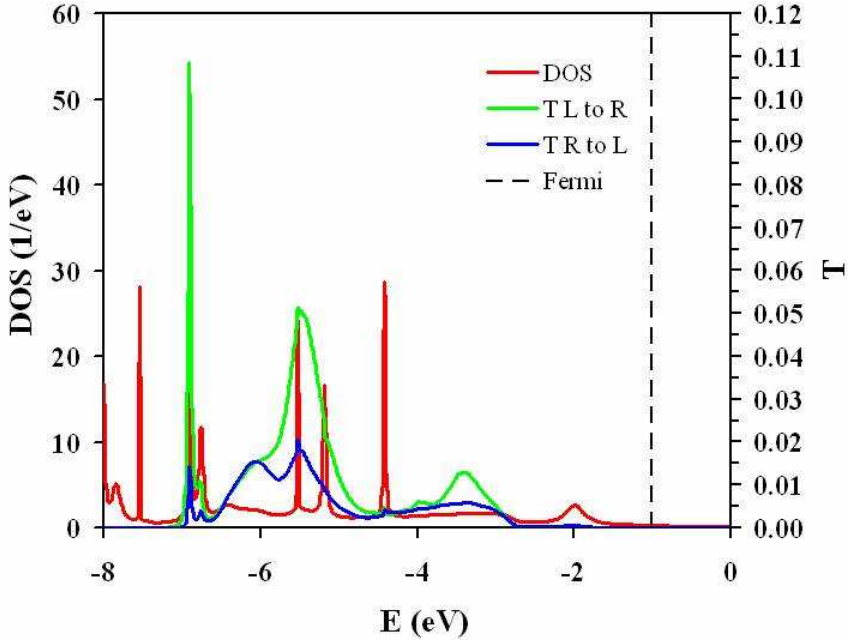

Figure 70. TR/DOS for delta anion

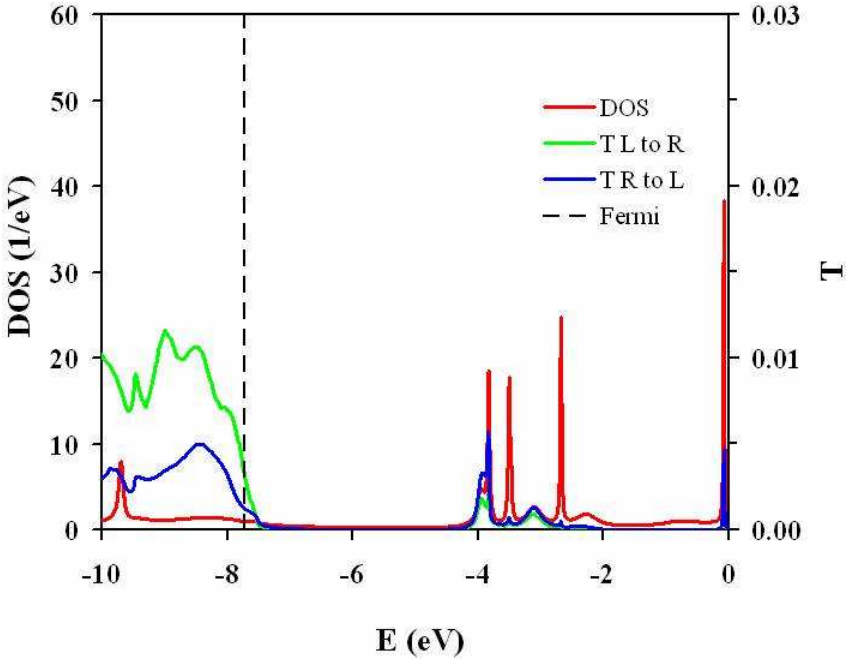

Figure 71. TR/DOS for delta cation

CHAPTER VI

SUMMARY AND CONCLUSIONS

From the molecular analysis it was found that the Oligoaniline molecule exhibits four stable conformational states with the orbitals delocalized to the same extent. The main difference in the four isomers was the orientation of the nitro-methyl groups with respect to the benzene rings. It was found that the Alpha and Delta conformations were geometrically similar in the sense that the nitro-methyl groups have the same orientation with the benzene rings on the side. Further results showed that this geometric similarity leads to similar energetic states for various Oligoaniline systems, implying that the methyl group orientation is the determining factor for the extent of delocalization around the middle benzene ring and ultimately, the conductivity. Through further molecular orbital analyses, the Beta conformation was found to have the most delocalization out of all the conformations, which is consistent with the fact that the methyl group orientation determines conductivity. The fact that there exists a high conducting state (Beta) and a low conducting state (Alpha, Delta) supports the fact that the different conducting states are associated with different molecular conformations, but an IETS analysis in conjunction with a dynamic field investigation proved that this was not the case. The IETS analysis showed the same IR and Raman activity for the Oligoaniline system, an indication that there are no significant changes to the conductivities for any of the conformations. However, an IETS analysis showed a notably different IR activity around the 1660 cm^{-1} wavelength for the Oligoaniline cation, which implies that charging effects play a major role in the conductivities. The investigation on dynamic field behavior showed that all of the conformations were converted to either Alpha or Delta, another result that lends credence that molecular conformational changes alone do not determine the conductivities.

The electrical analysis yielded consistent results with the molecular analysis, where it was found that Beta exhibited the highest current out of all the conformations in

the voltage range of concern. The electrical analysis on the Oligoaniline cation for all conformations showed an I-V curve similar to the experimental hysteresis curve, suggesting that ionization effects is indeed the major factor for the NDR switching behavior.

Based on the combined results from the molecular and electrical analyses, it seems likely that the switching behavior is a result of charging the molecule accompanied with a little change in the conformation. However, since the energy levels of the stable Alpha and Delta conformations are so similar, the effects of the molecular conformation on switching behavior can be minimized further. This conclusion is based on the consistent results from the MO diagrams, IETS analysis, and I-V calculations and will need supporting evidence from experiments in order to be substantiated

6.1 Future Work

Future work includes finding conditions for the ionization of the molecule, and also the mechanism for ionization. Temperature effects on conductivity should also be investigated to provide an explanation for the experimental results at the sub-atomic level. In addition, the results from this work can be applied to future moletronics systems to develop new means for modifications or synthesis.

REFERENCES

1. Y.Taur, *IBM J. Res. & Dev.*, **46**, No. 2/3 (2002)

2. M.A. Ratner, A. Aviram, *Chemical Physics Letters*, **29**, 277 (1974)

3. M.A. Ratner, *Materials Today*, **20** (2002)

4. J.R. Heath, M.A. Ratner, *Physics Today*, **43** (2003)

5. M.A. Reed, *FED*, **11**,57 (2000)

6. J.M. Seminario, L. Yan, *International Journal of Quantum Chemistry*, **102**, 711 (2005)

7. C.R. Nave, http://hyperphysics.phy-astr.gsu.edu/hbase/quantum/scheq.html, Mathematical Expressions for the Schrodinger Equation, February (2006)

8. H. Dorsett, and A. White, *Overview of Molecular Modeling and Ab initio Molecular Orbital Methods Suitable for Use with Energetic Materials*, DSTO Aeronautical and Maritime Research Laboratory, Salisbury, South Australia (2000)

9. W. Kohn, L. J. Sham. Phys. Rev., **140**, A1133 (1965)

10. A. D. Becke, *J. Chem. Phys.*, **98**, 5648 (1993)

11. A. D. Becke, *J. Chem. Phys.*, **98**, 1372 (1993).

12. J.P. Perdew, Y. Wang, *Phys. Rev. B*, **33**, 8800 (1986)

13. J.P. Perdew, Y. Wang, *Phys. Rev. B*, **45**, 13244 (1992)

14. J. Chen, M.A. Reed, A.M. Rawlett, J.M. Tour, *Science*, **286**, 1550 (1999)

15. M. Di Ventra, S.T. Pantelides, N.D. Lang, *Applied Physics Letters*, **76**, 3448 (2000)

16. J.M. Seminario, A.G. Zacarias, P.A. Derosa, *Journal of Chemical Physics*, **116**, 1671 (2002)

17. J. Chen, W. Wang, M.A. Reed, *Applied Physics Letters*, **77**, 1224 (2000)

18. L. Cai, M.A. Cabassi, H. Yoon, O.M. Cabarcos, C.L. McGuiness, A.K. Flatt, D.L. Allara, J.M. Tour, T.S. Mayer, *American Chemical Society – Nano Letters*, **5**, 2365 (2005)

19. M. J. Frisch, G. W. Trucks, H. B. Schlegel, G. E. Scuseria, M. A. Robb, J. R. Cheeseman, J. A. Montgomery, Jr., T. Vreven, K. N. Kudin, J. C. Burant, J. M. Millam, S. S. Iyengar, J. Tomasi, V. Barone, B. Mennucci, M. Cossi, G. Scalmani, N. Rega, G. A. Petersson, H. Nakatsuji, M. Hada, M. Ehara, K. Toyota, R. Fukuda, J. Hasegawa, M. Ishida, T. Nakajima, Y. Honda, O. Kitao, H. Nakai, M. Klene, X. Li, J. E. Knox, H. P. Hratchian, J. B. Cross, V. Bakken, C. Adamo, J. Jaramillo, R. Gomperts, R. E. Stratmann, O. Yazyev, A. J. Austin, R. Cammi, C. Pomelli, J. W. Ochterski, P. Y. Ayala, K. Morokuma, G. A. Voth, P. Salvador, J. J. Dannenberg, V. G. Zakrzewski, S. Dapprich, A. D. Daniels, M. C. Strain, O. Farkas, D. K. Malick, A. D. Rabuck, K. Raghavachari, J. B. Foresman, J. V. Ortiz, Q. Cui, A. G. Baboul, S. Clifford, J. Cioslowski, B. B. Stefanov, G. Liu, A. Liashenko, P. Piskorz, I. Komaromi, R. L. Martin, D. J. Fox, T. Keith, M. A. Al-Laham, C. Y. Peng, A. Nanayakkara, M. Challacombe, P. M. W. Gill, B. Johnson, W. Chen, M. W. Wong, C. Gonzalez, and J. A. Pople, *Gaussian 03, Revision C.02* Gaussian, Inc., Wallingford CT, 2004

20. J. S. Binkley, J. A. Pople, W. J. Hehre, *J. Am. Chem. Soc.* **102**, 939 (1980)

21. G. A. Petersson, M. A. Al-Laham, *J. Chem. Phys.* **94**, 6081 (1991)

22. G. A. Petersson, A. Bennett, T. G. Tensfeldt, M. A. Al-Laham, W. A. Shirley, J. Mantzaris, *J. Chem. Phys.* **89**, 2193 (1988)

23. R. A. Kendall, T. H. Dunning Jr., R. J. Harrison, *J. Chem. Phys.* **96**, 6796 (1992)

24. W. R. Wadt, P. J. Hay, *J. Chem. Phys.* **82**, 284 (1985)

25. M. D. Towler, A. Zupan, M. *Causa, Comput. Phys. Commun.*, **98**, 181 (1996)

26. J.M. Seminario, L.E. Cordova, P.A. Derosa, *Proceedings of the IEEE*, **91**, 1958 (2003)

27. V.R. Saunders, R. Dovesi, C. Roetti, R. Orlando, C.M. Zicovich-Wilson, N.M. Harrison, K. Doll, B. Cirvalleri, I.J. Bush, Ph. D'Arco, M. Llunell, *Crystal 03*, Torino Italy

28. J. M. Seminario, C. E. De La Cruz, P. A. Derosa, *J. Am. Chem. Soc.*, **123**, 5616 (2001)

29. R. T. Sanderson, *Science*, **114**, 670 (1951)

APPENDIX

INPUT FILES

Note: Only the input files of the Alpha conformation are shown

B.1 Symmetric one Pd contact atom Oligoaniline system

```
%chk=bZigzag_1Pd1Pd.chk
%mem=6GB
%nproc=4
#p freq=raman opt b3pw91/lanl2dz geom=connectivity

Symmetric Pd-Oligoaniline-Pd system of conformation alpha

0 1
 C                  3.74099164   -0.37738614    0.12192124
 C                  4.94295734   -0.93454011   -0.34851443
 C                  6.10477343   -0.16705166   -0.40961855
 C                  6.10499949    1.16664034   -0.01528229
 C                  4.91511644    1.72512834    0.45574712
 C                  3.75271822    0.97107825    0.53165030
 H                  4.97709837   -1.96665888   -0.67850489
 H                  7.01805007   -0.62568345   -0.77982132
 H                  7.01235554    1.76031869   -0.06834011
 H                  4.89265203    2.76156239    0.78250743
 H                  2.84358440    1.41690050    0.92120450
 N                  2.57832437   -1.14566111    0.24017975
 C                  1.29491675   -0.55224265    0.12275558
 C                  0.26928295   -0.92039872    1.00306649
 C                  1.00474892    0.37855577   -0.88342152
 C                 -1.00475047   -0.37854789    0.88347528
 H                  0.48451939   -1.61712776    1.80861287
 C                 -0.26928438    0.92040758   -1.00301109
 H                  1.78277515    0.66406416   -1.58472160
 C                 -1.29491748    0.55224980   -0.12270191
 H                 -1.78277772   -0.66405772    1.58477397
 H                 -0.48452383    1.61713974   -1.80855411
 N                 -2.57832602    1.14567473   -0.24012717
 C                 -3.74099142    0.37738926   -0.12192930
 C                 -3.75270225   -0.97105867   -0.53171570
 C                 -4.94297232    0.93451724    0.34849816
 C                 -4.91509974   -1.72511596   -0.45587713
 H                 -2.84355632   -1.41686165   -0.92126371
 C                 -6.10478697    0.16702097    0.40953850
 H                 -4.97712803    1.96662169    0.67853231
 C                 -6.10499812   -1.16665357    0.01514455
 H                 -4.89262156   -2.76153613   -0.78268062
```

```
H                 -7.01807430    0.62563448    0.77973772
H                 -7.01235310   -1.76033784    0.06815126
C                  2.66484062   -2.58291689    0.05490438
H                  2.87621511   -2.86383106   -0.98893974
H                  3.44844325   -3.00516713    0.69243890
H                  1.71345795   -3.03650159    0.33377590
C                 -2.66484099    2.58291535   -0.05473184
H                 -2.87623694    2.86374277    0.98913150
H                 -1.71344973    3.03651719   -0.33354750
H                 -3.44842822    3.00522244   -0.69224783

1 2 1.0 6 1.5 12 1.0
2 3 1.5 7 1.0
3 4 1.5 8 1.0
4 5 1.5 9 1.0
5 6 1.5 10 1.0
6 11 1.0
7
8
9
10
11
12 13 1.0 35 1.0
13 14 1.5 15 1.5
14 16 1.5 17 1.0
15 18 1.5 19 1.0
16 20 1.5 21 1.0
17
18 20 1.5 22 1.0
19
20 23 1.0
21
22
23 24 1.0 39 1.0
24 25 1.5 26 1.5
25 27 1.5 28 1.0
26 29 1.5 30 1.0
27 31 1.5 32 1.0
28
29 31 1.5 33 1.0
30
31 34 1.0
32
33
34
35 36 1.0 37 1.0 38 1.0
36
37
38
39 40 1.0 41 1.0 42 1.0
40
41
42
```

B.2 Symmetric single Au contact atom Oligoaniline system

```
%chk=bZigzag_1Au_1Au.chk
%mem=6GB
%nproc=4
#p freq=raman opt b3pw91/lanl2dz geom=connectivity

Zigzag System attached to 1 Au and 1 Au

0 1
 S                  8.82794199    0.97760648   -0.06450373
 C                  7.16598799    0.53109148    0.40646827
 C                  4.55637199   -0.14749352    1.24480027
 N                  3.28149099   -0.45986952    1.69363527
 C                  2.12477599    0.10683348    1.10822527
 C                 -0.21772901    1.18068848   -0.02453273
 N                 -1.37401901    1.74891148   -0.61070073
 C                 -2.64915801    1.43276848   -0.16593073
 C                 -5.26167301    0.74421448    0.65508427
 S                 -6.90277701    0.34078048    1.22882327
 C                  6.09350599    1.39169248    0.17447727
 C                  4.81525699    1.06197748    0.57714127
 C                  6.92207799   -0.65848152    1.07939327
 C                  5.64301899   -0.99743552    1.49430327
 H                  6.26971799    2.34020848   -0.31741773
 H                  4.00704699    1.75732448    0.39667327
 H                  7.74318699   -1.33627352    1.27637027
 H                  5.49758799   -1.93746352    2.00713727
 C                  3.10142799   -1.58441852    2.58969627
 H                  3.28713999   -2.54494652    2.09244027
 H                  3.76878399   -1.50742852    3.45080727
 H                  2.07573099   -1.59052452    2.94916727
 C                  0.79265099    0.65669048   -0.83045373
 C                  1.94542399    0.12854948   -0.27457873
 C                  1.11409199    0.63074448    1.91411127
 C                 -0.03867201    1.15881448    1.35815327
 H                  0.66072099    0.63858248   -1.90560873
 H                  2.71050799   -0.28815052   -0.91720973
 H                  1.24569199    0.64937348    2.98925427
 H                 -0.80383201    1.57527748    2.00089527
 C                 -1.19153901    2.88601748   -1.49035073
 H                 -0.16610401    2.89389948   -1.85067273
 H                 -1.37398901    3.84007848   -0.97950973
 H                 -1.85970201    2.82301048   -2.35192373
 C                 -2.90792601    0.22158748    0.49807227
 C                 -3.73509301    2.28659948   -0.40765173
 C                 -4.18557601   -0.10629752    0.90521927
 C                 -5.01529301    1.94249948   -0.00199173
 H                 -2.09822901   -0.47021152    0.68523127
 H                 -3.58752101    3.23290148   -0.90821273
 H                 -4.35824201   -1.04451052    1.41757827
 H                 -5.83613701    2.62161148   -0.19546573
```

```
Au                -7.78722701   -0.91067052   -0.57907973
Au                 9.54036677   -0.98842156   -1.17988918

1 2 1.0 44 1.0
2 11 1.5 13 1.5
3 4 1.0 12 1.5 14 1.5
4 5 1.0 19 1.0
5 24 1.5 25 1.5
6 7 1.0 23 1.5 26 1.5
7 8 1.0 31 1.0
8 35 1.5 36 1.5
9 10 1.0 37 1.5 38 1.5
10 43 1.0
11 12 2.0 15 1.0
12 16 1.0
13 14 1.5 17 1.0
14 18 1.0
15
16
17
18
19 20 1.0 21 1.0 22 1.0
20
21
22
23 24 2.0 27 1.0
24 28 1.0
25 26 2.0 29 1.0
26 30 1.0
27
28
29
30
31 32 1.0 33 1.0 34 1.0
32
33
34
35 37 2.0 39 1.0
36 38 1.5 40 1.0
37 41 1.0
38 42 1.0
39
40
41
42
43
44
```

B.3 Antisymmetric one Pd – one Au contact atom Oligoaniline system

```
%chk=bZigzag_1Pd_1Au.chk
%mem=4GB
%nproc=4
#p freq=raman opt b3pw91/lanl2dz geom=connectivity

Zigzag System attached to 1 Pd and 1 Au

0 2
 S                -7.83249100    1.06916200   -0.03861600
 C                -6.20649500    0.33490200   -0.02179200
 C                -3.65336500   -0.86976000   -0.08252900
 N                -2.40548600   -1.47147800   -0.15385000
 C                -1.20933500   -0.71906700   -0.08351600
 C                 1.20794300    0.71494900    0.07141100
 N                 2.40377000    1.46900400    0.14123700
 C                 3.65174000    0.86734600    0.07546300
 C                 6.20741100   -0.33275800    0.03423000
 S                 7.81373400   -1.10551000   -0.05374700
 C                -5.08188000    1.06102300   -0.41250800
 C                -3.83103200    0.47837200   -0.43831600
 C                -6.04267100   -1.00167700    0.31602800
 C                -4.79172900   -1.59948500    0.28772000
 H                -5.19488200    2.09504800   -0.71370000
 H                -2.98068700    1.06331400   -0.76086300
 H                -6.90507900   -1.58461000    0.61412900
 H                -4.70923600   -2.64017400    0.56694000
 C                -2.30460600   -2.91129000   -0.02453700
 H                -2.53999200   -3.25408800    0.99106500
 H                -2.97799300   -3.41347400   -0.72250900
 H                -1.28609900   -3.21688300   -0.24941000
 C                 0.17948100    0.94361300    0.98515700
 C                -1.01004800    0.23922400    0.90983600
 C                -0.18057500   -0.94778500   -0.99716700
 C                 1.00894200   -0.24339100   -0.92173700
 H                 0.32485400    1.66378200    1.78134500
 H                -1.78955800    0.42025000    1.63891800
 H                -0.32558700   -1.66758600   -1.79369400
 H                 1.78851200   -0.42466800   -1.65073500
 C                 2.30099500    2.90672800   -0.00868900
 H                 1.28286600    3.21417800    0.21558800
 H                 2.53255600    3.23566600   -1.02979500
 H                 2.97602100    3.41930400    0.68002400
 C                 3.82923800   -0.47950000    0.43507400
 C                 4.78951600    1.59456400   -0.30312600
 C                 5.07953600   -1.06388300    0.40473700
 C                 6.04141900    0.99934200   -0.32115200
 H                 2.97752700   -1.06640400    0.75028200
 H                 4.70508900    2.63145400   -0.59562900
 H                 5.18932700   -2.10435700    0.68389300
 H                 6.90359300    1.58083200   -0.62271000
```

```
Pd                -8.63562513    0.45894869    2.07693239
Au                 8.64730674   -0.81249678    2.14538914

1 2 1.0 43 1.0
2 11 1.5 13 1.5
3 4 1.0 12 1.5 14 1.5
4 5 1.0 19 1.0
5 24 1.5 25 1.5
6 7 1.0 23 1.5 26 1.5
7 8 1.0 31 1.0
8 35 1.5 36 1.5
9 10 1.0 37 1.5 38 1.5
10 44 1.0
11 12 2.0 15 1.0
12 16 1.0
13 14 1.5 17 1.0
14 18 1.0
15
16
17
18
19 20 1.0 21 1.0 22 1.0
20
21
22
23 24 2.0 27 1.0
24 28 1.0
25 26 2.0 29 1.0
26 30 1.0
27
28
29
30
31 32 1.0 33 1.0 34 1.0
32
33
34
35 37 2.0 39 1.0
36 38 1.5 40 1.0
37 41 1.0
38 42 1.0
39
40
41
42
43
44
```

B.4 Antisymmetric trimer Pd – Au contact atoms Oligoaniline system

```
%chk=bZigzag_3Pd_3Au.chk
%mem=7GB
%nproc=4
#p freq=raman b3pw91/lanl2dz geom=connectivity

Zigzag System attached to 3 Pd and 3 Au

0 2
 C                  7.16899400    0.52279600    0.40176200
 C                  4.55937800   -0.15578900    1.24009400
 N                  3.28449700   -0.46816500    1.68892900
 C                  2.12778200    0.09853800    1.10351900
 C                 -0.21472300    1.17239300   -0.02923900
 N                 -1.37101300    1.74061600   -0.61540700
 C                 -2.64615200    1.42447300   -0.17063700
 C                 -5.25866700    0.73591900    0.65037800
 C                  6.09651200    1.38339700    0.16977100
 C                  4.81826300    1.05368200    0.57243500
 C                  6.92508400   -0.66677700    1.07468700
 C                  5.64602500   -1.00573100    1.48959700
 H                  6.27272400    2.33191300   -0.32212400
 H                  4.01005300    1.74902900    0.39196700
 H                  7.74619300   -1.34456900    1.27166400
 H                  5.50059400   -1.94575900    2.00243100
 C                  3.10443400   -1.59271400    2.58499000
 H                  3.29014600   -2.55324200    2.08773400
 H                  3.77179000   -1.51572400    3.44610100
 H                  2.07873700   -1.59882000    2.94446100
 C                  0.79565700    0.64839500   -0.83516000
 C                  1.94843000    0.12025400   -0.27928500
 C                  1.11709800    0.62244900    1.90940500
 C                 -0.03566600    1.15051900    1.35344700
 H                  0.66372700    0.63028700   -1.91031500
 H                  2.71351400   -0.29644600   -0.92191600
 H                  1.24869800    0.64107800    2.98454800
 H                 -0.80082600    1.56698200    1.99618900
 C                 -1.18853300    2.87772200   -1.49505700
 H                 -0.16309800    2.88560400   -1.85537900
 H                 -1.37098300    3.83178300   -0.98421600
 H                 -1.85669600    2.81471500   -2.35663000
 C                 -2.90492000    0.21329200    0.49336600
 C                 -3.73208700    2.27830400   -0.41235800
 C                 -4.18257000   -0.11459300    0.90051300
 C                 -5.01228700    1.93420400   -0.00669800
 H                 -2.09522300   -0.47850700    0.68052500
 H                 -3.58451500    3.22460600   -0.91291900
 H                 -4.35523600   -1.05280600    1.41287200
 H                 -5.83313100    2.61331600   -0.20017200
 S                 -6.89544821    0.33354767    1.22260573
 Au                -8.48585289    0.98709520   -0.40910890
```

```
Au                -9.98644383    0.56539343   -2.64203150
Au               -10.07806530    2.91485248   -1.44140306
S                  8.82705876    0.96826608   -0.06810785
Pd                10.63632491    0.57892617   -1.58294149
Pd                10.72102670    2.35257019    0.39731088
Pd                12.95440860    1.31323432   -0.55441958

1 9 1.5 11 1.5 45 1.0
2 3 1.0 10 1.5 12 1.5
3 4 1.0 17 1.0
4 22 1.5 23 1.5
5 6 1.0 21 1.5 24 1.5
6 7 1.0 29 1.0
7 33 1.5 34 1.5
8 35 1.5 36 1.5 41 1.0
9 10 2.0 13 1.0
10 14 1.0
11 12 1.5 15 1.0
12 16 1.0
13
14
15
16
17 18 1.0 19 1.0 20 1.0
18
19
20
21 22 2.0 25 1.0
22 26 1.0
23 24 2.0 27 1.0
24 28 1.0
25
26
27
28
29 30 1.0 31 1.0 32 1.0
30
31
32
33 35 2.0 37 1.0
34 36 1.5 38 1.0
35 39 1.0
36 40 1.0
37
38
39
40
41 42 1.0
42 43 1.0 44 1.0
43 44 1.0
44
45 46 1.0 47 1.0
46 48 1.0 47 1.0
47 48 1.0
```

```
 48
```

B.5 Comjob Input File

```
#Common name of the files
bZigzag_3Pd_3Au
#Number of processors to be used
4
#Requested memory in the com file
6GB
#Requested memory in the job file
6GB
#Wall time requested
0:00:00
#Method and basis set
b3pw91/lanl2dz
#Direction of the applied field
Z
#Charge and multiplicity
0,2
#Comment line
Zigzag with 3 Pd and 3 Au contacts
#Working directory
/home/mike/bZigzag_3Pd_3Au/Zigzag
#Mass storage directory
/home/mike/bZigzag_3Pd_3Au/Zigzag
#number of field intensities to be used
51
#Fields intensities
0
2
4
6
8
10
12
14
16
18
20
22
24
26
28
30
32
34
36
38
```

```
40
42
44
46
48
50
-2
-4
-6
-8
-10
-12
-14
-16
-18
-20
-22
-24
-26
-28
-30
-32
-34
-36
-38
-40
-42
-44
-46
-48
-50
0
0
```

B.6 MoCAF Input File

```
DFT
bZigzag_3Pd_3AuF
bZigzag_3Pd_3AuF
bZigzag_3Pd_3AuF
bZigzag_3Pd_3AuF
4,1,1
242,M
66,R
8,M
66,L
Pd
METAL
3,9,6,4
Au
METAL
3,9,6,4
0.5,0.5
-4.449
-4.449
0.5
bZigzag_3Pd_3AuF-TR.dat
bZigzag_3Pd_3AuF-CO.dat
-10.,0.,1000
-4.5,4.5,51
0.01
21.70
1.0,1.0
```

VITA

Name:	Michael Wei-Leung Wang
Address:	16305 22nd DR SE, Mill Creek WA 98012
Email Address:	michaelwwang@tamu.edu
Education:	B.S., Chemical Engineering, University of Washington, 2004
	M.S., Chemical Engineering, Texas A&M University, 2006